USCIPI REPORT #630

Digital Color Image Restoration

by

Clanton E. Mancill

August 1975

Signal and Image Processing Institute
UNIVERSITY OF SOUTHERN CALIFORNIA
Department of Electrical Engineering-Systems
Powell Hall of Engineering
University Park/MC-0272
Los Angeles, CA 90089 U.S.A.

UNCLASSIFIED

Security Classification

DOCUMENT CONTROL DATA - R & D

(Security classification of title, body of abstract and indexing annotation must be entered when the overall report is classified)

1. ORIGINATING ACTIVITY (Corporate author)
Image Processing Institute
University of Southern California, University Park
Los Angeles, California 90007

2a. REPORT SECURITY CLASSIFICATION
UNCLASSIFIED

2b. GROUP

3. REPORT TITLE
DIGITAL COLOR IMAGE RESTORATION

4. DESCRIPTIVE NOTES (Type of report and inclusive dates)
Technical Report, August 1975

5. AUTHOR(S) (First name, middle initial, last name)
Clanton E. Mancill

6. REPORT DATE
August 1975

7a. TOTAL NO. OF PAGES
156

7b. NO. OF REFS
39

8a. CONTRACT OR GRANT NO.
F08606-72-C-0008

b. PROJECT NO.
ARPA Order No. 1706

c.

d.

9a. ORIGINATOR'S REPORT NUMBER(S)
USCIPI Report 630

9b. OTHER REPORT NO(S) (Any other numbers that may be assigned this report)

10. DISTRIBUTION STATEMENT
Approved for release: distribution unlimited

11. SUPPLEMENTARY NOTES

12. SPONSORING MILITARY ACTIVITY
Advanced Research Projects Agency
1400 Wilson Boulevard
Arlington, Virginia 22209

13. ABSTRACT

The restoration of color errors in digitally recorded color images is considered in this dissertation. A vector space model of a general digital color image recording system is derived and the equations representing the model and the equations of colorimetry are expressed in matrix form. Computer algorithms are derived which correct color errors introduced by imperfections in the color recording system. The sources of color error which are considered include sensor spectral responses which depart from ideal color matching curves, crosstalk between color signal channels, and system nonlinearities. The special case of a color film-digital scanner system is examined in detail, although the methods derived apply to a wider class of color or multispectral sensing and recording systems. The success of the correction algorithms is demonstrated using a computer simulation of the film-scanner system. The algorithms for correction of spectrally imperfect sensors are also tested using a specially created six band multispectral test image.

The generalized matrix inverse is used extensively in this report. Least squares, minimum norm, and Wiener estimation algorithms, in the form of generalized inverses, are applied to the correction of sensor imperfections. The utility of the generalized inverse in the spectral domain is also demonstrated by applying it to some related color problems. These include the estimation of the spectral response of a sensor from sample readings, and computer generation of spectral waveforms with desired colorimetric properties.

* *

14. Key Words: Colorimetry, Image Processing, Estimation theory, Color Film Error Correction, Generalized Matrix Inverse Applications, Multispectral Processing.

DD FORM 1 NOV 65 1473

UNCLASSIFIED

Security Classification

14 KEY WORDS	LINK A		LINK B		LINK C	
	ROLE	WT	ROLE	WT	ROLE	WT

ABSTRACT

The restoration of color errors in digitally recorded color images is considered in this dissertation. A vector space model of a general digital color image recording system is derived and the equations representing the model and the equations of colorimetry are expressed in matrix form. Computer algorithms are derived which correct color errors introduced by imperfections in the color recording system. The sources of color error which are considered include sensor spectral responses which depart from ideal color matching curves, crosstalk between color signal channels, and system nonlinearities. The special case of a color film-digital scanner system is examined in detail, although the methods derived apply to a wider class of color or multispectral sensing and recording systems. The success of the correction algorithms is demonstrated using a computer simulation of the film-scanner system. The algorithms for correction of spectrally imperfect sensors are also tested using a specially created six band multispectral test image.

The generalized matrix inverse is used extensively in this report. Least squares, minimum norm, and Wiener estimation algorithms, in the form of generalized inverses, are applied to the correction of sensor imperfections. The

utility of the generalized inverse in the spectral domain is also demonstrated by applying it to some related color problems. These include the estimation of the spectral response of a sensor from sample readings, and computer generation of spectral waveforms with desired colorimetric properties.

TABLE OF CONTENTS

LIST OF FIGURES

LIST OF TABLES

ACKNOWLEDGEMENTS

The advice and support of many people contributed to the preparation of this dissertation. The author wishes especially to thank the members of his guidance committee, Dr. W.K. Pratt, Dr. T.E. Harris, and Dr. W. Frei. The advice and guidance of Dr. William K. Pratt, the committee chairman and director of the Image Processing Institute, is most sincerely acknowledged. Many others, faculty and students, have also contributed suggestions and ideas which have been incorporated into this report. Discussions with Dr. Robert H. Wallis were particularly helpful to the author. The support of the clerical and laboratory staff of the Institute is deeply appreciated, especially the expert typing of Miss Marilyn Chan.

This research was supported in part by the Advanced Research Projects Agency of the Department of Defense and was monitored by the Air Force Test Range under Contract No. F08606-72-C-0008. In addition, the author would like to express thanks to the Hughes Aircraft Company and the National Aeronautics and Space Administration for support provided during the author's postgraduate career.

Description of photographs in color plate

(4-16) True color image

(4-17) Narrowband sensor image

(4-18) Pseudo-inverse estimated image, narrowband sensor input

(4-19) Wiener inverse estimated image, narrowband sensor input

(4-20) Long wavelength sensor image

(4-21) Wiener inverse estimated image, long wavelength sensor input

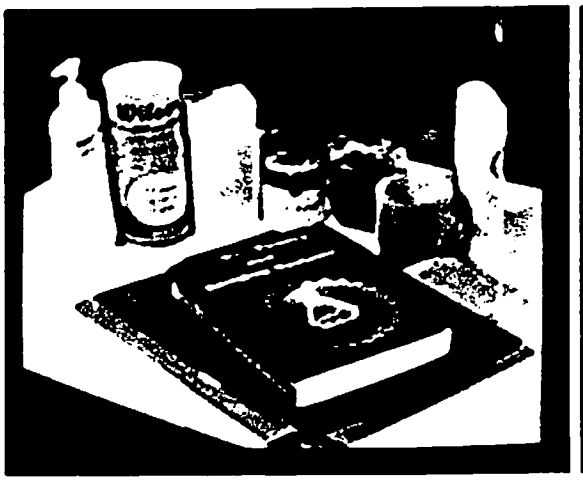

Figure (4-16)

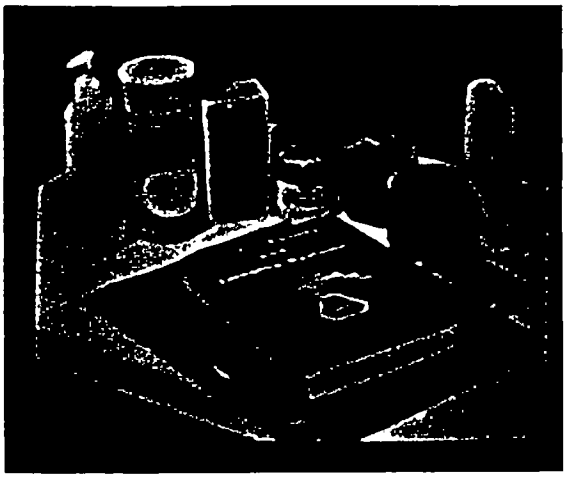

Figure (4-17)

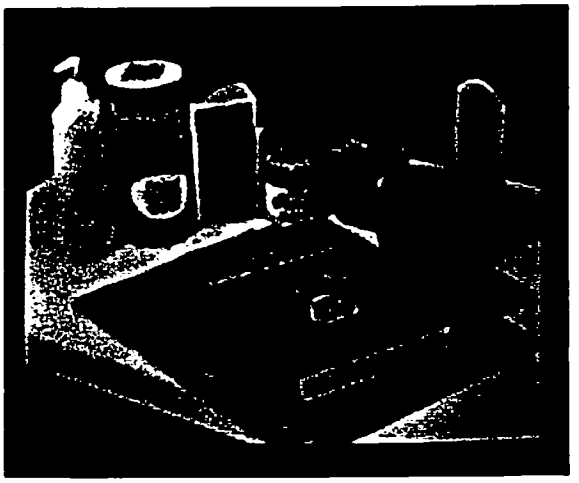

Figure (4-18)

Figure (4-19)

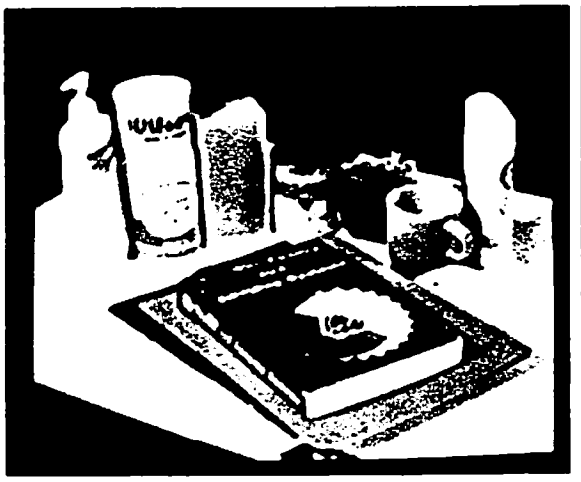

Figure (4-20)

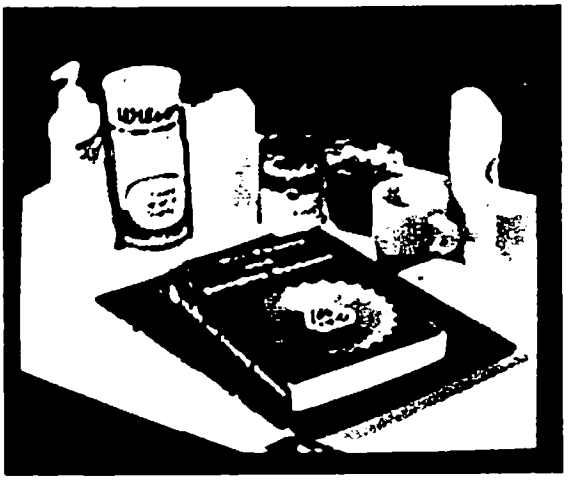

Figure (4-21)

1. Introduction

This report concerns the application of sampled data processing and estimation methods to the restoration of digitally recorded color images. The restoration of color values which have been degraded by sensor and storage imperfections is an objective which has been pursued since color image recording systems were invented. The methods of color restoration which have been heretofore explored have varied with each method of color image recording. The first, and by far the most common, medium of color image recording is color photographic film. Most color film images do not undergo any post-development restoration at all. Those film images which are restored are usually modified only by photographic masking, which attempts to provide pleasingly saturated colors and a proper white balance. Masking and other photographic restoration methods are extremely limited in their ability to correct color errors. They are slow, inflexible and usually apply the same correction to all points in the image. When color values are converted to electrical signals, as in color television and in color scanning devices, much more can be done to correct color errors, often in a real-time interactive mode. Here again, the object is most commonly the production of a pleasing saturated picture, not the increase of color fidelity as measured by a quantitative criterion.

With the comparatively recent development of digital image recording, it becomes possible to extend further the capabilities of color image restoration. All the power and flexibility of the stored program digital computer, which have been proved as successful in the restoration and enhancement of digital monochrome imagery, can be applied to color image restoration. The digital computer can be utilized in the optimization and testing of restoration algorithms as well as in the execution of these algorithms to restore large quantities of digital color imagery.

This report will examine the computer application of some standard mathematical tools and operations to the task of restoring errors introduced by sensor and storage imperfections in a general color image recording system. The system imperfections which are considered include non-ideal sensor spectral responses, crosstalk between color signal channels, and errors introduced by system nonlinearities. A color film-electronic scanner color system is analyzed in some detail, but the methods developed can be applied to a wider class of color analyzing and recording systems. In addition, some of the mathematical restoration tools utilizing generalized inverses are applied to other color problems such as the spectral calibration of color scanners and the computer generation of spectral waveforms with desired colorimetric properties.

The dissertation consists of seven chapters. Chapter 2 presents a short tutorial on colorimetry, color reproduction and restoration. Chapter 3 discusses the advantages of digital color restoration and vector space modelling of color systems. Tristimulus estimation using linear estimation methods is treated in Chapter 4. Chapter 5 discusses methods of inverting the nonlinear film-scanner equations in order to estimate film exposure values. Some related applications of digital color methods are treated in Chapter 6 and some conclusions and general remarks about the dissertation are presented in Chapter 7.

2. Color Reproduction

The long established field of color science historically has consisted of two branches: colorimetry, which is the measurement of color, and color reproduction. These two areas of study have been related only slightly and, for two reasons, have not been put on a rigorous basis until recent years. First, established color standards came into use only after the formation of the Commission Internationale d'Eclairage (CIE) in the early 1930's. Secondly, until the development of color television in the 1950's, color reproduction was achieved by photographic methods. Because of the complexity of subtractive color photography, its capabilities were advanced primarily by empirical means, and not through the use of colorimetry, which is based on the simpler theory of additive primary colors. In the last two decades, color reproduction technology has adopted the terminology and methods of colorimetry, and the two branches of color science have become more unified.

In Chapter 2 which follows, three topics will be discussed. First, the basics of colorimetry will be given, including a brief discussion of color error formulas. Second, the principles of color reproduction and the important sources of reproduction errors will be described. Finally, some of the standard techniques of color

restoration, both photographic and electronic, will be discussed.

2.1 Colorimetry

Colorimetry, the science of color measurement, is based on the experimental observation that, over some range of colors and observing conditions, any color stimulus (defined as radiant flux detected by an observer's visual system and evoking a sensation of color [1]) can be matched by an additive mixture of three fixed primary color stimuli.

The experimental laws governing the relations between the spectral intensity distribution of a color stimulus and the amounts of each primary color stimulus required to match it form the basis of colorimetry. The fundamental color matching equations are

$$\begin{aligned} \int C(\lambda)\, S_R(\lambda)\, d\lambda &= \int C_P(\lambda)\, S_R(\lambda)\, d\lambda \\ \int C(\lambda)\, S_G(\lambda)\, d\lambda &= \int C_P(\lambda)\, S_G(\lambda)\, d\lambda \\ \int C(\lambda)\, S_B(\lambda)\, d\lambda &= \int C_P(\lambda)\, S_P(\lambda)\, d\lambda \end{aligned} \qquad (2\text{-}1)$$

where $C(\lambda)$ is the spectral intensity distribution of the color to be matched and $C_P(\lambda)$ is the spectral intensity distribution of the weighted sum of primary colors which

matches $C(\lambda)$. The characteristics of the standard average observer with normal color vision are given by the spectral sensitivity curves $S_R(\lambda)$, $S_G(\lambda)$, and $S_B(\lambda)$ and the spectral intensity of the matching primaries are $P_R(\lambda)$, $P_G(\lambda)$, and $P_B(\lambda)$. The primary colors are usually suitably chosen red, green, and blue lights.

If the weights or amounts of each primary which together match $C(\lambda)$ are given by $A_R(C)$, $A_G(C)$ and $A_B(C)$, then

$$C_p(\lambda) = A_R(C)\ P_R(\lambda) + A_G(C)\ P_G(\lambda) + A_P(C)\ P_B(\lambda) \qquad (2\text{-}2)$$

Then if I_R, I_G, I_B are defined as below, a color match requires

$$I_R \triangleq \int C(\lambda) S_R(\lambda) d\lambda = \int [A_R(C) P_R(\lambda) + A_G(C) P_G(\lambda) + A_B(C) P_B(\lambda)] S_R(\lambda) d\lambda \qquad (2\text{-}3a)$$

$$I_G \triangleq \int C(\lambda) S_G(\lambda) d\lambda = \int [A_R(C) P_R(\lambda) + A_G(C) P_G(\lambda) + A_B(C) P_B(\lambda)] S_G(\lambda) d\lambda \qquad (2\text{-}3b)$$

$$I_B \triangleq \int C(\lambda) S_B(\lambda) d\lambda = \int [A_R(C) P_R(\lambda) + A_G(C) P_G(\lambda) + A_B(C) P_B(\lambda)] S_B(\lambda) d\lambda \qquad (2\text{-}3c)$$

where $A_R(C)$, $A_G(C)$, $A_B(C)$ are called the primary matching values of the color C. When these primary matching values are normalized by the primary matching values of a reference white color W, the resulting normalized values are called the tristimulus values of C

$$T_1(C) = \frac{A_1(C)}{A_1(W)} \qquad (2\text{-}4a)$$

$$T_2(C) = \frac{A_2(C)}{A_2(W)} \qquad (2\text{-}4b)$$

$$T_3(C) = \frac{A_3(C)}{A_3(W)} \qquad (2\text{-}4c)$$

Equations (2-3) and (2-4) can be combined in matrix form to give the following equation of color matching

$$\begin{bmatrix} I_R \\ I_G \\ I_B \end{bmatrix} = \begin{bmatrix} d_{11} & d_{12} & d_{13} \\ d_{21} & d_{22} & d_{23} \\ d_{31} & d_{32} & d_{33} \end{bmatrix} \begin{bmatrix} A_1(W) & 0 & 0 \\ 0 & A_2(W) & 0 \\ 0 & 0 & A_3(W) \end{bmatrix} \begin{bmatrix} T_1(C) \\ T_2(C) \\ T_3(C) \end{bmatrix} \qquad (2\text{-}5)$$

where

$$d_{ij} = P_j(\lambda)\, S_i(\lambda)\, d\lambda \qquad (2\text{-}6)$$

and in the subscripts i,j R=1, G=2, B=3.

The color matching equations, expressed above in different but equivalent equations (2-1), (2-3), and (2-5), illustrate the main objective of colorimetry: to determine whether or not two given stimuli, $C(\lambda)$ and $C_p(\lambda)$, match in color. The two colors match, colorimetrically, when their tristimulus values are equal.

It is important to observe that colorimetry does not

attempt to characterize the sensation which an observer perceives when he receives a color stimulus. To do this would require a much more complex model involving spatial and temporal parameters relating to state adaption, stimuli surrounding the test stimuli and other parameters. Colorimetry is not designed to provide a general color perception model, only to answer the simpler but still important question of whether two colors match or not.

The presence of a linear integration of spectral intensity over wavelength in the color matching equations is a reflection of the underlying assumptions of linearity and additivity in color matching. Linearity and additivity, which hold accurately over a wide range of observing conditions [1], require:

(1) that the match between any two colors continues to hold when the spectral distributions of the two colors are each scaled up or down by the same constant factor; and,

(2) that if colors A and B match, and if colors C and D match then the additive color mixtures (A+C) and (B+D) also match.

Under these assumptions, it is easily seen that any color $C(\lambda)$ may be thought of as a weighted sum of spectral, i.e., monochromatic, colors. Because of linearity and additivity, the tristimulus values of the spectral

distribution $C(\lambda)$ can be obtained by integrating the tristimulus values of the spectral components of $C(\lambda)$ over all wavelengths. Combining eqs. (2-1), (2-3) and (2-5) gives

$$T_1(C) = C(\lambda)\, T_1(\lambda)\, d\lambda$$

$$T_2(C) = C(\lambda)\, T_2(\lambda)\, d\lambda \qquad (2\text{-}7)$$

$$T_3(C) = C(\lambda)\, T_3(\lambda)\, d\lambda$$

where

$$\begin{bmatrix} T_1(\lambda) \\ T_2(\lambda) \\ T_3(\lambda) \end{bmatrix} = \begin{bmatrix} 1/A_1(\lambda) & 0 & 0 \\ 0 & 1/A_2(W) & 0 \\ 0 & 0 & 1/A_3(W) \end{bmatrix} \begin{bmatrix} \quad \\ d_{ij} \\ \quad \end{bmatrix}^{-1} \begin{bmatrix} S_R(\lambda) \\ S_G(\lambda) \\ S_B(\lambda) \end{bmatrix} \qquad (2\text{-}8)$$

The functions $T_1(\lambda)$, $T_2(\lambda)$, $T_3(\lambda)$ are called the color matching curves of the set of primaries $P_R(\lambda)$, $P_G(\lambda)$, $P_B(\lambda)$. These curves completely describe human visual color response under the colorimetric model by determining through eq.(2-7) the tristimulus values, or primary weights, needed to match any color. It will subsequently be shown that $T_1(\lambda)$, $T_2(\lambda)$, $T_3(\lambda)$ are the optimum spectral sensitivities for a color sensor whose outputs directly drive display primaries $P_R(\lambda)$, $P_G(\lambda)$, $P_B(\lambda)$. Figure (2-1) contains a plot of the color matching curves corresponding to equal radiance narrowband primaries at 700.0, 546.1, and

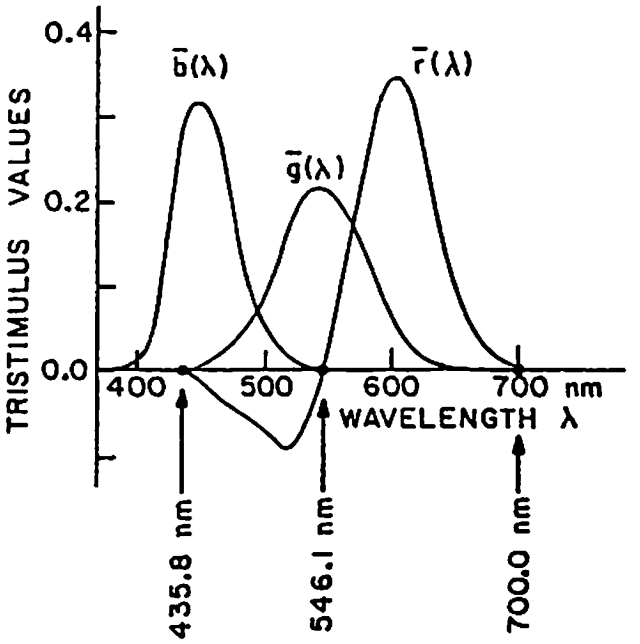

Figure (2-1) Color matching curves for narrowband primaries

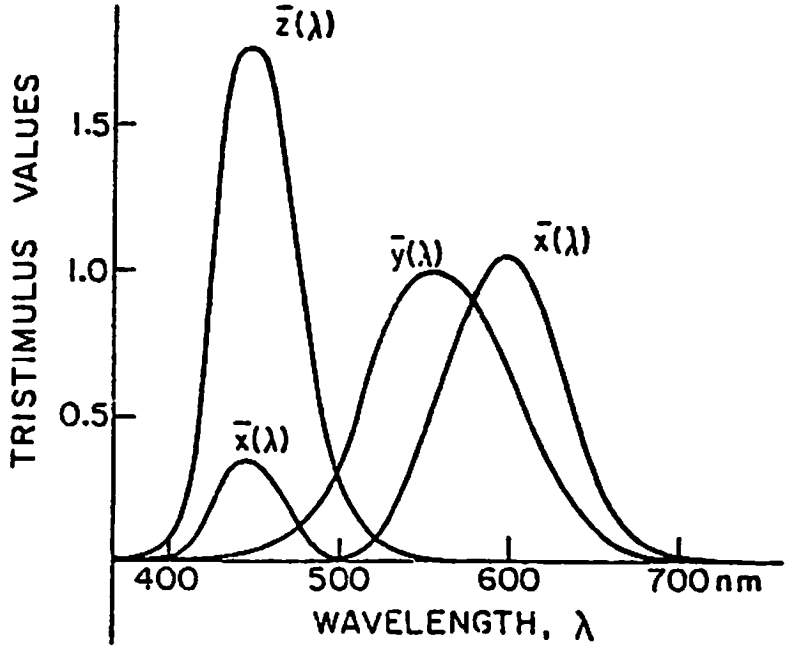

Figure (2-2) CIE XYZ color matching curves

435.8 nanometers, with a reference white whose power spectral density is constant with wavelength (equal energy white).

The color matching curves of eq. (2-8) depend on the matching primaries $P_R(\lambda)$, $P_G(\lambda)$, $P_B(\lambda)$ only through the matrix $D=[\ d_{ij}\ ]$ of eq. (2-6). Therefore, the three color matching curves corresponding to a particular primary set may be derived from those corresponding to another primary set by a 3x3 matrix multiplication, so that each new curve is a weighted sum of the three original color matching curves. It follows from eq. (2-7) that the tristimulus values of a color with respect to the new primaries are equal to the old tristimulus values multiplied by the same 3x3 matrix.

It is of interest to note that color matching curves $T_1(\lambda)$, $T_2(\lambda)$, $T_3(\lambda)$ are obtained directly by means of color matching experiments with test subjects, rather than by calculating them from the visual sensitivity curves $S_{R'}$, $S_{G'}$, S_B through eq. (2-8). The visual sensitivity curves are, even today, known with less accuracy than are the color matching curves, since it is difficult to measure them directly. The responses $S_{R'}$, $S_{G'}$ and S_B cannot be determined from the color matching curves via eq. (2-8) since $S_{R'}$, $S_{G'}$, S_B are contained in each element d_{ij} of $\underline{D}$. For this reason, color matching is nearly always done by

comparing the tristimulus values of two colors obtained from equations of the form of eq. (2-7) rather than by using the spectral sensitivities of the eye directly, as in eqs. (2-1).

The determination of tristimulus values of eqs. (2-7) requires that $T_1(\lambda)$, $T_2(\lambda)$, $T_3(\lambda)$ represent a particular set of "standard observer" color matching curves such as the CIE 1931 standard observer curves $X(\lambda)$, $Y(\lambda)$, $Z(\lambda)$ shown in figure (2-2). In this case, the tristimulus equations become

$$X = R\int C(\lambda)\ X(\lambda)\ d\lambda$$

$$Y = R\int C(\lambda)\ Y(\lambda)\ d\lambda \qquad (2\text{-}9)$$

$$Z = R\int C(\lambda)\ Z(\lambda)\ d\lambda$$

where R may be chosen arbitrarily when only the relative tristimulus values are of interest. When R is chosen to be $R=K \approx 680$ lumens/watt, the value of Y is then the luminous flux, in lumens, of the color $C(\lambda)$.

When a color consists of radiant flux reflected (or transmitted) by a nonradiating object, it is called an object-color stimulus. A reflected object color is specified by the spectral distribution $P(\lambda)\ I(\lambda)$ where $P(\lambda)$ is the spectral reflectivity and $I(\lambda)$ is the spectral intensity (power) distribution of the light source. The

tristimulus equations are then

$$X = R\int P(\lambda)\ I(\lambda)\ X(\lambda)\ d\lambda$$

$$Y = R\int P(\lambda)\ I(\lambda)\ Y(\lambda)\ d\lambda \qquad (2\text{-}10)$$

$$Z = R\int P(\lambda)\ I(\lambda)\ Z(\lambda)\ d\lambda$$

where R is usually chosen so that for a perfectly reflecting and perfectly diffusing object ($P(\lambda)=1.0$ at all wavelengths), the luminance Y has a value of 100. This may be ensured by defining R as

$$R \triangleq \frac{100}{\int I(\lambda)\ Y(\lambda)\ d\lambda} \qquad (2\text{-}11)$$

The spectral distribution of the illuminant, $I(\lambda)$, is usually assumed to be one of the CIE standard illuminants:

CIE illuminant A represents a black-body emitter at 2856 K (approximates the spectral distribution of an incandescent light bulb).

CIE illuminant C represents average daylight with a correlated color temperature of approximately 6770 K.

CIE illuminant D_{65} represents a phase of daylight with a correlated color temperature of approximately 6500 K (using more recent measurements than those of illuminant C).

CIE illuminant D_{55} and D_{75} represent phases of daylight with correlated color temperatures of 5500 and 7500 K, respectively.

The spectral distributions of these illuminants are shown

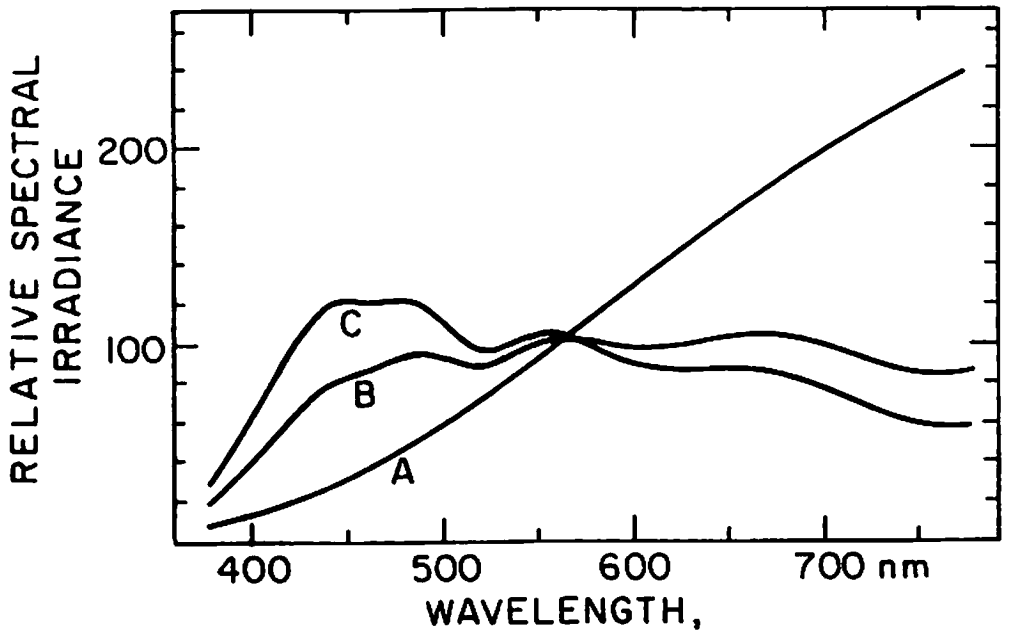

Figure (2-3a) CIE standard illuminants A, B, C

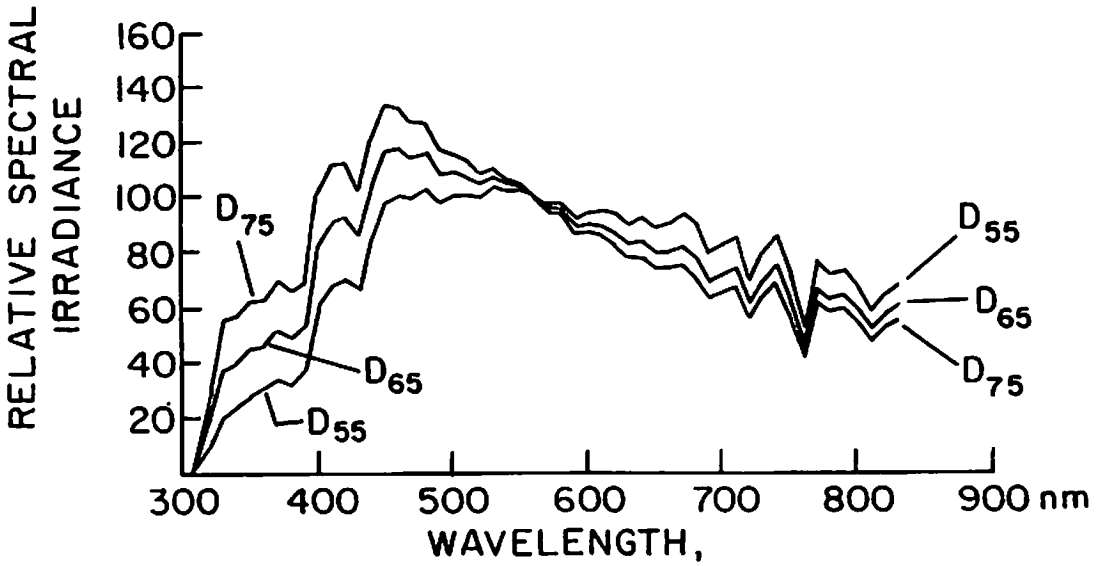

Figure (2-3b) CIE standard illuminants D_{55}, D_{65}, D_{75}

in figure (2-3).

Although any color stimulus is uniquely specified colorimetrically by giving its tristimulus values in any of the standard observer coordinate systems, it is more convenient for plotting purposes to reduce the dimensionality of a color from three to two by normalizing each tristimulus value by the sum of the three tristimulus values. These normalized values are called chromaticity values and are represented by the lower case symbol of the corresponding tristimulus symbol. For example,

$$t_i = \frac{T_i}{T_1 + T_2 + T_3} \qquad (2\text{-}12)$$

for i=1,2,3 or

$$x = \frac{X}{X + Y + Z}$$

$$y = \frac{Y}{X + Y + Z} \qquad (2\text{-}13)$$

$$z = \frac{Z}{X + Y + Z}$$

Since x+y+z=1, only two chromaticities, usually x and y, need be specified. When a third number is required to complete the specification of the color, the luminance value Y is often given also. The complete color specification is then x,y,Y.

Two chromaticity values may be used as rectangular

coordinates in a chromaticity diagram. The CIE 1931 (x,y) chromaticity diagram is shown in figure (2-4) with the locus of spectral (monochromatic) colors from λ=380 nanometers to λ=780 nanometers included. It may be shown easily that the location on a chromaticity diagram of a positively weighted sum of two color stimuli must lie on the straight line connecting the chromaticity coordinates of the two color stimuli. It follows that any realizable color, i.e., a positively weighted sum of spectral colors, must lie within the locus of spectral colors on a chromaticity diagram. When tristimulus values are normalized so that (1,1,1) corresponds to a reference white, the reference white is then located at (1/3,1/3) on the chromaticity diagram.

Color Difference Formulas

It was previously stated that colorimetry attempts to answer the question of whether two colors appear to a human observer to match or not. Two colors match colorimetrically when their tristimulus values are equal. The definition of colorimetry can be broadened to include the measurements of the color difference when the tristimulus values of two colors are not equal. A formula is desired which operates on the tristimulus values of two colors and produces a number which is proportional to the perceived difference between the colors for an average

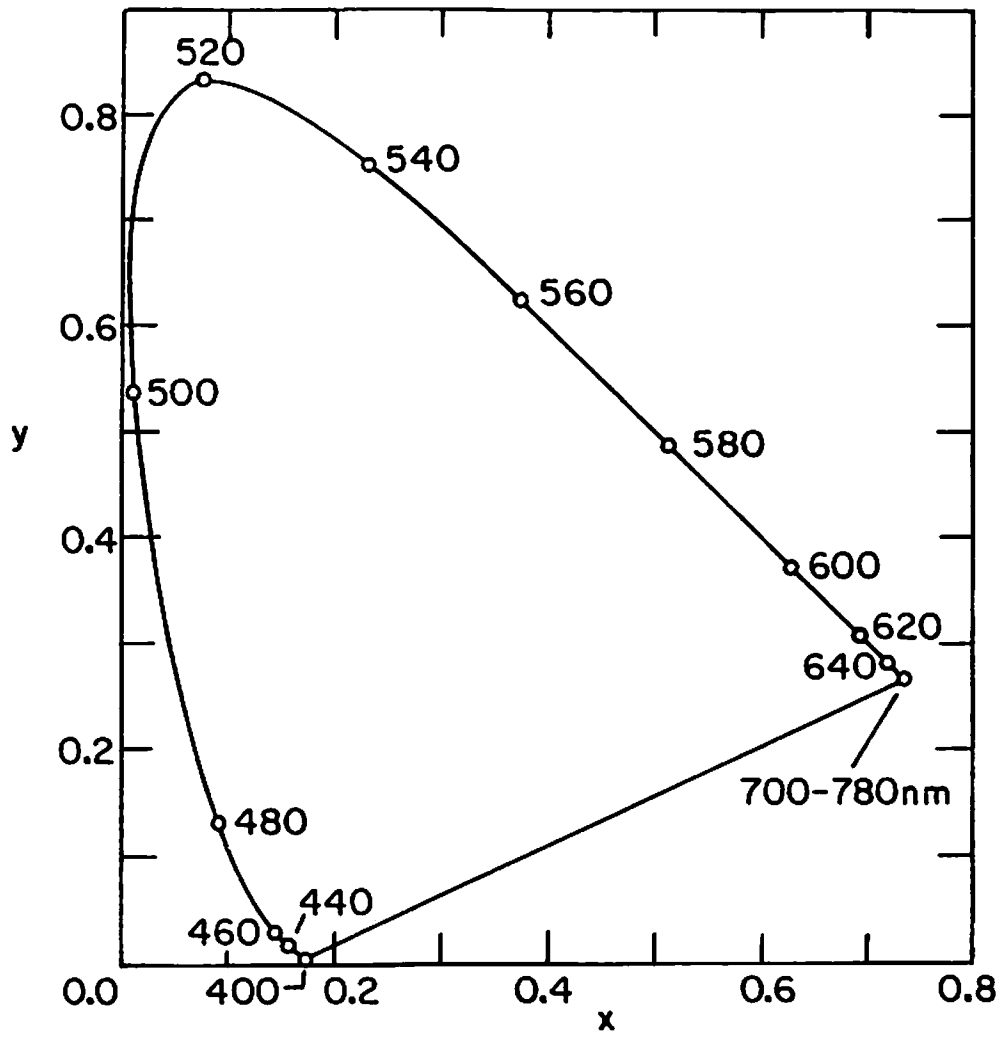

Figure (2-4) CIE x-y chromaticity diagram

observer with normal color vision. Obtaining such a formula is difficult since the subjective estimation of color differences by an observer is far less accurate than is strict color matching, and the influence of viewing conditions is very strong [2].

Still, there are several useful color difference formulas based on the 1931 CIE standard observer (XYZ) system. One system which attempts to provide a chromaticity diagram in which equal distances correspond approximately to equal visual differences is the 1960 CIE uniform chromaticity scale (UCS) diagram. This system is derived from a projective transformation of the 1931 CIE chromaticity diagram [3]. The transformation equations are

$$u = \frac{4X}{X + 15Y + 3Z}$$

$$v = \frac{6Y}{X + 15Y + 3Z} \qquad (2\text{-}14)$$

where u,v are UCS chromaticities and the UCS tristimulus values are called U,V and W. The UCS chromaticity diagram showing the locus of spectral colors is given in figure (2-5). The 1960 CIE-UCS system has been extended to include luminance differences in the U*,V*,W* system [4], defined by

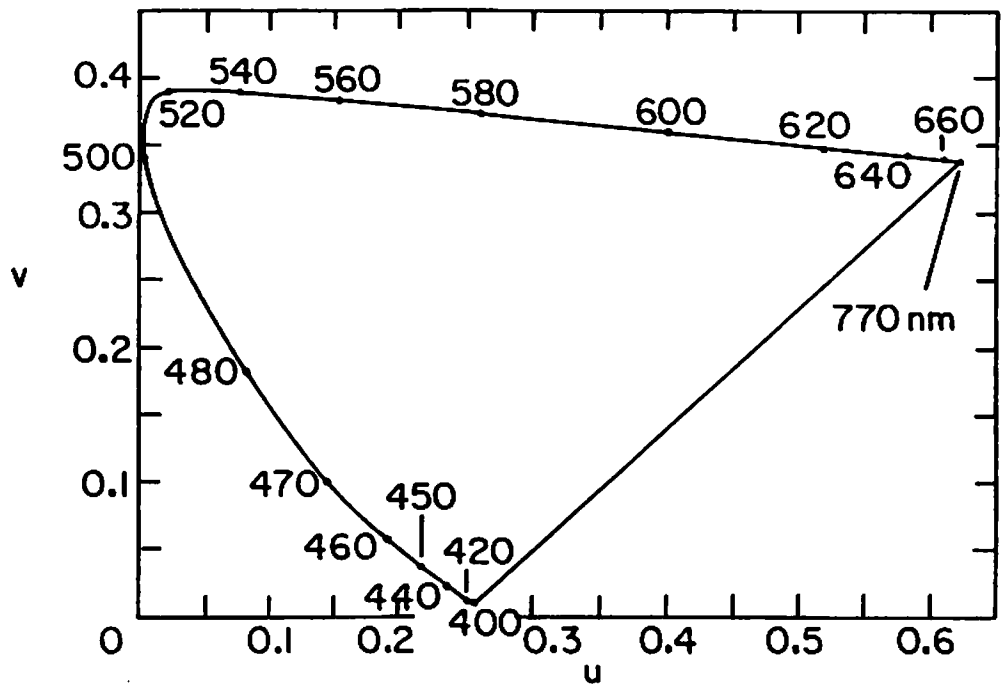

Figure (2-5) CIE UCS chromaticity diagram

$$W^* = 25Y^{1/3} - 17$$

$$U^* = 13W(u - u_o) \qquad (2\text{-}15)$$

$$V^* = 13W(v - v_o)$$

for $1 \leq Y \leq 100$, where u_o, v_o are the UCS chromaticities of the reference white. The resulting color difference formula for colors U^*, V^*, W^* and U^*, V^*, W^* is given by

$$\Delta E = [(U_1^* - U_2^*)^2 + (V_1^* - V_2^*)^2 + (W_1^* - W_2^*)^2]^{1/2} \qquad (2\text{-}16)$$

Another widely used uniform color coordinate system is the cube root system [5]. The formulas for the cube root coordinates L, a, b are given by

$$L = 25.29G^{1/3} - 18.38$$
$$a = 106.0\ (R^{1/3} - G^{1/3})$$
$$b = 42.34\ (G^{1/3} - B^{1/3})$$

where R=1.02 X, G=Y, and B=0.847 Z. The color distance formula is then the Euclidean distance in L, a, b space

$$\Delta E = [(\Delta L)^2 + (\Delta a)^2 + (\Delta b)^2]^{1/2} \qquad (2\text{-}17)$$

In each of the two systems described above, the U*V*W* and the L a b systems, one coordinate (W* or L) corresponds to the perceived brightness of the color, while the other two coordinates form a plane in which the origin corresponds to an achromatic grey. In each system, color

saturation increases with distance from the origin, while hue or dominant wavelength varies with angle about the origin. In all such perceptually uniform systems, the coordinates are nonlinear functions of the tristimulus values, while the tristimulus values are always linear functions of the color spectral distribution $C(\lambda)$.

2.2 Color Reproduction

In this section, additive and subtractive color reproduction will be described using the methods and expressions of colorimetry. Colorimetry possesses serious limitations as a basis for the reproduction of color images which are large, spatially complex, and possibly time varying. Color matching curves, the basic functions of colorimetry, are obtained by the matching of two small, uniform patches of color which are of three to ten degrees in angular size, seen against a black surround. It is well known that perceived color sensations, and, to a lesser extent, color matches, change when the surrounding area of the test colors is changed visually [6]. Still, colorimetry has served as the foundation of color television design, in the absence of a better visual model, and the results have been quite satisfactory [7].

Color reproduction methods which are based on the rules of colorimetry attempt to satisfy the following two

conditions:

(1) The spectral sensitivities of the color sensors are a set of color matching curves.

(2) The sensor outputs drive display primaries which are the primaries corresponding to the sensor color matching curves (or the sensor outputs have been transformed to correspond to the display primaries).

The two most important sources of color reproduction errors occur when the two above conditions are not met. Imperfect spectral sensitivities and deficiencies of the primaries are present, to some extent, in all color reproduction systems, whether photographic, television, or lithographic.

Imperfect spectral sensitivities occur for two reasons. First, real sensors such as photographic emulsions and vidicon tubes do not have sensitivities which are color matching curves, though appropriate optical filtering may allow an arbitrarily close fit to color matching curves, at the cost of some loss of system sensitivity and signal-to-noise ratio. A second reason is that spectral sensitivities may be intentionally degraded in order to compensate partially for errors introduced in other parts of the system. An example of this is the wide spectral spacing of the peak sensitivities of the three layers of some color films. The widely spaced

sensitivities introduce an exaggerated saturation of colors which helps to compensate for loss of saturation in the developed transparency caused by undesired layer absorptions. Undesired absorptions will be treated at greater length later.

A quantitative figure of merit for color sensors is the colorimetric quality factor q defined by Neugebauer [8]. The quality factor of a spectral sensitivity curve is unity when the curve is any color matching curve. The quality factor diminishes as the sensitivity curve departs more and more from its nearest (in the least squares sense) color matching curve. The quality factor q is obtained by forming a collection of functions from three color matching curves and any complete orthonormal set, such as the usual set of sine and cosine functions. This collection is orthonormalized by the Gram-Schmitt process giving an orthonormal function set

$$U_1(\lambda),\ U_2(\lambda),\ U_3(\lambda),\ \ldots\ldots\ldots,\ U_n(\lambda),\ \ldots\ldots$$

the first three of which are color matching curves. Such an orthonormal set is shown in figure (2-6). Figure (2-6a) shows the first three functions, all color matching curves. The first (and only nonnegative) member of the set is the luminous efficiency curve. The second three functions of the set, derived using sine and cosine functions, are shown in figure (2-6b).

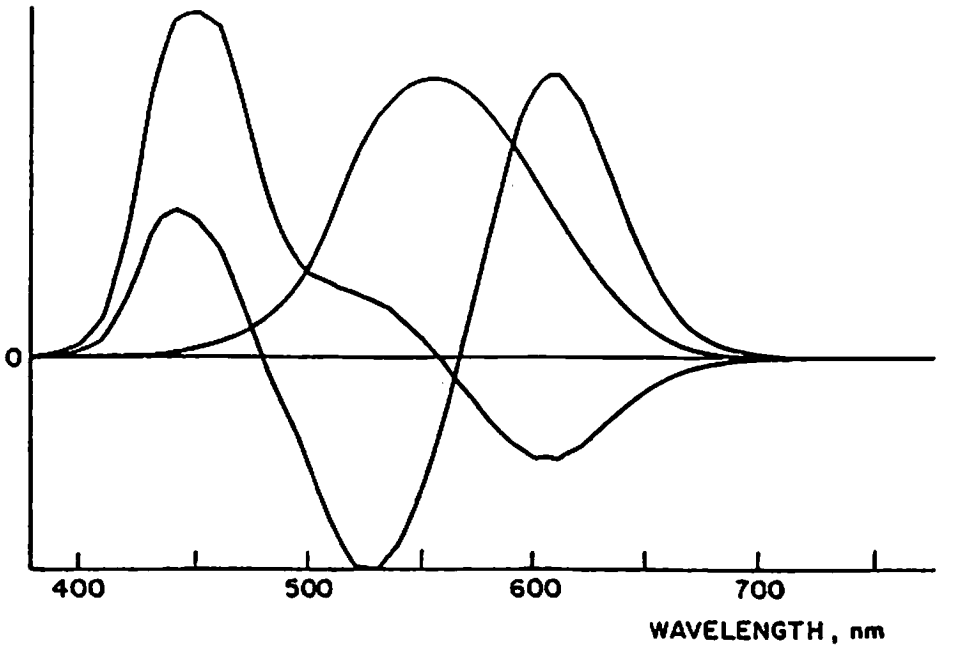

Figure (2-6a) Orthonormal color matching curves

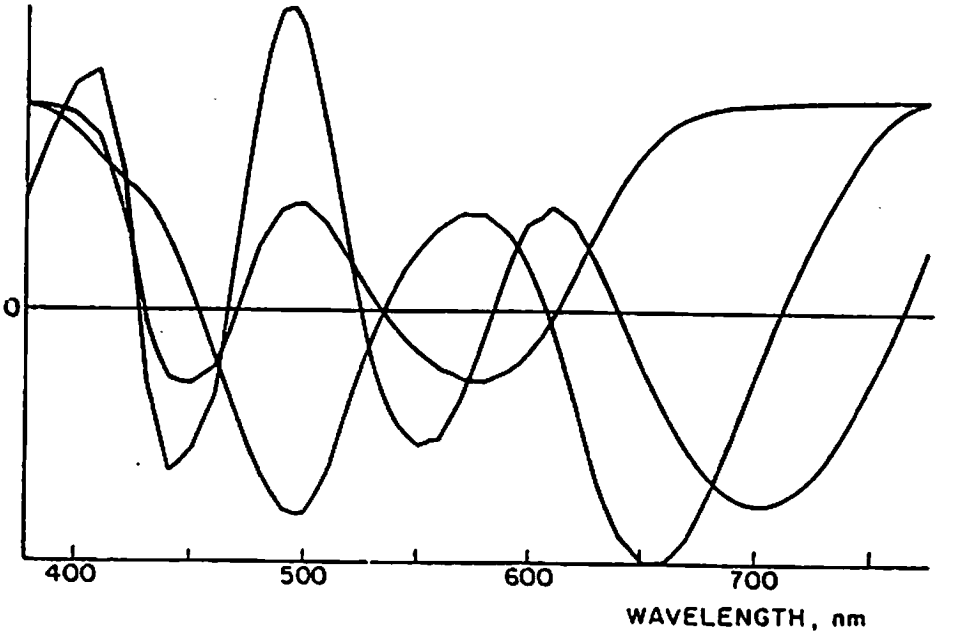

Figure (2-6b) Second three orthonormal functions

The given filter or sensor function $f(\lambda)$ is expanded in this orthonormal set, so that

$$f = \sum_{i=1}^{\infty} f_i U_i \tag{2-18}$$

where

$$f_i = \langle f U_i \rangle \triangleq \int f(\lambda) U_i(\lambda) d\lambda \tag{2-19}$$

the quality factor q is then defined to be the ratio of the energy of f in the first three coefficients of (2-18) to the total energy of f as given by

$$Q \triangleq \frac{\sum_{i=1}^{3} f_i^2}{\sum_{i=1}^{\infty} f_i^2} = \frac{f_1^2 + f_2^2 + f_3^2}{\langle f^2 \rangle} \tag{2-20}$$

A useful property of the representation of eq. (2-18) is that the least-squares nearest color matching curve to $f(\lambda)$ may be obtained by summing the first three components of the expansion

$$f_{CMC} = \sum_{i=1}^{3} f_i U_i \tag{2-21}$$

The value of the quality factor q required for a color sensor depends on the application of the sensor. The

sensors in colorimeters usually have q factor values of 0.99 or higher, achieved by careful adjustment of filter characteristics. In color television cameras, the q factors of the three color sensors are also high, perhaps 0.90 or better. The sensor curves are usually chosen to be close to the color matching curves corresponding to the standard NTSC display primaries, where the negative lobes of the ideal curves are neglected [9]. In color photography, the film layer sensitivities may have q factor values as small as 0.6, or even less, because colorimetric accuracy may have been sacrificed in favor of other properties, as mentioned earlier.

The second major source of errors in color reproduction is the problem of cross-talk or undesired absorptions. In color television, this might be caused by imperfect signal decoding, so that the signal driving the red display primary might be contaminated by the blue and green display signals. Misalignment in a shadow mask picture tube, allowing the electron beam of one primary gun to illuminate phosphors of the other two primaries, is another example of crosstalk in color television. In color photography and color lithography the equivalent problem is called undesired absorption. A color film transparency has a cyan (red-absorbing) layer which should control the red transmission of the transparency, with the other two layers (magenta and yellow) absorbing no red light at all. In

reality, red light is absorbed to some extent by the magenta and yellow layers. Figure (2-7) shows the spectrophotometric absorption curves of a typical set of photographic dyes. The cyan and magenta layers absorb strongly in the blue (400-460 nm) region, where ideally their optical densities should be zero. The cyan dye also exhibits unwanted absorption in the green portion of the spectrum. In each case, one of the color signals, red, green, or blue, is contaminated by one or both of the other two color signals. An ideal set of color reproduction dyes would be similar to those illustrated in figure (2-8). The rectangular spectral passband maximizes energy transmittance for a given dye saturation purity, while the non-overlapping stopbands remove the undesired absorption. Each dye affects one and only one spectral region and the resulting ideal subtractive color system is equivalent to an additive color system. Since unity spectral transmittance or reflectance is not achieved by real dyes at any wavelength, undesired absorption is always present in any real subtractive color reproduction system.

The result of crosstalk or undesired absorption is color error, usually a loss of saturation as a strong signal in one color channel excites the other two channels to some extent, tending to neutralize the saturation of the color at the display.

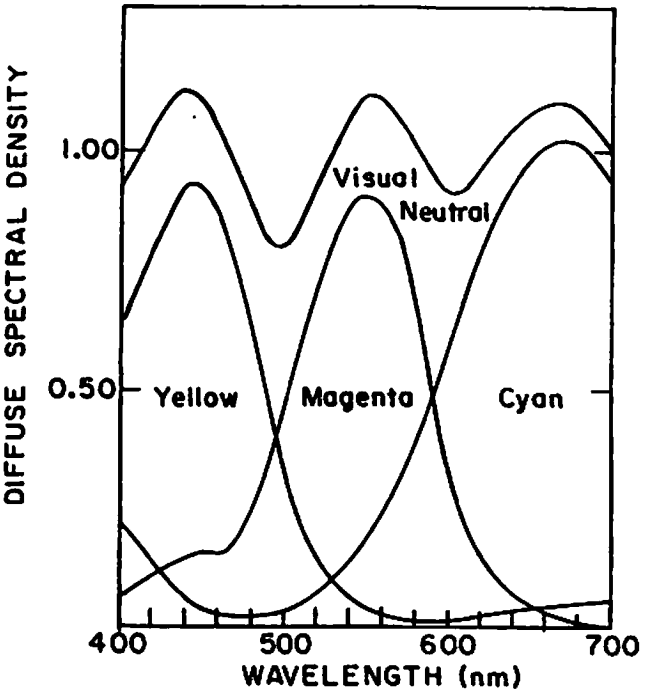

Figure (2-7) Photographic dye spectral absorption

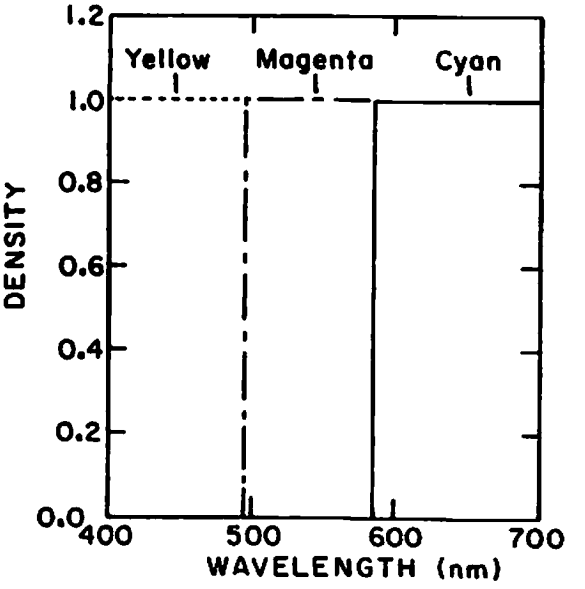

Figure (2-8) Ideal dye spectral absorption

In addition to sensor imperfections and crosstalk, there are several other sources of color errors which are of lesser importance, but which cannot be neglected in a general discussion of color errors. One such source of errors is the limiting of color signals by one or more components in the color system. Examples include dynamic range limitations in a color television camera tube or display and the limited range of film densities in a color photographic system. The effects of limiting may be seen by examining the density versus log exposure curve (sometimes called the Hurter and Driffield curve or H and D curve) of a typical reversal color film, shown in figure (2-9). When the exposure values of the three layers all lie to left of the upper bend in the H and D curve, the densities limit at "black" and all color information is lost (Case A). When all three exposure values lie to the right of the right bend in the D log E curve, the densities limit at "white" (Case B). When at least one exposure value limits while one or two exposure values lie on the linear portion of the D log E curve, the output color will not be neutral and its hue and saturation will in general exhibit large errors (Case C). Only when all three exposure values at an image point lie on the linear portion of their respective curves is it possible to maintain accurate brightness, hue and saturation values relative to other properly exposed points in the image (Case D).

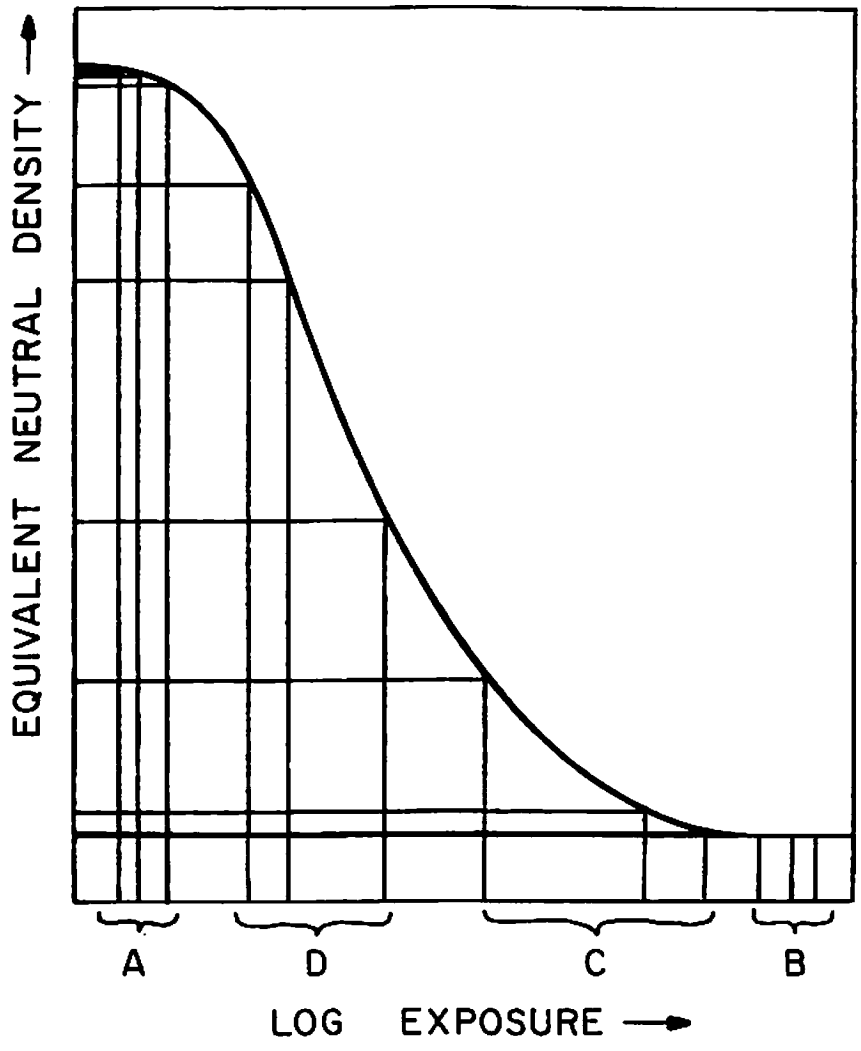

Figure (2-9) Limiting in photographic film

Another source of color error is gamut limitations in the display. It was previously stated that the position on a chromaticity diagram of a weighted sum of two primary lights lies on the line connecting the position of the primaries. It follows that the reproducible gamut of a three primary display must lie within the triangle on the chromaticity diagram defined by the positions of the three primaries. In additive displays such as television monitors, the color gamut is great enough to include all but a few relatively infrequent highly saturated colors. Subtractive photographic systems are further restricted in gamut by the undesired dye absorptions with a resulting inability to reproduce saturated colors at high lightness levels [10].

2.3 Restoration of Color Errors

Restoration of color errors caused by system imperfections of the types discussed in the previous section is conventionally done in one of two ways, depending on whether the color reproduction system is additive or subtractive. Color television is the only widely used additive color imaging system. In color television, undesired spectral absorption cannot take place, and its additive equivalent, crosstalk among the three color signals, is negligible when the signal decoding

and shadow mask alignment in the receiver are correct. Imperfect spectral sensitivities of the camera tube are always present, however, and some kind of signal matrixing [11,12,13] is usually, but not always, provided to correct the errors. The sensor errors arise because the color matching curves corresponding to the picture tube phosphor primaries always have negative values over some portion of the wavelength spectrum, while real sensor characteristics have only nonnegative values. In theory, ideal sensors could be made by providing a real sensor of the correct spectral shape for each negative lobe in the color matching curves, and subtracting its output from that of the appropriate positive lobe sensor of each curve. This would require eight or nine sensors and is never done in practice. Instead, three sensors are used whose spectral characteristic curves approximate the main positive lobes of the color matching curves of the receiver primaries [11]. In many cases, no further restoration is done, and color errors are present owing to the absence of the negative sensor lobes. These errors usually appear as a loss of color saturation at the receiver. In some television cameras, a linear matrix operation is applied to the three color signals in order to better approximate receiver tristimulus values. The matrix typically has negative off-diagonal elements, which approximate the action of the missing negative lobes by subtracting a

fraction of each of the other signal values from each signal. The exact values of the matrix elements are typically chosen by minimizing the average color error, as measured by one of the "uniform" color difference formulas, over some ten or twenty test color samples [12]. Signal matrixing can reduce television color errors due to imperfect sensor characteristics to a very small average level [11,12].

In the case of subtractive color imaging, i.e. photography, the most common restoration method is photographic masking. Masking can be described as the modification of one image by the information contained in another [14,15]. Photographic masking is intended primarily to correct for undesired absorption of dyes. A negative image, or mask, is generated for each case of significant cross-talk among the three-color images. When these masks, up to six in number, are placed in exact registration with the three superimposed original cyan, magenta, and yellow images, the cross-talk components of the original dye images are largely cancelled by the masks [14]. Masking is therefore a similar operation to matrixing in color television, even though the sources of the errors are different in the two cases. In the television case, a matrix with negative off-diagonal elements operates on the three exposure signals in order to correct for imperfect sensor characteristics. Photographic

masking applies a matrix with negative off-diagonal elements to the vector of film layer densities (which vary as the log of the exposures) in order to correct for undesired dye absorptions.

Because of the effort required in preparing and registering the masks, masking is mainly used in cases where many reproductions are required from a single original. Masking is widely used in photo-mechanical color reproduction (for example, photo-lithography). In photo-mechanical reproduction, masking is incorporated into the process of preparing separation negatives for each of the printing dyes[16]. Since the separations are often produced by a color scanner, the masking operation is readily achieved by manipulation of the scanner electrical signals [15,16].

References

1. Wyszecki, G., Color Science, John Wiley, New York (1967).

2. Wyszecki, G., Chapter 2 of Color: Theory and Imaging Systems , Soc.Photog.Sci.Eng. publication (1973).

3. McAdam, D.L., "Projective Transformations of ICI Color Specifications," J.Opt.Soc.America 27, pp. 294-299 (1937).

4. Wyszecki, G., and H. Wright, "Field Trial of the 1964 CIE Color-Difference Formula," J.Opt.Soc.America 55, p. 1166-1174 (1965).

5. Glasser, L., et al., "Cube-Root Color Coordinate System," J.Opt.Soc.America 48, pp. 736-740 (1958).

6. Cornsweet, T., Visual Perception, Academic Press (1970).

7. Proceedings IEEE, Color Television Issues, 39, 10 (1951) and 42, 1 (1954).

8. Neugebauer, H.E.J., "Quality Factor for Filters Whose Spectral Transmittances are Different from Color Mixture Curves, and Its Application to Color Photography," J.Opt.Soc.America 46, 10 pp. 821-824 (1956).

9. DeMarsh, L.E., Chapter 7 of Color: Theory and Imaging Systems , Soc.Photog.Sci.Eng. publication (1973).

10. Clapper, F.R., R. Gendron and S. Brownstein, "Color Gamuts of Additive and Subtractive Color Reproduction Systems," J.Opt.Soc.America 63, pp 625-629 (1973).

11. DeMarsh,op. cit.

12. Jones, A.H., "Optimum Color Analysis Characteristics and Matrices for Color Television Cameras With Three Receptors," Jour.SMPTE 77,p 108 (1968)

13. DeMarsh,L., and J.Pinney, "Studies of Some Colorimetric Problems in Color Television," Jour.SMPTE 79,p 338 (1970)

14. Pearson, M., Chapter 6 of Color: Theory and Imaging Systems , Soc.Photog.Sci.Eng. publication (1973).

15. Hunt, R.W.G., The Reproduction of Colour , John Wiley, New York (1967)

16. Yule, J.A.C, Principles of Color Reproduction, John Wiley, New York (1967)

3. Digital Color Restoration

Color errors which are generated by an imperfect color reproduction system can be corrected digitally. A sampled color image is described by a 3-dimensional array of numbers, usually nxnx3, where there are n samples in each of two spatial dimensions, with 3 color values stored at each spatial image point. When a color image exists in such a sampled form, or can be put into sampled form, the great speed and flexibility of a digital computer can be put to use in correcting the color errors introduced by imperfections in the sensors and storage devices which recorded the original image. In contrast, correction of color errors by photographic means, for example by photographic masking, is a slow and complex process. The production of several masking transparencies and their exact registration is required for each image which is to be corrected. The correcting power of masking is limited to altering the density of each transparency layer by a weighted sum of the two other layer densities at that point, as was described in Chapter 2. In digital restoration, however, the correcting algorithms may be complex, nonlinear, spatially varying, and may have spatial memory. The speed of a digital computer when used along with a television display also allows a degree of interactive processing which is not possible with photographic restoration. The penalties incurred in

digital image restoration include the requirement for the necessary equipment and loss of accuracy associated with sampled data processing.

3.1 Vector Space Formulation of Color Analysis

In order to perform color restoration in a digital computer, the necessary functions and equations must be converted to discrete, sampled-data form. In this form, the common linear operations of color measurement and color reproduction become matrix-vector operations instead of integral operations. For example, an integral operation on a spectral waveform $C(\lambda)$ of the form

$$x_i = \int_{\lambda_L}^{\lambda_U} S_i(\lambda)\, C(\lambda)\, d\lambda, \qquad (3\text{-}1)$$

for i=1,2,3 can be discretized by replacing the continuous variable λ with a finite set of points $\lambda_1, \lambda_2, \ldots \lambda_n$ and forming the approximate discrete equation

$$x_i = \sum_{j=1}^{n} w_j\, S_i(\lambda_j)\, C(\lambda_j) \qquad (3\text{-}2)$$

where $w_1, w_2, \ldots w_n$ are the weighting coefficients of the quadrature integration formula used [1]. By defining a vector $\underline{c}$ whose i th component is $C(\lambda_i)$, and a matrix whose ij th component is $w_j S_i(\lambda_j)$, eq. (3-2) can be compactly stated in matrix form by

$$\underline{x} = \underline{S}\,\underline{c} \tag{3-3}$$

where

$$\underline{x} = \begin{bmatrix} x_1 \\ x_2 \\ x_3 \end{bmatrix} \qquad \underline{c} = \begin{bmatrix} c(\lambda_1) \\ c(\lambda_2) \\ \vdots \\ c(\lambda_n) \end{bmatrix} \tag{3-4}$$

and

$$\underline{S} = \begin{bmatrix} w_1\, S_1(\lambda_1) & w_2\, S_1(\lambda_2) \;\ldots\ldots\; w_n\, S_1(\lambda_n) \\ w_1\, S_2(\lambda_1) & \\ w_1\, S_3(\lambda_1) & \ldots\ldots\ldots\ldots\ldots\ldots\; w_n\, S_3(\lambda_n) \end{bmatrix} \tag{3-5}$$

Since many of the important equations of colorimetry and color reproduction are of the form of eq. (3-1), matrix operators and equations are very useful in the analysis of sampled data models of color imaging systems and in colorimetry [2]. The equations of colorimetry are strictly sampled data equations in any case, since color matching curves are obtained by experiments with human observers at a finite number of optical wavelengths [3]. The continuous color matching curves which are sometimes published are obtained by interpolation of the original sample values.

The utility of matrix notation can be demonstrated by examining color matching and metamerism [4]. Two spectrophotometric distributions of light are said to be color matched if they cannot be distinguished from each

other by a human observer. Two such colors are called a metameric pair. The tristimulus values are the same for each member of a metameric pair (or set) of colors [3].

In the vector space formulation, let

$$\underline{t} = \begin{bmatrix} t_1 \\ t_2 \\ t_3 \end{bmatrix} \tag{3-6}$$

and

$$\underline{T} = \begin{bmatrix} u_1(\lambda_1) & u_1(\lambda_2) & \cdots & u_1(\lambda_n) \\ u_2(\lambda_1) & u_2(\lambda_2) & \cdots & u_2(\lambda_n) \\ u_3(\lambda_1) & u_3(\lambda_2) & \cdots & u_3(\lambda_n) \end{bmatrix} \tag{3-7}$$

where $\underline{t}$ is called the tristimulus vector, $U_1(\lambda)$, $U_2(\lambda)$, and $U_3(\lambda)$ are color mixture functions for a standard set of observing conditions, and the set $(\lambda_1, \lambda_2, \ldots, \lambda_n)$ are a uniformly spaced set of wavelengths covering (as a minimum) the domain over which the color mixture functions are significantly different from zero. The value of n usually lies in the range of 15 to 80. Also let

$$\underline{E} = \begin{bmatrix} E(\lambda_1) & 0 & \cdots & 0 \\ 0 & E(\lambda_2) & \cdots & 0 \\ \vdots & & & \vdots \\ 0 & 0 & \cdots & E(\lambda_n) \end{bmatrix} \tag{3-8}$$

where $E(\lambda)$ is the spectral energy distribution of the light source and

$$\underline{r} = \begin{bmatrix} R(\lambda_1) \\ R(\lambda_2) \\ \vdots \\ R(\lambda_n) \end{bmatrix} \tag{3-9}$$

with $R(\lambda)$ representing the spectral reflectance of a reflective sample. If the color is from a reflective sample, then

$$\underline{c} = \underline{E}\underline{r} \tag{3-10}$$

The tristimulus values $\underline{t}$ for a reflective sample are given by

$$\underline{t} = \underline{T}\underline{E}\underline{r} \tag{3-11}$$

If $\underline{r}_s$ and $\underline{r}_m$ represent the spectral reflectances of a sample and a matching sample respectively, then

$$\underline{t} = \underline{T}\underline{E}\underline{r}_s = \underline{T}\underline{E}\underline{r}_m \tag{3-12}$$

or

$$\underline{T}\underline{E}[\underline{r}_s - \underline{r}_m] = \underline{0} \tag{3-13}$$

Two reflectivities are thus said to be metameric with respect to an illuminant $\underline{E}$ and a standard observer $\underline{T}$ when their difference vector lies in the null space of the matrix $\underline{T}\underline{E}$.

3.2 Modelling Color Imaging Systems

In order to achieve accurate color restoration digitally, an accurate vector model of the color imaging system is necessary. A general model of an imaging system which senses and stores color values is shown schematically in figure (3-1). At each image point, a spectral power distribution, represented in sample form by the vector $\underline{c}$ of dimension n, serves as the input to a set of sensitivity functions represented by the matrix $\underline{S}$, with outputs consisting of the three components of the vector $\underline{x}$. The elements $\underline{S}$, $\underline{C}$, and $\underline{x}$ are defined and related by eqs. (3-3), (3-4), and (3-5). As an example, the rows of $\underline{S}$ might be samples of the three layer sensitivities of a color photographic film. In general, the linear operation modeled by the matrix $\underline{S}$ is followed by a nonlinear function of $\underline{x}$ which results in another 3-vector $\underline{w}$. The nonlinear operation $\underline{F}$ might represent limiting of signals in a color television system, or the nonlinear relationship between layer exposure and layer density in color photographic film. The three components of $\underline{w}$ are stored and are at some later time used as input signals to a process $\underline{G}$, generally nonlinear, which displays the signals as an output spectral distribution $\underline{c}$, again represented by n samples.

The functional relationship between the input spectral

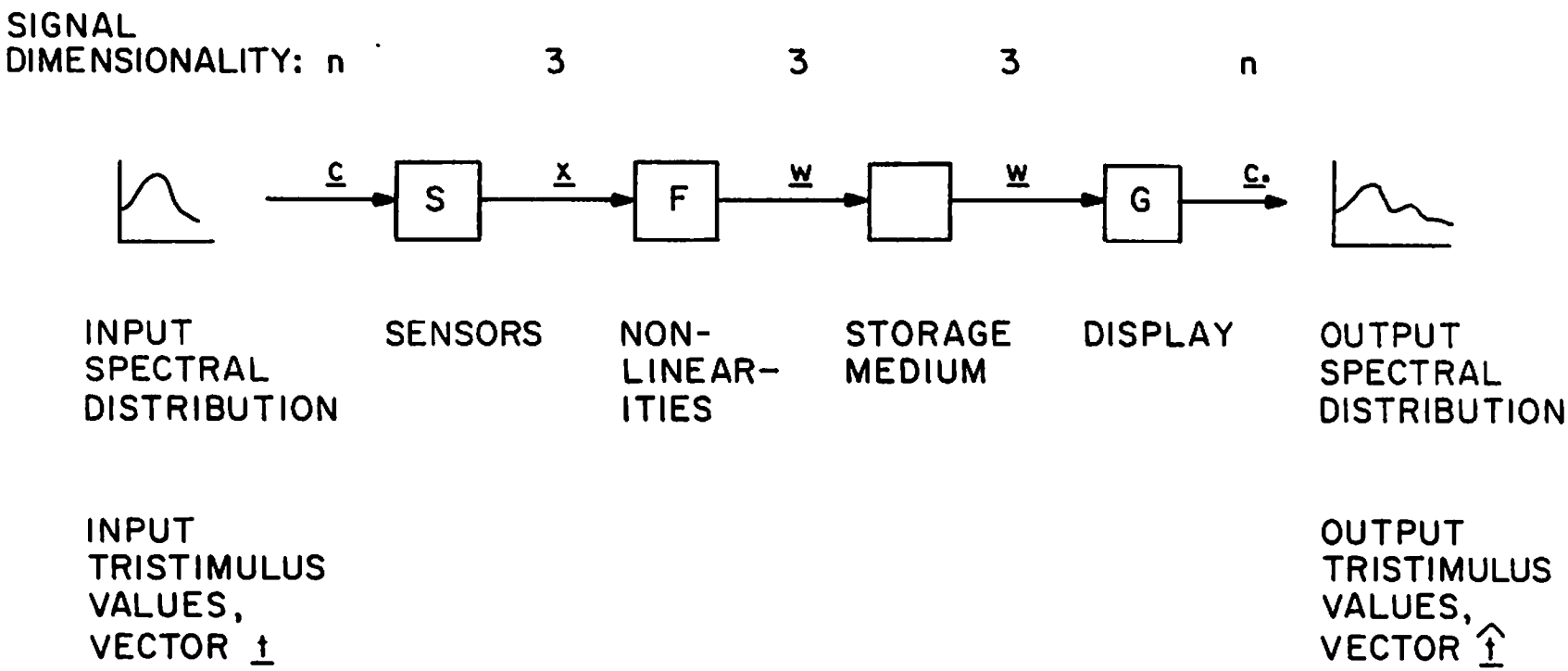

Figure (3-1) General color imaging system

distribution $\underline{c}$ and the displayed distribution $\underline{c}_o$ for this model can be written as

$$\underline{c}_o = \underline{GFSc} \qquad (3\text{-}15)$$

where $\underline{G}$ and $\underline{F}$ are general vector operations of appropriate dimensionality and are nonlinear, in general. It is clearly impossible for the modeled system to generate a $\underline{c}_o$ vector equal to the input vector $\underline{c}$. The $\underline{S}$ operation has reduced the dimensionality of $\underline{c}$ from n (usually 30, 40, or 80) to 3, with an irreversible loss of information. It is possible, in theory, to generate a $\underline{c}_o$ which is metameric to $\underline{c}$, since each color is colorimetrically specified by three tristimulus values. For a colorimetrically perfect color reproduction system, the input and output tristimulus vectors, $\underline{t}$ and $\underline{t}_o$ are equal at each image point, or

$$\underline{t}_o = \underline{Tc}_o = \underline{TGFSc} = \underline{Tc} = \underline{t} \qquad (3\text{-}16)$$

This relation holds if the following two statements are true:

1) The rows of $\underline{S}$ are color matching curves. If this is true, then $\underline{x}=\underline{Sc}$ is a tristimulus vector of $\underline{c}$ and may be easily converted to the tristimulus vector corresponding to any other set of color matching curves (for example the rows of $\underline{T}$).

2) The operator $\underline{G}\,\underline{F}$ is an inverse tristimulus

operator; that is, it takes a tristimulus vector $\underline{x}$ and generates a waveform $\underline{c}$ which is a solution of the linear equation $\underline{x}=\underline{S}\underline{c}$. This implies that $\underline{G}\ \underline{F}$ is a linear operator even though $\underline{F}$ is generally nonlinear.

When these two conditions are met, the color at each pixel in the reproduced image will match colorimetrically the corresponding point in the input image. As stated in Chapter 2, real color reproduction systems do not meet these conditions exactly. Sensor spectral characteristics are usually only approximations to a set of color matching curves, and the subsequent recording display sequence operation $\underline{G}\ \underline{F}$ is always nonlinear owing to the limiting of signals and other nonlinearities in the storage medium or the display [5, 6].

In order to perform digital restoration on a digitized color image, the foregoing model must be extended to include the color scanner which digitized the displayed image. In subsequent sections, the special case of reversal color film as an image storage medium will be examined. To perform digital processing on a photographically recorded transparency, the transparency must be scanned by a color analyzing system which outputs three color signal values at each point of a chosen spatial grid array. The completely general color analyzing system model including a scanner is shown in figure (3-2), with

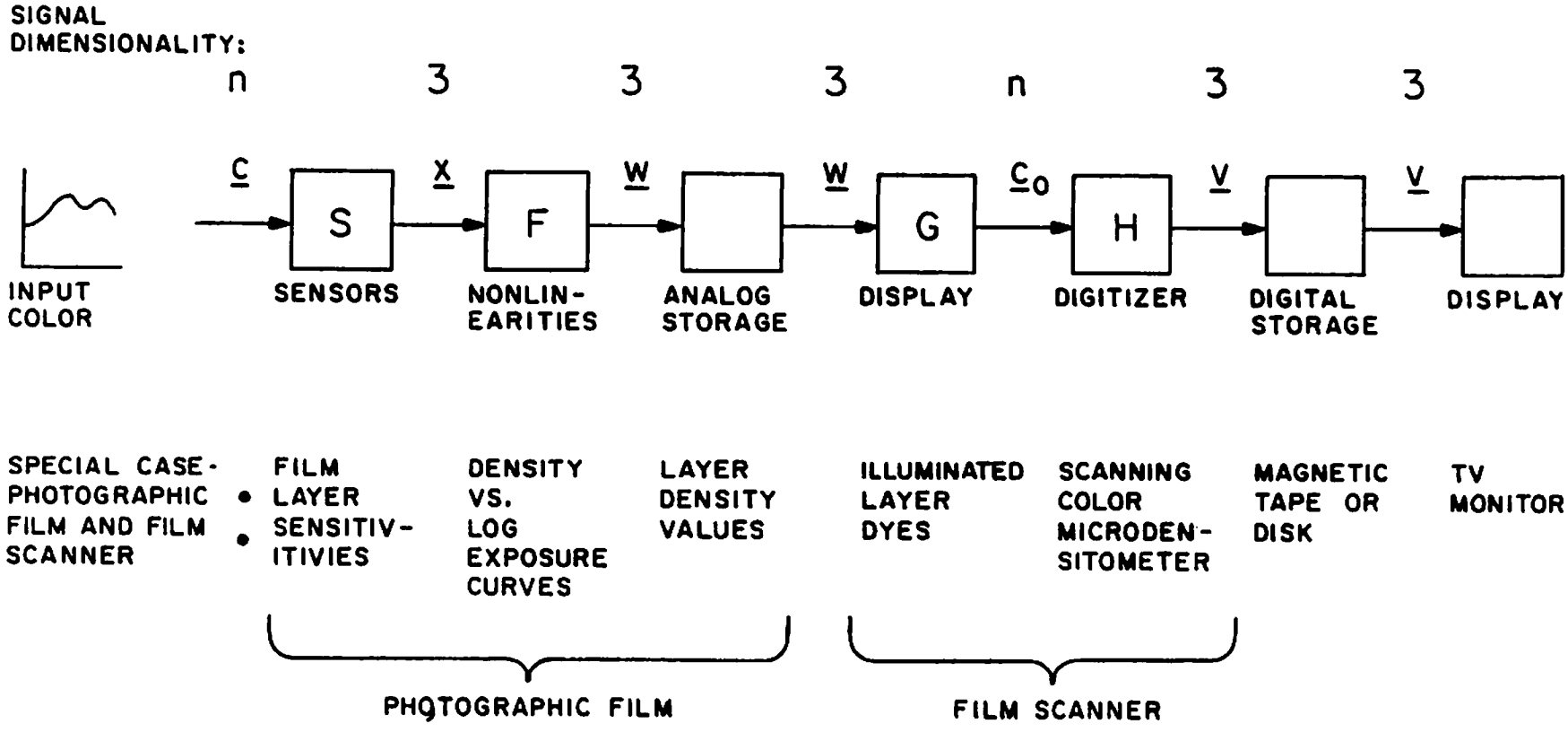

Figure (3-2) Color image recording and digitizing system

the film-scanner special case specified beneath the general system component blocks. It should be noted that while all of the component blocks shown are present in a digitized film color system, they may not all be present in other digital image color systems. A digital television system, for example, might not display and/or store the images before digitization.

For the digital color analyzing system of figure (3-2), the relation between the input color vector $\underline{c}$ and the stored observable $\underline{v}$ is given by

$$\underline{v} = \underline{HGFSc} \tag{3-17}$$

where $\underline{H}$, the characteristic function of the scanner, is a nonlinear function of $\underline{c}$, but may be linear to a good approximation over a wide range of signal levels [7]. If the signal $\underline{v}$ were used to drive a display television monitor, a colorimetric match between the displayed color and the input color $\underline{c}$ will be obtained if $\underline{v}$ is the tristimulus vector of $\underline{c}$ in the system defined by the television display primaries. If $\underline{T}$ is the matrix of color matching curves in that system, then

$$\underline{v} = \underline{Tc} \tag{3-18}$$

or

$$\underline{HGFS} = \underline{T} \qquad (3\text{-}19)$$

for a colorimetrically ideal digital color system.

3.3 The Color Estimation Problem

The problem to be solved can be stated as follows: How can the tristimulus values of an input color to the system of figure (3-2) be most accurately determined when the two conditions of the ideal colorimetric reproduction system do not hold? By observing the digitized signal $\underline{v}(x,y)$ over some discrete array of image points in the x and y spatial dimensions, it is desired to estimate $\underline{t}(x,y)$, the tristimulus vector at each image point, where $\underline{t}$ is derivable from the input spectral distribution $\underline{c}$ by the relation $\underline{t}=\underline{T}\underline{c}$.

The estimation problem may be broken into two parts, each corresponding to one of the conditions of ideal reproduction which are violated by real color reproduction systems. Correspondingly, eq. (3-17), which describes the whole system sequence, may be broken into two serial operations

$$\underline{x} = \underline{S}\underline{c} \qquad (3\text{-}20)$$

and

$$\underline{v} = \underline{HGFx} \tag{3-21}$$

The estimation process proceeds in two steps. First, an estimate of $\underline{x}$ is determined from the observable $\underline{v}$ by inverting eq. (3-21). Second the estimated $\underline{x}$ is used to estimate $\underline{c}$ by inverting eq. (3-20). It will be shown later that the desired tristimulus estimate $\hat{\underline{t}}$ is best estimated by taking the estimated $\hat{\underline{c}}$ and letting $\hat{\underline{t}}=\underline{T}\hat{\underline{c}}$. The two requirements of ideal colorimetric reproduction may be related to the above equations as follows:

1) The matrix $\underline{S}$ in eq. (3-20) must have rows consisting of color matching curves.

2) The operation $\underline{HGF}$ in eq. (3-21) must be linear and invertible.

In an idealized case where condition (2) is true, $\underline{x}$ is obtained from eq. (3-16) by simple matrix inversion

$$\underline{x} = (\underline{HGF})^{-1}\,\underline{v} \tag{3-22}$$

If condition (1) is also true, then $\underline{x}$ is a tristimulus vector of $\underline{c}$ and there exists a 3x3 matrix $\underline{A}$ such that

$$\underline{T} = \underline{AS} \tag{3-23}$$

and, therefore

$$\underline{t} = \underline{Tc} = \underline{ASc} = \underline{Ax} \qquad (3\text{-}24)$$

For a real, non-ideal system, no matrix $\underline{A}$ satisfying eq. (3-23) exists and $\underline{HGF}$ is usually invertible only over some range of signal values.

In summary, it is desired to invert the set of equations

$$\underline{x} = \underline{Sc} \qquad (3\text{-}25)$$

$$\underline{v} = \underline{HGFx} \qquad (3\text{-}26)$$

in order to obtain an estimate of the tristimulus vector $\underline{t}$ which is optimal in some as yet undefined sense. Equation (3-26) is non-linear, deterministic (if observation noise can be neglected) and is exactly determined ($\underline{x}$ and $\underline{v}$ each are three dimensional). Equation (3-25) is linear, stochastic (because of observation noise on $\underline{x}$ and possibly because of statistical assumptions which may be made about $\underline{c}$) and is underdetermined ($\underline{c}$ is of higher dimension than $\underline{x}$). The two step estimation method is diagrammed in figure (3-3).

Chapter 4 will examine methods of solution of eq. (3-25). Chapter 5 will examine solution methods for eq. (3-26), with emphasis on the film-scanner color analysis

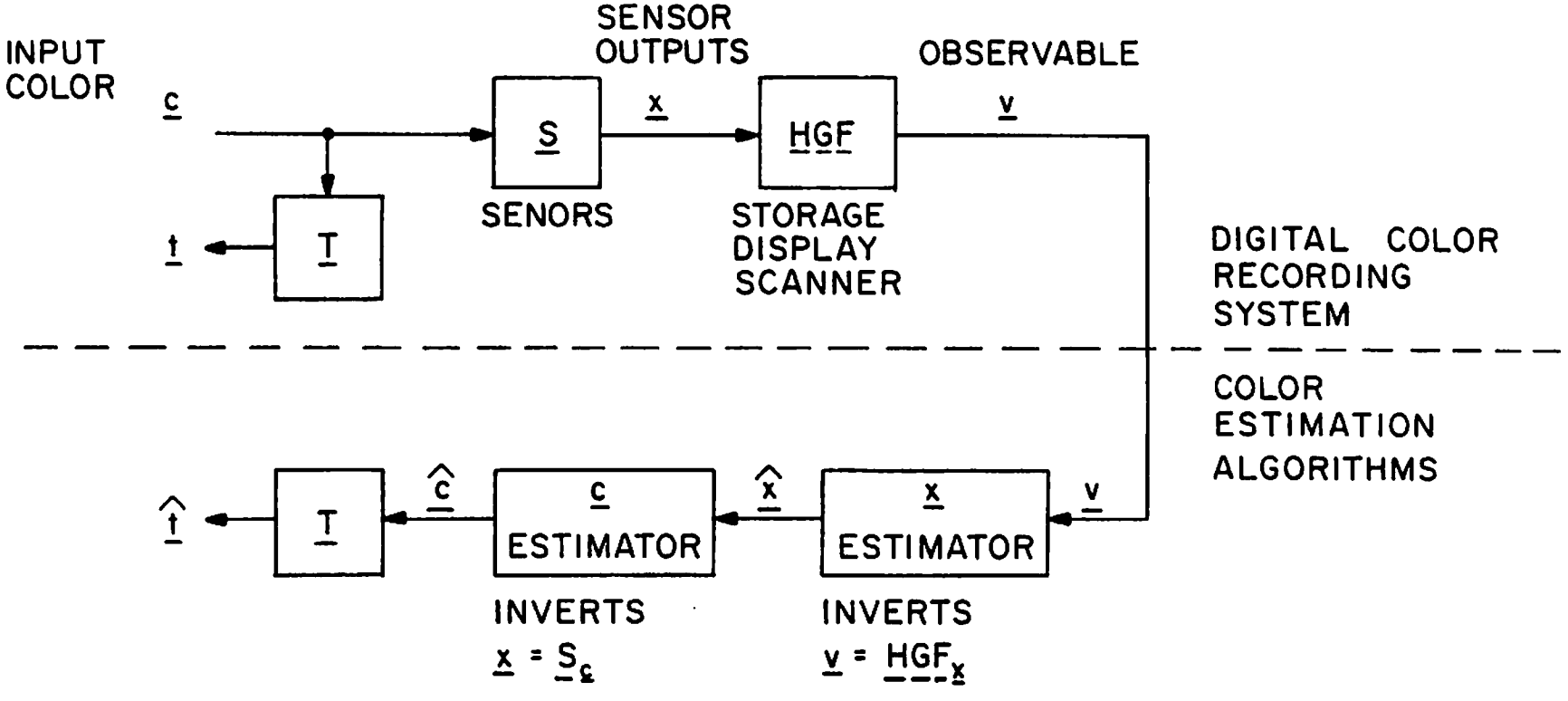

Figure (3-3) Digital color recording system and tristimulus estimation sequence

system.

References

1. Lewis, T.O., and P.L. Odell, Estimation in Linear Models, Prentice-Hall, Englewood Cliffs, New Jersey, (1971).

2. Miller, C.W., "The Matrix Algebra and Color Reproduction," J. Opt. Soc. Am., 31, pp.477-482 (1941)

3. Wyszecki, G., and W.S. Stiles, Color Science, John Wiley, New York (1967).

4. Allen, E., "Basic Equations Used in Computer Color Matching," J. Opt. Soc. Am., 56, 9, p. 1256, (1966).

5. Evans, R.M., W.T. Hanson, Jr., and W.L. Brewer, Principles of Color Photography, John Wiley, New York (1953).

6. Yule, J.A.C., Principles of Color Reproduction, John Wiley, New York (1967).

7. Hunt, R.W.G., The Reproduction of Colour, 2nd edition, John Wiley, London (1967).

4. Tristimulus Estimation

The final step in the color restoration process is the estimation of the tristimulus values at each image point in the original scene. This estimate must use as its input quantities signals which are outputs of imperfect spectral sensors, and which are usually themselves indirectly obtained from other observable quantities. This chapter is concerned with the estimation of tristimulus values from spectral sensor outputs which are assumed to be directly observable.

In vector notation, the equations to be solved are

$$\underline{x} = \underline{\underline{S}}\underline{c}+\underline{e} \qquad (4\text{-}1)$$

and

$$\underline{t}=\underline{\underline{T}}\underline{c} \qquad (4\text{-}2)$$

where

$\underline{\underline{S}}$: 3xn array of sensor spectral sensitivities

$\underline{\underline{T}}$: 3xn array of color matching curves

$\underline{c}$: n$\underline{x}$1 spectral distribution vector of input color

$\underline{x}$: 3x1 vector of sensor outputs

$\underline{e}$: 3x1 vector of observation errors

$\underline{t}$: 3x1 vector of tristimulus values of $\underline{c}$

The problem is to estimate $\underline{t}$ when $\underline{\underline{S}}$ and $\underline{\underline{T}}$ are known, $\underline{c}$ and

$\underline{e}$ are unknown, and $\underline{x}$ is observed.

4.1 Linear Estimation Methods

Since eq. (4-1) is a linear equation and since the techniques of linear estimation are well developed [1,2,3], it is natural to attempt to estimate $\underline{t}$ from $\underline{x}$ using linear estimation methods. In order to optimize any estimator, however, it is necessary to choose a fidelity criterion, an expression which quantifies the color difference between any two sets of tristimulus values, $\underline{t}_1$ and $\underline{t}_2$. Such a fidelity criterion should ideally satisfy two conflicting conditions:

1) The fidelity criterion should be perceptually uniform, i.e., the error value given by the fidelity criterion should be proportional to the perceived color error over the entire tristimulus space.

2) Maximization of the fidelity criterion should lead to estimator equations which are solvable in closed form and with a high degree of generality.

There are several existing color distance formulas which are perceptually uniform to a good approximation [7,8]. These color distance formulas (see Section 2.1) are complicated functions of the tristimulus values of the colors, and, when used as color fidelity criteria, do not satisfy the solvability condition stated above. In order

to obtain solvable equations, it is necessary to use a quadratic error criterion, a type of error criterion whose use is almost universal in linear estimation theory. Hence, let the error criteria in the tristimulus and spectral distribution spaces be the quadratic forms

$$e_t = [(\underline{t}_1 - \underline{t}_2)^T \underline{M}(\underline{t}_1 - \underline{t}_2)]^{1/2} \qquad (4\text{-}3)$$

and

$$e_c = [(\underline{c}_1 - \underline{c}_2)^T \underline{N}(\underline{c}_1 - \underline{c}_2)]^{1/2} \qquad (4\text{-}4)$$

where $\underline{M}$ and $\underline{N}$ are 3x3 and nxn positive definite matrices, respectively. Then the many techniques of linear estimation which have been developed over the years may be directly applied to the tristimulus estimation problem. These error criteria, or color distance formulas, are not perceptually uniform, but they do satisfy two important conditions which a useful color distance formula should obey:

1) Reducing the color distance between two colors as determined by either of these two formulas will, in general, provide an improved color match between the two colors.

2) When the color distance e_t or e_c is equal to zero, the two colors are perceptually equivalent under a colorimetric model. The converse is true for e_t but not for e_c.

In the remainder of this chapter, several widely used linear estimation methods will be applied to the tristimulus estimation problem. The problem will first be approached under a linear regression model. Under this model, the spectral distribution $\underline{c}$ is assumed to be nonrandom but unknown. No statistical information on $\underline{c}$ is assumed available, but a priori knowledge in the form of a smoothness constraint is utilized to improve the estimate. Least squares estimation and minimum norm methods are among the techniques employed to solve eqs. (4-1) and (4-2) under the regression model. The tristimulus estimation problem will also be approached using a stochastic color model. Under this model, $\underline{c}$ is assumed to be a random vector whose first two moments either are known or can be approximated. The problem can then be solved using well known Wiener estimation methods.

4.2 Estimation Under a Linear Regression Model

In Chapter 3 it was shown that if sensor spectral sensitivities can be expressed as linear weighted sums of color matching curves, then tristimulus values can be directly obtained from the sensor outputs when there is no observation noise. For cases in which this condition does not hold, a matrix B can be found which approximates the color matching matrix T by $\underline{B}\underline{S}$ in the least squares sense.

Then a tristimulus estimator can be obtained by letting

$$\hat{\underline{t}} = \underline{BSc} = \underline{Bx} \tag{4-7}$$

In order to find the least squares approximation or fit of T by $\underline{S}$ it is necessary to find the best least squares fit of each row of $\underline{T}$ by a weighted sum of the rows of $\underline{S}$. Let

$$\begin{bmatrix} \underline{u}_1^T \\ \underline{u}_2^T \\ \underline{u}_3^T \end{bmatrix} = \underline{T} \tag{4-8}$$

and

$$\begin{bmatrix} \underline{b}_1^T \\ \underline{b}_2^T \\ \underline{b}_3^T \end{bmatrix} = \underline{B} \tag{4-9}$$

Then it is desired to find the vectors $\underline{b}_i$ for i=1,2,3 which minimize $\|\underline{u} - \underline{S}^t \underline{b}_i\|$ where the n-dimensional Euclidean vector norm is defined by

$$||\underline{x}|| = (\underline{x}^T \underline{x})^{1/2} \tag{4-10}$$

Using the well known least squares estimation theorem [4], the desired vectors are

$$\underline{b}_i = (\underline{SS}^T)^{-1} \underline{S}\, \underline{u}_i \qquad i = 1, 2, 3 \tag{4-11}$$

Taking the transpose of each side and observing that $\underline{SS}$ is symmetric,

$$\underline{b}_i^T = \underline{u}_i^T \underline{S}^T (\underline{SS}^T)^{-1} \tag{4-12}$$

Using (4-12), (4-8), and (4-9),

$$\underline{B} = \underline{T}\, \underline{S}^T (\underline{SS}^T)^{-1} \tag{4-13}$$

Substituting this expression for $\underline{B}$ into eq. (4-7) gives the least squares tristimulus estimator

$$\hat{\underline{t}} = \underline{T}\, \underline{S}^T (\underline{SS}^T)^{-1}\, \underline{x} \tag{4-14}$$

The matrix product $\underline{S}^T(\underline{SS}^T)^{-1}$ is defined as the pseudo-inverse matrix $\underline{S}^+$ of the 3xn matrix $\underline{S}$, when $\underline{S}$ has linearly independent rows [2]. The least squares estimator, eq. (4-14) is therefore of the form

$$\hat{\underline{t}} = \underline{T}\, \hat{\underline{c}} = \underline{T}\, \underline{S}^+\, \underline{x} \tag{4-17}$$

where $\hat{\underline{c}}=\underline{S}^+\underline{x}$ is an estimator of the unknown color vector $\underline{c}$, obtained by solving the (underdetermined) equation $\underline{x}=\underline{Sc}$ for $\underline{c}$ using $\underline{S}^+$, the pseudo-inverse of $\underline{S}$. Any vector $\underline{c}$ of the form

$$\underline{c} = \underline{S}^+\, \underline{x} + (\underline{I} - \underline{S}^+\underline{S})\, \underline{v} \tag{4-18}$$

where $\underline{v}$ is any n vector, is also a solution of $\underline{x}=\underline{Sc}$. This may be seen by multiplying each side of (4-18) by $\underline{S}$,

$$\underline{Sc} = \underline{SS}^{+}\,\underline{x} + (\underline{S} - \underline{SS}^{+}\underline{S})\,\underline{v} = \underline{x} \qquad (4\text{-}19)$$

since $\underline{SS}^{+}=\underline{I}$. Of all the solutions given by eq. (4-18), the vector $c=\underline{S}^{+}\underline{x}$, obtained by setting $\underline{v}=\underline{0}$ in (4-18) is the solution of minimum Euclidean norm. This becomes evident by observing that the particular solution $S^{+}\underline{x}$ is orthogonal to the homogeneous solution $(\underline{I}-\underline{S}^{+}\underline{S})\underline{v}$. For any $\underline{v}$

$$[(\underline{I} - \underline{S}^{+}\underline{S})\,\underline{v}]^{T}\,\underline{S}^{+}\underline{x} = \underline{v}^{T}(\underline{I} - \underline{S}^{+}\underline{S})\,\underline{S}\,\underline{x} = \underline{0} \qquad (4\text{-}20)$$

Since the length (norm) of the sum of a fixed vector $S\,\underline{x}$ and a vector orthogonal to $\underline{S}^{+}\underline{x}$ is minimized when the orthogonal vector is of zero length, $c=\underline{S}^{+}\underline{x}$ is the minimum (Euclidean) norm solution of $\underline{x}=\underline{Sc}$.

The particular estimate of $\underline{c}$ given by $\underline{c}=\underline{S}^{+}\underline{x}$ is only one of the many solutions to the underdetermined equation $\underline{x}=\underline{Sc}$. Minimum norm estimation provides other solutions which may be better in the sense of minimizing a quadratic norm given by

$$||\underline{c}||_{N} = (\underline{c}^{T}\,\underline{Nc})^{1/2} \qquad (4\text{-}21)$$

The nxn matrix $\underline{N}$ must be positive definite and symmetric and is chosen so that $||\underline{c}||_{N}$ is a measure of a property of $\underline{c}$ which is to be minimized. Particular choices of $\underline{N}$, such as those leading to minimal energy or maximal smoothness of $\underline{c}$, will be discussed after deriving the general minimum norm estimator.

The task is to choose a $\underline{c}$ which minimizes $\underline{c}^T\underline{N}\underline{c}$ while satisfying $\underline{S}\underline{c}=\underline{x}$. This can be accomplished using Lagrange multipliers. Let

$$J(\underline{c}) \triangleq \underline{c}^T \underline{N}\underline{c} + \underline{\lambda}^T(\underline{S}\underline{c} - \underline{x}) \qquad (4\text{-}22)$$

where λ is a 3-vector of LaGrange multipliers. The scalar term $J(\underline{c})$ is minimized when its first derivative is zero

$$\frac{\partial J}{\partial \underline{c}} = 2\underline{N}\underline{c} + \underline{S}^T\underline{\lambda} = 0$$

which yields

$$\underline{c} = -\frac{1}{2}\underline{N}^{-1}\underline{S}^T\underline{\lambda} \qquad (4\text{-}23)$$

Solving eq.(4-23) and $\underline{x}=\underline{S}\underline{c}$ for λ as a function of $\underline{x}$ gives

$$\underline{x} = \underline{S}\underline{c} = -\frac{1}{2}\underline{S}\underline{N}^{-1}\underline{S}^T\underline{\lambda}$$

or

$$\lambda = -2(\underline{S}\underline{N}^{-1}\underline{S}^T)^{-1}\underline{x} \qquad (4\text{-}24)$$

Substituting (4-24) into (4-23) gives the solution

$$\hat{\underline{c}} = \underline{N}^{-1}\underline{S}^T(\underline{S}\underline{N}^{-1}\underline{S}^T)^{-1}\underline{x} \qquad (4\text{-}25)$$

Again forming the tristimulus estimate $\hat{\underline{t}}=\underline{T}\hat{\underline{c}}$,

$$\hat{\underline{t}} = \underline{T}\underline{N}^{-1}\underline{S}^T(\underline{S}\underline{N}^{-1}\underline{S}^T)^{-1}\underline{x} \qquad (4\text{-}26)$$

This is the minimum $\underline{N}$ norm estimate of $\underline{t}$. By letting $\underline{N}=\underline{I}$, the identity matrix, the least squares estimator of eq.

(4-14) is obtained. The relationship between the least squares and minimum norm solutions for general $\underline{N}$ is given in the following theorem [5], which is given without proof:

Theorem - Let $\underline{N}$ be positive definite and $\underline{S}$ be real. Let $\underline{A}^{+}_{MN}$ be the $\underline{M}$-least squares minimum $\underline{N}$-norm inverse of $\underline{A}$. Then,

$$((\underline{S}^{T})^{+}_{N^{-1}I})^{T} = \underline{S}^{+}_{IN} \qquad (4\text{-}27)$$

The theorem states that the minimum $\underline{N}$ norm estimator is equivalent to the $\underline{N}^{-1}$ least squares estimator. This means that if the least squares estimator eq.(4-14) used $(\underline{c}^{T}\underline{N}^{-1}\underline{c})$ as its n-space norm instead of $(\underline{c}^{T}\underline{c})$, it would be identical to the expression of eq.(4-26).

The choice of the nxn matrix $\underline{N}$ in the $\underline{N}$-normis determined by the particular solution which is to be chosen from the many solutions of $\underline{x}=\underline{S}\underline{c}$. If $\underline{N}=\underline{I}$, the identity matrix, the norm becomes

$$||\underline{c}||^{2} = \underline{c}^{T}\underline{c}$$

which is equivalent to the energy of $\underline{c}$. Another approach in restricting the estimate of $\underline{c}$ is to try to choose $\underline{N}$ so as to incorporate a priori knowledge of $\underline{c}$ into the estimate. One such piece of a priori knowledge is that the spectral intensity curve which $\underline{c}$ represents is "smooth" in some sense. A useful smoothness criterion is that of the average squared second difference of $\underline{c}$ [6]. If this

smoothness criterion is used, the solution to $\underline{x}=\underline{S}\underline{c}$ which minimizes the quantity $\underline{c}^T\underline{N}\underline{c}$ is sought, where

$$\underline{c}^T\underline{N}\underline{c} = \sum_{i=2}^{n-1}[(c_{i+1} - c_i) - (c_i - c_{i-1})]^2 = \sum_{i=2}^{n-1}(c_{i+1} - 2c_i + c_{i-1})^2$$

If a vector $\underline{y}=\underline{D}\underline{c}$ is defined by

$$y = \begin{bmatrix} y_1 \\ y_2 \\ \vdots \\ y_{n-2} \end{bmatrix} \triangleq \begin{bmatrix} 1 & -2 & 1 & 0 & 0 & \cdots & 0 \\ 0 & 1 & -2 & 1 & 0 & \cdots & 0 \\ 0 & 0 & 1 & -2 & 1 & \cdots & 0 \\ \vdots & & & & & & \vdots \\ 0 & . & . & 0 & 1 & -2 & 1 \end{bmatrix} \begin{bmatrix} c_1 \\ c_2 \\ \vdots \\ c_n \end{bmatrix} = \underline{D}\underline{c} \quad (4\text{-}28)$$

then $\underline{y}^T\underline{y}$ is the desired average squared second difference. Thus,

$$\underline{c}^T\underline{N}\underline{c} = \sum_{i=3}^{n-2} y_i^2 = \underline{y}^T\underline{y} = \underline{c}^T\underline{D}^T\underline{D}\underline{c}$$

and the nxn matrix $\underline{N}$ is then

$$\underline{N} = \underline{D}^T\underline{D} = \begin{bmatrix} 1 & -2 & 1 & 0 & 0 & \cdots & \\ -2 & 5 & -4 & 1 & 0 & & \\ 1 & -4 & 6 & -4 & 1 & 0 & \cdots \\ 0 & 1 & -4 & 6 & -4 & 1 & 0 \\ \vdots & & & & & & \vdots \end{bmatrix} \quad (4\text{-}29)$$

The matrix $\underline{N}$ thus derived cannot be directly substituted into eq.(4-26), the minimum norm estimator, since it is singular (each row and column sum to zero). This obstacle can be removed by replacing $\underline{N}$ by $\underline{N} + \epsilon\underline{I}$ where ϵ is a positive constant, small compared to unity.

The least squares and minimum norm solutions treated thus far are deterministic solutions to eqs. (4-1) and (4-2). The observation noise $\underline{e}$ in eq. (4-1) was assumed to be negligible. Tristimulus estimation under a regression model will now be extended to include additive observation noise whose first two moments are assumed known. The regression model is given by the set of equations

$$\underline{x} = \underline{\underline{S}}\underline{c} + \underline{e} \qquad (4\text{-}30a)$$

$$E(\underline{e}) = \underline{0} \qquad (4\text{-}30b)$$

$$E(\underline{e}\underline{e}^T) = \underline{\underline{R}}_{ee} \qquad (4\text{-}30c)$$

where E denotes the ensemble expectation operator, and $\underline{\underline{R}}_{ee}$ is therefore the 3x3 symmetric, positive definite covariance matrix of the observation error $\underline{e}$. Equations (4-30) are a special case of the general linear regression problem. What is found is a set of three 3-vectors $\underline{l}_i$ for i=1,2,3 such that $\underline{l}_i^T\underline{x}$ is an estimator of t_i, the i th element of $\underline{t}$. Thus,

$$\hat{t}_i = \underline{l}_i^T \underline{x} \simeq \underline{u}_i^T \underline{c} = t_i$$

where $\underline{u}_i$ is the i th row of the tristimulus matrix $\underline{\underline{T}}$. Clearly it would be desirable that

$$E(\underline{\hat{t}}) = \underline{t}$$

If $\hat{\underline{t}}$ satisfies this relationship for all true values of $\underline{t}$, the estimator is said to be unbiased. For an unbiased $\hat{\underline{t}}$

$$E(\underline{\ell}_i^T \underline{x}) = \underline{u}_i^T \underline{c}$$

Now,

$$E(\underline{\ell}_i^T \underline{x}) = \underline{\ell}_i^T E(\underline{x}) = \underline{\ell}_i^T \underline{S}\underline{c}$$

So, for an unbiased estimator

$$\underline{\ell}_i^T \underline{S}\underline{c} = \underline{u}_i^T \underline{c}$$

for all $\underline{c}$, or

$$\underline{S}^T \underline{\ell}_i = \underline{u}_i \qquad (4\text{-}31)$$

If this condition holds, then $t_i = \underline{u}_i^T \underline{c}$ is said to be unbiasedly estimable.

Unfortunately, the quantity t_i is not unbiasedly estimable in the case of tristimulus estimation. The condition of eq. (4-31) does not hold in general, since it requires that the color-matching curve $\underline{u}_i$ be expressible as a weighted sum of the three rows of $\underline{S}$ (which are the three sensor spectral sensitivities). Note that this condition is equivalent to the condition of eq. (3-23). Since the dimensionality n of the rows of $\underline{S}$ is far greater than three, eq.(4-31) cannot hold for general $\underline{S}$. An equivalent description is that unbiased estimation is not possible when the regression model is underdetermined.

Although an unbiased estimator is not obtainable, it is possible to seek a minimum bias estimator. A linear function $\underline{l}_i^T \underline{x}$ is said to be a minimum bias estimator of $\underline{u}_i^T \underline{c}$ if

$$||\underline{S}^T \underline{\ell}_i - \underline{u}_i|| = \inf_{\underline{\ell}} ||\underline{S}^T \underline{\ell} - \underline{u}_i||$$

Minimum bias estimators are not unique, in general. It is desired, then, to find an estimator which has least variance in the class of linear minimum bias estimators. This estimator is called the best linear minimum bias estimator (BLMBE). The variance of a scalar random variable a is defined to be

$$V(a) = E(a - E(a))^2$$

Let $\underline{l}_i^T \underline{x}$ be an estimator of $\underline{u}_i^T \underline{c}$. Then,

$$E(\underline{\ell}_i^T \underline{x} - \underline{u}_i^T \underline{c}) = (\underline{\ell}_i^T \underline{S} - \underline{u}_i^T) \underline{c} \qquad (4\text{-}32)$$

is the bias and the variance is

$$V(\underline{\ell}_i^T \underline{x}) = \underline{\ell}_i^T \underline{R}_{ee} \underline{\ell}_i \qquad (4\text{-}33)$$

The problem is to minimize $\underline{l}_i^T \underline{R}_{ee} \underline{l}_i$ in the class of $\underline{l}$ for which $\|\underline{S}^T \underline{l}_i - \underline{u}_i\|$ is a minimum. The norm in the three dimensional space is defined to be the Euclidean norm

$$||\underline{\ell}|| = (\underline{\ell}^T \underline{\ell})^{1/2}$$

Let the norm in R^n be defined by $\|\underline{x}\| = (\underline{x}^T \underline{M} \underline{x})^{1/2}$ where $\underline{M}$ is positive definite. The answer is given by the minimum

I-norm M-least squares solution of the inconsistent equation $\underline{S}^T\underline{l}=\underline{u}$

$$\underline{\ell}_i = (\underline{S}^T)^+_{MI}\, \underline{u}_i$$

The estimator of $\underline{u}_i^T\underline{c}$ is

$$\hat{t}_i = \underline{\ell}^T\underline{x} = \underline{u}_i^T[(\underline{S}^T)^+_{MI}]^T\, \underline{x} = \underline{u}_i^T\, \underline{S}^+_{IM-1}\, \underline{x} \qquad (4\text{-}34)$$

using the duality result of eq.(4-27). The variance of the estimator, assuming uncorrelated observation error, is

$$V(\underline{\ell}^T\underline{x}) = \underline{\ell}^T\, \underline{R}_{ee}\, \underline{\ell} = \alpha^2\, \underline{\ell}^T\underline{\ell} = \alpha^2\, \underline{u}_i^T(\underline{S}^T)^+_{MI}[(\underline{S}^T)^+_{MI}]\, \underline{u}_i \qquad (4\text{-}35)$$

where

$$\underline{R}_{ee} = \alpha^2\, \underline{I}$$

An explicit expression for the BLMBE for uncorrelated observation noise is given by

$$\hat{t}_i = \underline{u}_i^T\, \underline{MS}^T\, (\underline{SMS}^T)^{-1}\, \underline{x}$$

The best linear minimum bias tristimulus vector estimator is then

$$\underline{\hat{t}} = \underline{TMS}^T\, (\underline{SMS}^T)^{-1}\, \underline{x} \qquad (4\text{-}36)$$

where

$$\underline{\hat{t}} = \begin{bmatrix} \hat{t}_1 \\ \hat{t}_2 \\ \hat{t}_3 \end{bmatrix}$$

It can be seen that, if $\underline{M}=\underline{I}$, the BLMBE is equivalent to the least squares estimator of eq. (4-14). If $\underline{M}=\underline{N}^{-1}$, the BLMBE is equivalent to the minimum norm estimator of eq. (4-26).

In the event that the observation noise is correlated, the regression model can be extended to account for it. Let

$$E(\underline{e}) = \underline{0} \tag{4-37a}$$

$$E(\underline{e}\underline{e}^T) = \alpha^2 \underline{W} \tag{4-37b}$$

where $\underline{W}$ is non-singular and positive definite and α is unknown. Since $\underline{W}$ is non-singular and positive definite, $\underline{H}$ exists such that

$$\underline{W}^{-1} = \underline{H}^T\underline{H} = \underline{H}^2 \tag{4-38}$$

Let

$$\underline{z} = \underline{Hx}$$

$$\underline{e}_1 = \underline{He}$$

$$\underline{S}_1 = \underline{HS}$$

Then

$$\underline{z} = \underline{S}_1\underline{c} + \underline{e}_1 \tag{4-39a}$$

$$E\underline{e}_1 = \underline{0} \tag{4-39b}$$

and

$$E\underline{e}_1\,\underline{e}_1^T = \alpha^2\,\underline{I} \tag{4-40}$$

The model defined by eqs.(4-39) and (4-40) has uncorrelated noise, and can be solved as before. The estimator of $\underline{t}$ is given again by eq. (4-36) where $\underline{S}$ is replaced by $\underline{S}_1$, and $\underline{x}$ is replaced by $\underline{z}$. Thus,

$$\hat{\underline{t}} = \underline{TMS}_1^T\,(\underline{S}_1\,\underline{M}\,\underline{S}_1^T)^{-1}\,\underline{z}$$

or

$$\hat{\underline{t}} = \underline{TMS}^T\,\underline{H}^T(\underline{HSMS}^T\,\underline{H}^T)^{-1}\,\underline{Hx} = \underline{TMS}^T\,(\underline{SMS}^T)^{-1}\,\underline{x} \tag{4-41}$$

The resulting estimator of eq.(4-41) is identical to the uncorrelated noise estimator of eq.(4-36). The estimator's independence of the noise correlation is a result of the fact that the equation being solved is underdetermined. It is of interest to look at the overdetermined and exactly determined cases. If $\underline{M}=\underline{I}$, the general solution to the correlated noise problem eq. (4-37) and (4-38) is given by

$$\hat{\underline{c}} = (\underline{HS})^{+} \underline{Hx} \tag{4-42}$$

where, again, $(\underline{HS})^{+}$ is the Moore-Penrose pseudo-inverse of $\underline{HS}$ [3]. For the overdetermined case, the pseudo-inverse is defined by

$$\underline{A}^{+} = (\underline{A}^{T}\underline{A})^{-1} \underline{A}^{T} \tag{4-43}$$

where $\underline{A}$ is mxn with m>n and rank $(\underline{A})$=n. In the underdetermined case, the pseudo-inverse is defined by

$$\underline{A}^{+} = \underline{A}^{T}(\underline{AA}^{T})^{-1} \tag{4-44}$$

where $\underline{A}$ is mxn with m<n and rank $(\underline{A})$=m. In the exactly determined case, m=n and $\underline{A}^{+}=\underline{A}^{-1}$. Substituting these expressions into eq.(4-42) in turn gives for the overdetermined case

$$\hat{\underline{c}} = (\underline{S}^{T} \underline{W}^{-1}\underline{S})^{-1} \underline{S}^{T} \underline{W}^{-1} \underline{x} \tag{4-45}$$

In the underdetermined case

$$\hat{\underline{c}} = \underline{S}^{T}(\underline{SS}^{T})^{-1} \underline{x} \tag{4-46}$$

In the exactly determined case

$$\hat{\underline{c}} = \underline{S}^{-1} \underline{x} \tag{4-47}$$

The best linear estimator is independent of the correlation properties of the noise when the system to be solved is underdetermined or exactly determined.

In the tristimulus estimation problem, which is underdetermined, the linear estimators which have been discussed thus far (least squares, minimum norm, and BLMBE) are all of the general form

$$\underline{\hat{t}} = \underline{T}\underline{\hat{c}} = \underline{T}\underline{S}^{-}\underline{x} \tag{4-48}$$

where $\underline{S}^{-}$ is a generalized inverse of $\underline{S}$. When the vector norms in R^3 and R^n are taken to be Euclidean norms (i.e., $\underline{M}=\underline{N}=\underline{I}$), the different generalized inverses all become the pseudo-inverse, and all three estimators are identical

$$\underline{\hat{t}} = \underline{T}\underline{\hat{c}} = \underline{T}\underline{S}^{+}\underline{x} = \underline{T}\underline{S}^{T}(\underline{S}\underline{S}^{T})^{-1}\underline{x} \tag{4-49}$$

4.3 Stochastic Color Estimation

The regression model of the previous section included additive observation noise whose first two statistical moments were assumed known. The spectral distribution vector $\underline{c}$ of the input color was assumed to be unknown but nonrandom; no statistical assumptions on $\underline{c}$ were included in the estimation model. In the following discussion, the model is altered to include a random $\underline{c}$ vector. The random color model is given by

$$\underline{x} = \underline{S}\underline{c} + \underline{e} \tag{4-50}$$

and

$$\underline{t} = \underline{T}\underline{c} \tag{4-51}$$

where, again, $\underline{S}$ and $\underline{T}$ are known 3xn matrices, $\underline{x}$ is the observable 3-vector and $\underline{t}$ is the tristimulus 3-vector which is to be estimated. The statistical properties of the unknown n-vector $\underline{c}$ and 3-vector $\underline{e}$ are given by

$$E\underline{c} = \underline{m}_c \tag{4-52a}$$

$$E[(\underline{c} - \underline{m}_c)\ (\underline{c} - \underline{m}_c)^T] = \underline{R}_{cc} \tag{4-52b}$$

$$E\underline{e} = \underline{0} \tag{4-53a}$$

$$E(\underline{e}\underline{e}^T) = \underline{R}_{ee} \tag{4-53b}$$

$$E(e_i\ c_j) = 0 \tag{4-53c}$$

for i=1,2,3 and j=1,2,...,n. A linear estimator of $\underline{c}$ of the form

$$\hat{\underline{c}} = \underline{a} + \underline{A}\underline{x} \tag{4-54}$$

will now be sought for which $\underline{a}$ is a real vector and $\underline{A}$ is a real matrix chosen so that

$$\underline{Q}_c \triangleq E[(\underline{c} - \hat{\underline{c}})\ (\underline{c} - \hat{\underline{c}})^T] \tag{4-55}$$

is minimized. The minimization of $\underline{Q}_c$ is defined to mean that for any other linear estimator $\hat{\underline{c}}'$ and its corresponding $\underline{Q}_c'$, the matrix $\underline{Q}_c' - \underline{Q}_c$ is positive semi-definite. When $\underline{Q}_c$ is minimized, the expected squared

errors of the components of $\hat{\underline{c}}$ (the diagonal elements of $\underline{Q}$) are each minimized. This insures that

$$e^2 \triangleq E[(\underline{c} - \hat{\underline{c}})^T (\underline{c} - \hat{\underline{c}})] \tag{4-57}$$

the sum of the squared component errors of $\underline{c}$, is also minimized. Most importantly, the minimization of $\underline{Q}_c$ also results in the minimization of the matrix of tristimulus errors $\underline{Q}_t$ when a tristimulus estimator $\hat{\underline{t}}$ is derived from $\hat{\underline{c}}$ by letting $\hat{\underline{t}}=\underline{T}\hat{\underline{c}}$. Let

$$\underline{Q}_t \triangleq E[(\underline{t}-\hat{\underline{t}})(\underline{t}-\hat{\underline{t}})^T] = E[\underline{T}(\underline{c}-\hat{\underline{c}})(\underline{c}-\hat{\underline{c}})^T \underline{T}^T] = \underline{T}\underline{Q}_c\underline{T}^T \tag{4-58}$$

If $\underline{Q}'_c - \underline{Q}_c$ is positive semi-definite, then

$$\underline{Q}'_t - \underline{Q}_t = \underline{T}(\underline{Q}'_c - \underline{Q}_c)\,\underline{T}^T$$

is also positive semi-definite since the rows of $\underline{T}$ are linearly independent, and $\underline{Q}_t$ is therefore minimized when $\underline{Q}_c$ is minimized. The spectral distribution estimator which is sought has the form of eq. (4-54) and minimizes eq. (4-55). The solution is the well known discrete Wiener estimator (see reference [3] for a derivation), given by

$$\underline{a} = \underline{m}_c - \underline{A}\underline{m}_x \tag{4-59}$$

and

$$\underline{A} = \underline{R}_{cx}\,\underline{R}_{xx}^{-1} \tag{4-60}$$

where

$$\underline{R}_{cx} = E[(\underline{c} - \underline{m}_c)(\underline{x} - \underline{m}_x)^T] \tag{4-61a}$$

$$\underline{R}_{xx} = E[(\underline{x} - \underline{m}_x)(\underline{x} - \underline{m}_x)^T] \tag{4-61b}$$

and

$$\underline{m}_x = \underline{S}\underline{m}_c \tag{4-61c}$$

Substituting eqs. (4-59) and (4-60) into eq. (4-54) gives

$$\hat{\underline{c}} = \underline{m}_c + \underline{R}_{cx}\,\underline{R}_{xx}^{-1}\,(\underline{x} - \underline{m}_x) \tag{4-62}$$

By manipulating eqs.(4-50) and (4-61),the necessary correlation matrices are found to be

$$\underline{R}_{cx} = E[(\underline{c} - \underline{m}_c)(\underline{x} - \underline{m}_x)^T] = \underline{R}_{cc}\,\underline{S}^T$$

and

$$\underline{R}_{xx} = E[(\underline{x} - \underline{m}_x)(\underline{x} - \underline{m}_x)^T] = \underline{S}\,\underline{R}_{cc}\,\underline{S}^T + \underline{R}_{ee}$$

Substituting these last two relations into (4-62) gives

$$\underline{c} = \underline{m}_c + \underline{R}_{cc}\,\underline{S}^T\,(\underline{S}\,\underline{R}_{cc}\,\underline{S}^T + \underline{R}_{ee})^{-1}\,(\underline{x} - \underline{m}_x)$$

The corresponding Wiener tristimulus estimator, $\hat{\underline{t}}=\underline{T}\hat{\underline{c}}$, is given by

$$\hat{\underline{t}} = \underline{T}(\underline{m}_c + \underline{R}_{cc}\,\underline{S}^T\,(\underline{S}\,\underline{R}_{cc}\,\underline{S}^T + \underline{R}_{ee})^{-1}\,(\underline{x} - \underline{m}_x) \qquad (4\text{-}63)$$

The color covariance matrix $\underline{R}_{cc}$ might reasonably be approximated by a first order Markov covariance matrix of the form

$$\underline{R}_{cc} = \begin{bmatrix} 1 & \rho & \rho^2 & \rho^3 & \cdots & \rho^{n-1} \\ \rho & 1 & \rho & \cdots & & \vdots \\ \rho^2 & \rho & 1 & & & \rho \\ \vdots & & & & & \\ \rho^{n-1} & & \cdots & & & 1 \end{bmatrix} \qquad (4\text{-}64)$$

where ρ, the correlation coefficient, is a positive constant less than unity.

4.4 Tristimulus Estimation Results

The tristimulus estimators which have been discussed in the foregoing sections have been tested by means of a computer simulation which uses ten test colors and also by using a computer simulation which incorporates real multispectral images. The set of ten test colors consisted of measured reflectivities (reference 4-9) of natural and man-made objects which are typical of those which might occur in a scene to be reproduced. The ten spectral reflectivities are shown in figure (4-1). They correspond

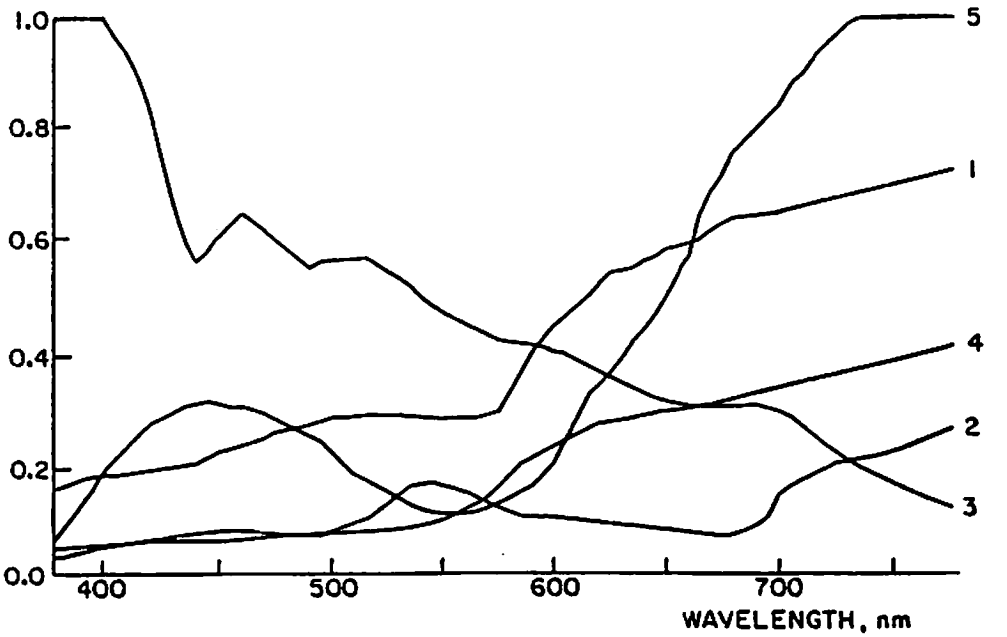

Figure (4-1) First five test spectral reflectivities

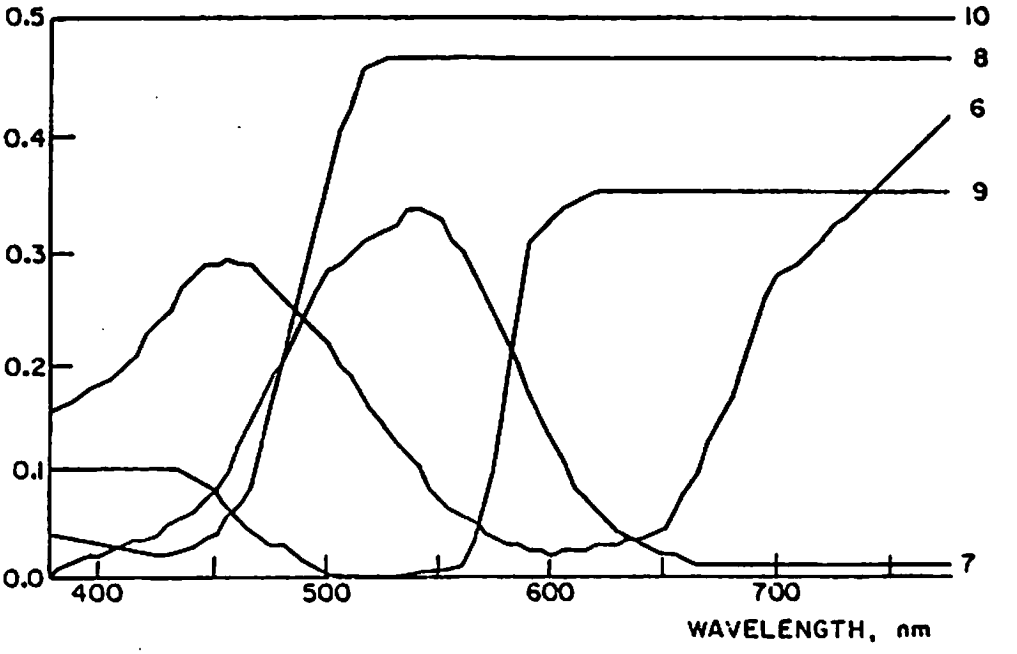

Figure (4-2) Second five test spectral reflectivities

to the following objects:

1) flesh
2) grass
3) sky blue
4) red brick
5) purple flower
6) blue dye
7) green dye
8) yellow dye
9) red dye
10) flat neutral gray

These reflectivities were multiplied at each wavelength by a daylight illuminant function (CIE Illuminant C) to generate the ten input test colors. Each reflectivity curve represents a measured reflectivity, except (3) and (4). Number (3) is a curve which, when multiplied by Illuminant C, gives a typical spectral energy curve of light from the sky. Number (4) is a hypothetical neutral reflector whose reflectivity is 0.5 at all wavelengths. The spectral energy curve of CIE Illuminant C is shown in figure (2-3).

The spectral sensitivity characteristics which were incorporated into the model were of several kinds. An important set, representing a typical reversal color film and lens combination, is shown in figure (4-3). These curves are the spectral products of the film layer taking

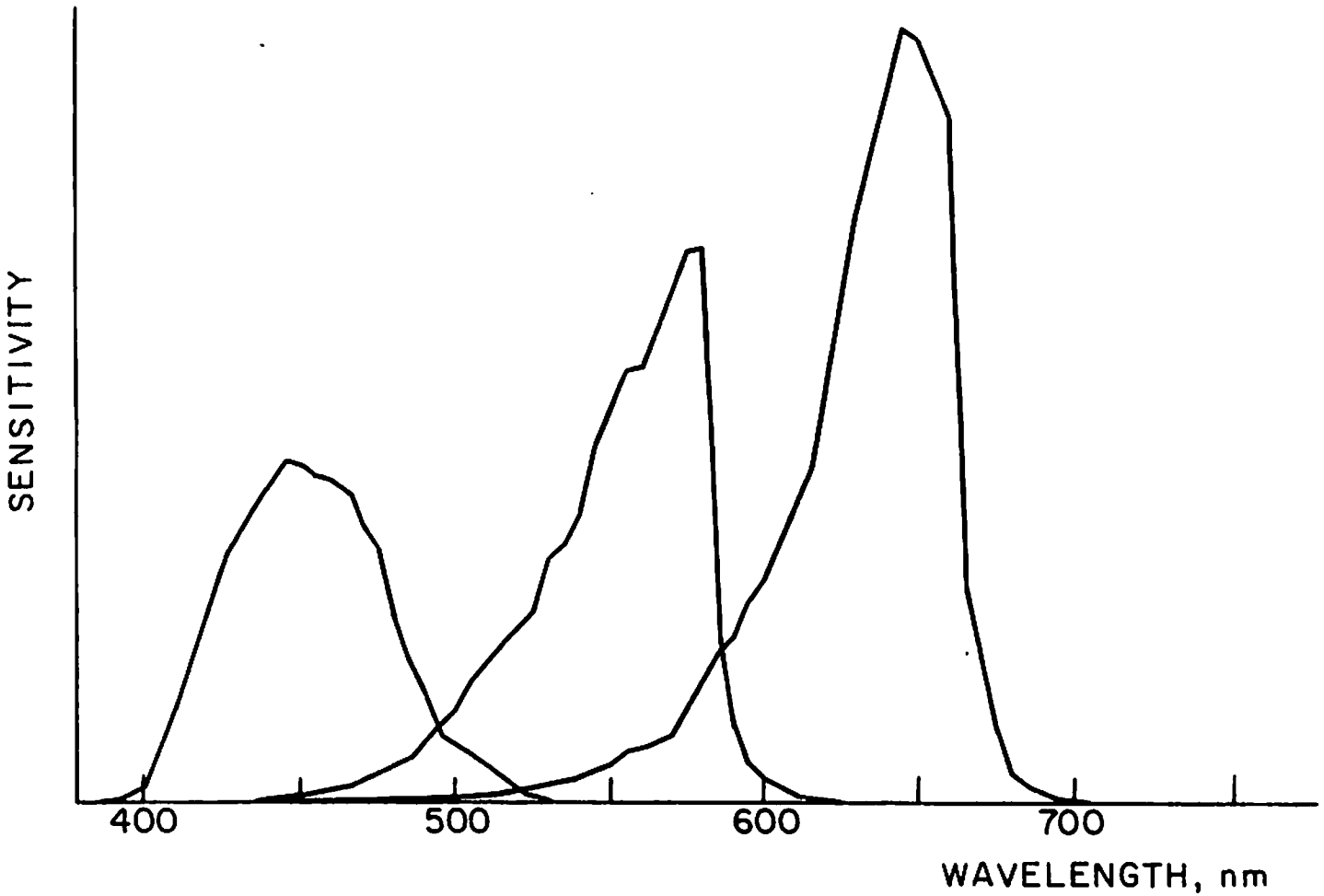

Figure (4-3) Spectral sensitivities, lens and film

sensitivities, figure (4-4a) and the lens optics transmissivity, figure (4-4b). The 80 samples of each of the 3 curves of figure (4-3) become the elements of the 3x80 sensitivity matrix $\underline{S}$. The colorimetric quality factors Q for the red, green, and blue sensor curves of $\underline{S}$ are, respectively, 0.414, 0.822, and 0.983. The green and especially, the blue sensors of this sensor set are very good approximations to color matching curves. The red sensor, by contrast, is not close to any color matching curve primarily because it peaks at about 650 nanometers, a wavelength which is about 50 nm. longer than the peak wavelength of any ideal color matching red sensor. The difference can be seen by comparing the sensor characteristics $\underline{S}$, figure (4-3), with the set of color matching curves which are nearest to $\underline{S}$ in the least squares sense, shown in figure (4-5). The green sensor of $\underline{S}$ is also shifted slightly toward the longer wavelengths relative to its ideal colorimetric position, but not so much as the red sensor. The reason for the exaggerated spread of peak sensitivities in the color film is, as described in Chapter 2, to increase color saturation for a more pleasing (but less accurate) color rendition.

The linear estimators of the input waveform $\underline{c}$ can be graphically compared using the film sensor $\underline{S}$. The estimators are of the form

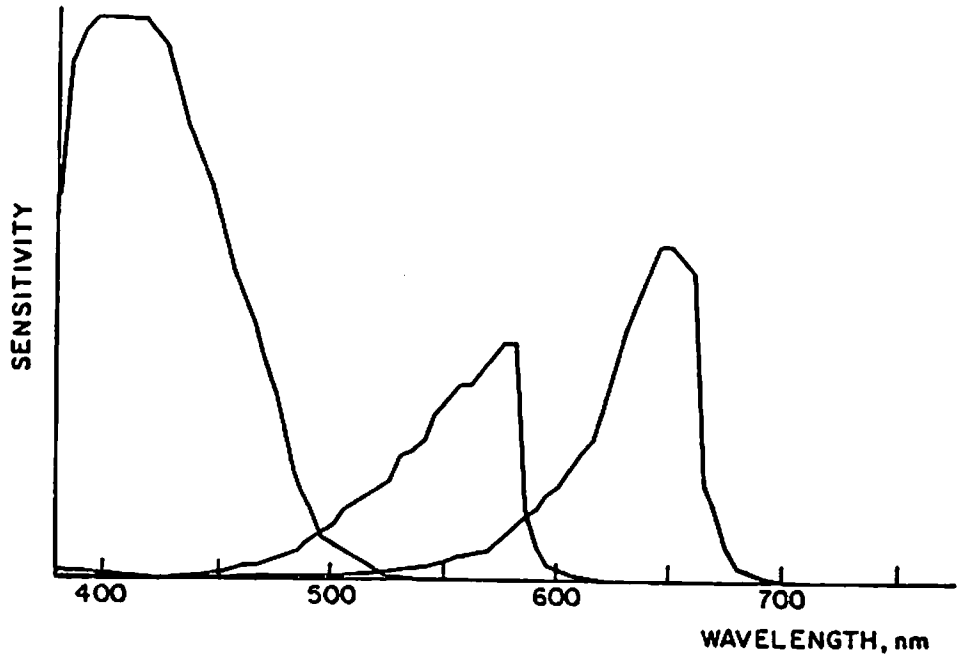

Figure (4-4a) Color film layer spectral sensitivities

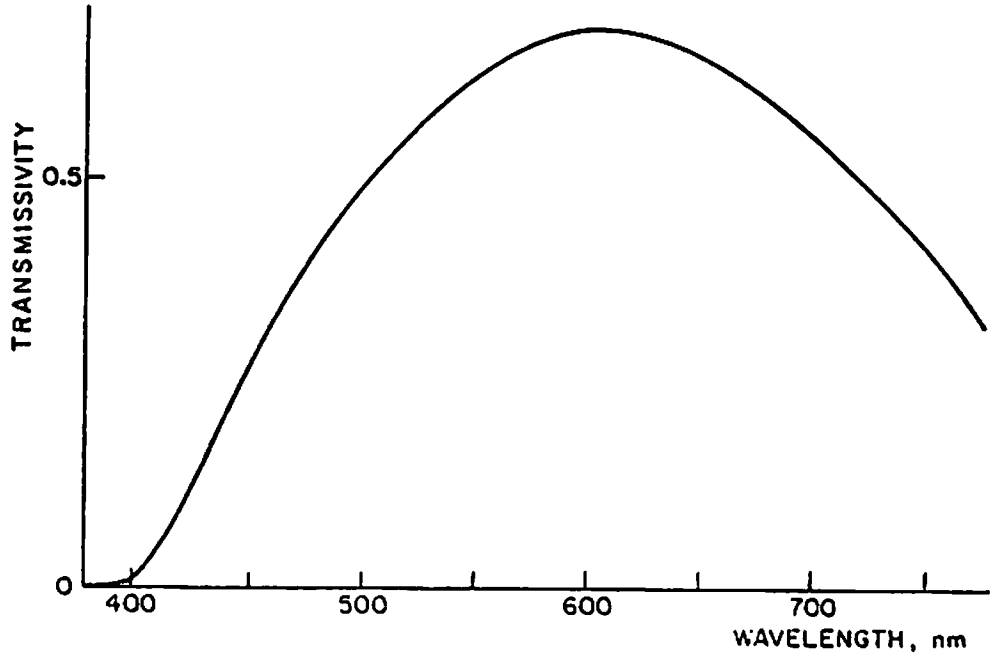

Figure (4-4b) Lens absorption characteristic

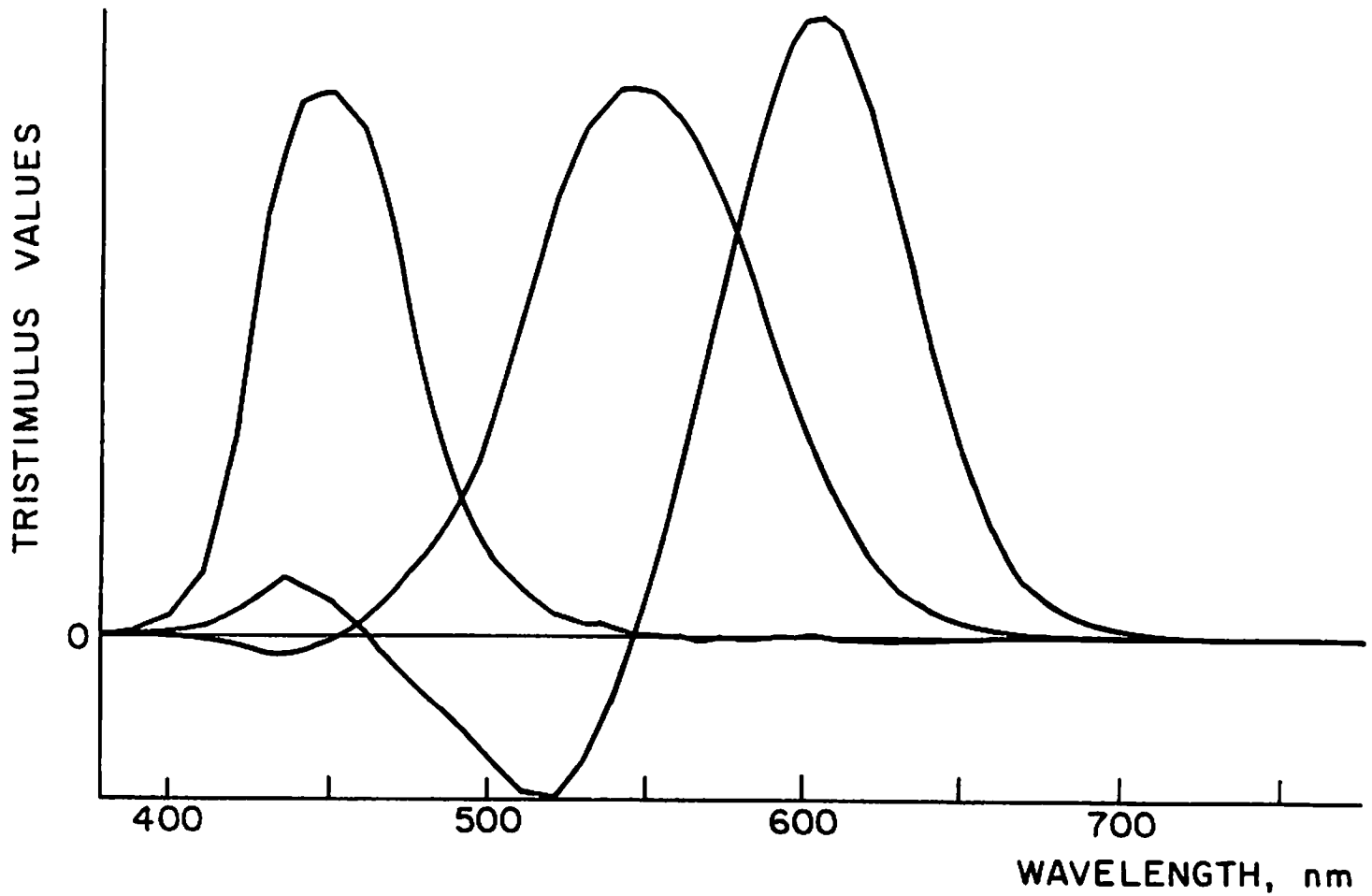

Figure (4-5) Color matching curves nearest to film-lens sensors

$$\hat{\underline{c}} = \underline{c}_o + \underline{S}^- \underline{x}$$

where $\underline{S}^-$ is a generalized inverse of $\underline{S}$ and $\underline{c}_o$ is the zero vector except in the Wiener case. The generalized inverses are one of the following:

1) pseudo-inverse:

$$\underline{S}^+ = \underline{S}^T(\underline{S}\underline{S}^T)^{-1}$$

2) constrained inverse:

$$\underline{S}_c^- = \underline{N}^{-1}\ \underline{S}^T(\underline{S}\underline{N}^{-1}\ \underline{S}^T)^{-1}$$

3) Wiener inverse:

$$\underline{S}_W^- = \underline{M}\underline{S}^T(\underline{S}\underline{M}\underline{S}^T)^{-1}$$

where $\underline{N}$ is the smoothing matrix defined in eq. (4-29), and $\underline{M}$ is the Markov covariance matrix given by eq. (4-64). Since $\underline{S}$ is a 3x80 matrix, each $\underline{S}^-$ is an 80x3 matrix whose columns may be graphed as the rows of $\underline{S}$ were graphed in figure (4-3). The columns of $\underline{S}^+$, the pseudo-inverse of S, are shown in figure (4-6). The columns of $\underline{S}_c^-$ and $\underline{S}_w^-$ are shown in figures (4-7) and (4-8). Figure (4-8a) shows the Wiener inverse using a correlation coefficient ρ=0.5 and figure (4-8b) shows the Wiener inverse with ρ=0.9. The estimate $\underline{c}$ of the input spectral waveform are weighted sums of the columns of the appropriate $\underline{S}^-$ (summed with a mean vector in the Wiener case).

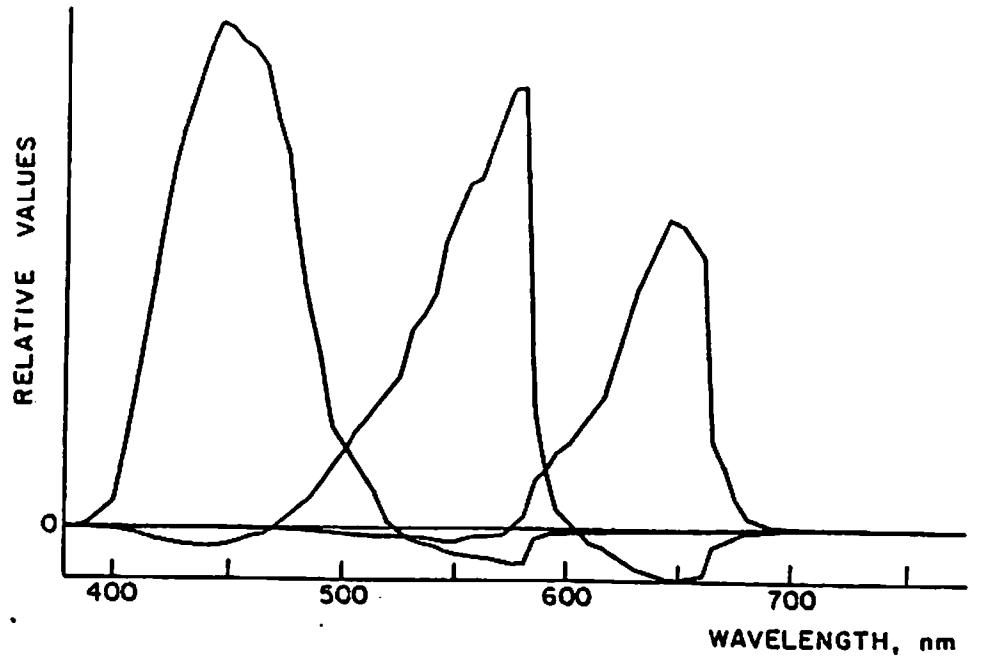

Figure (4-6) Columns of pseudo-inverse operator

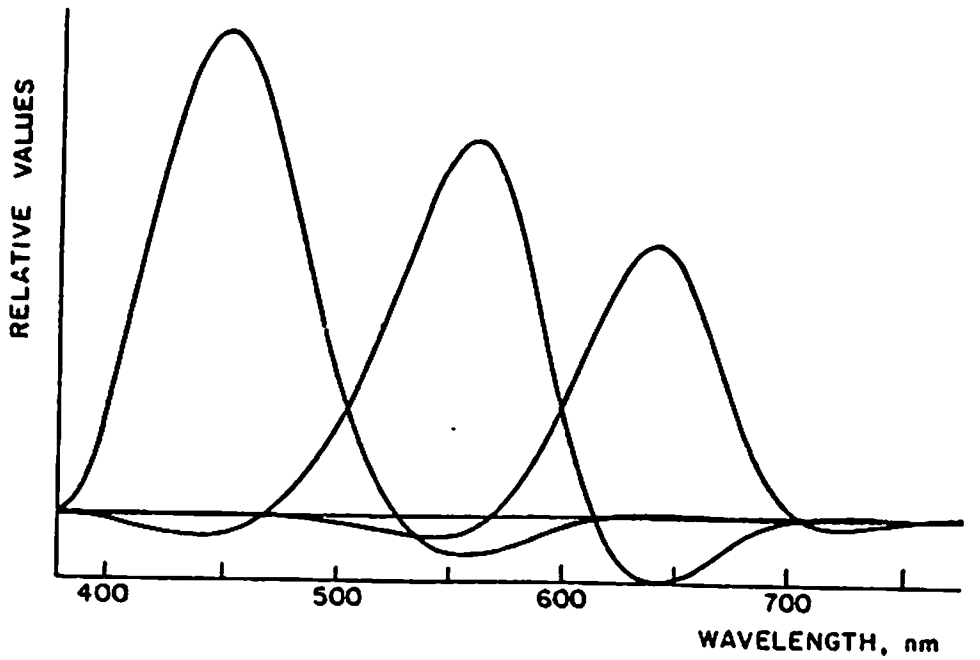

Figure (4-7) Columns of smoothing inverse operator

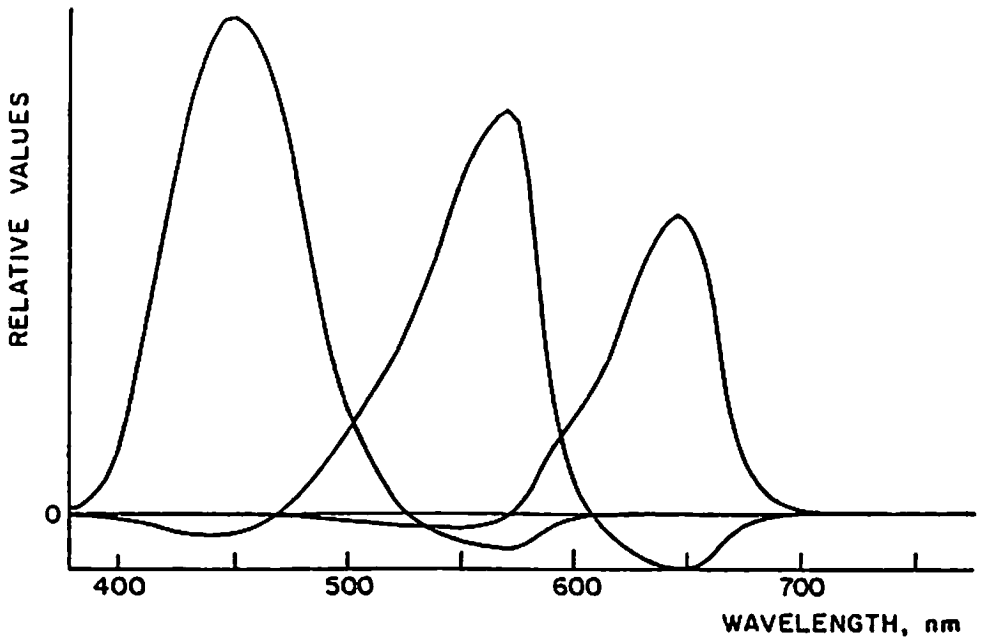

Figure (4-8a) Columns of Wiener inverse operator, $\rho = 0.5$

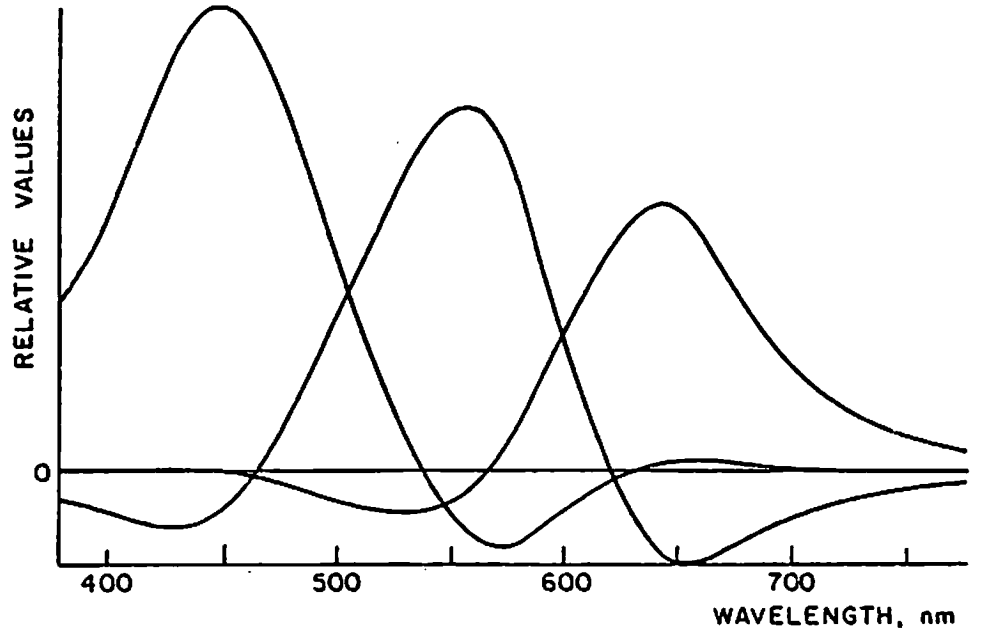

Figure (4-8b) Columns of Wiener inverse operator, $\rho = 0.9$

Examples of the waveforms generated by the estimators are shown in figures (4-9), (4-10), and (4-11). The solid curve of figure (4-9) shows a test color (sky blue) obtained as the product of the illuminant of figure (4-2) and a "reflectivity" given by curve number 3 of figure (4-1a). The dotted line in the figure is the pseudo-inverse estimator of $\underline{c}$ given by $\underline{c}=\underline{S}^{+}\underline{x}$ where, as usual, $\underline{x}=\underline{S}\underline{c}$. Figure (4-10) shows the constrained smoothing estimate $\underline{c}=\underline{S}_{c}^{-}\underline{x}$ compared with the same input test color. Figure (4-11) shows the corresponding estimate of $\underline{c}$ for the case of the Wiener estimate (ρ=0.9). The estimator is

$$\hat{\underline{c}} = \underline{m}_{c} + \underline{MS}^{T}(\underline{SMS}^{T})^{-1}\,(\underline{x} - \underline{Sm}_{c})$$

where the mean vector $\underline{m}$ was taken to be 0.3 $I(\lambda)$. The function $I(\lambda)$ is the illuminant, figure (2-3), and 0.3 corresponds to a somewhat arbitrary average reflectivity. Of these three solutions, the one which imposes the most smoothing on the solution, the Wiener estimate with ρ =0.9, is clearly closest to the original waveform.

The performance of the tristimulus estimators is shown in Table (4-1) for each of the ten test colors. These results are summarized in Table (4-2) by averaging the data over the ten test colors. Color errors are described three ways: luminance error (where luminance = 1.0 corresponds to the illuminant against unit reflectivity), chrominance error (Euclidean distance in UCS chromaticity space), and

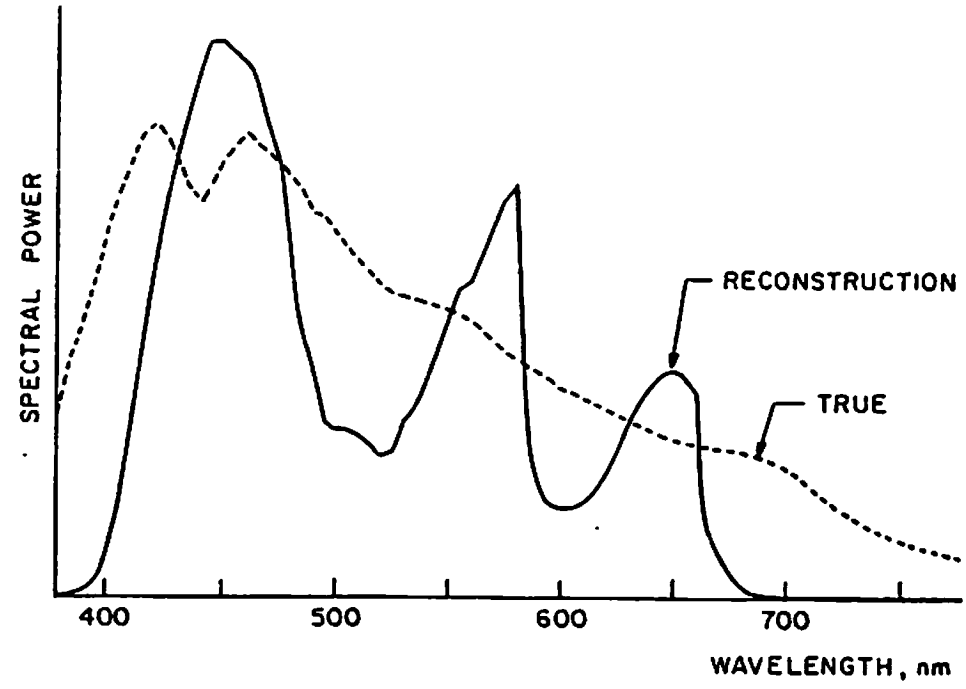

Figure (4-9) Pseudo-inverse reconstruction of color 3

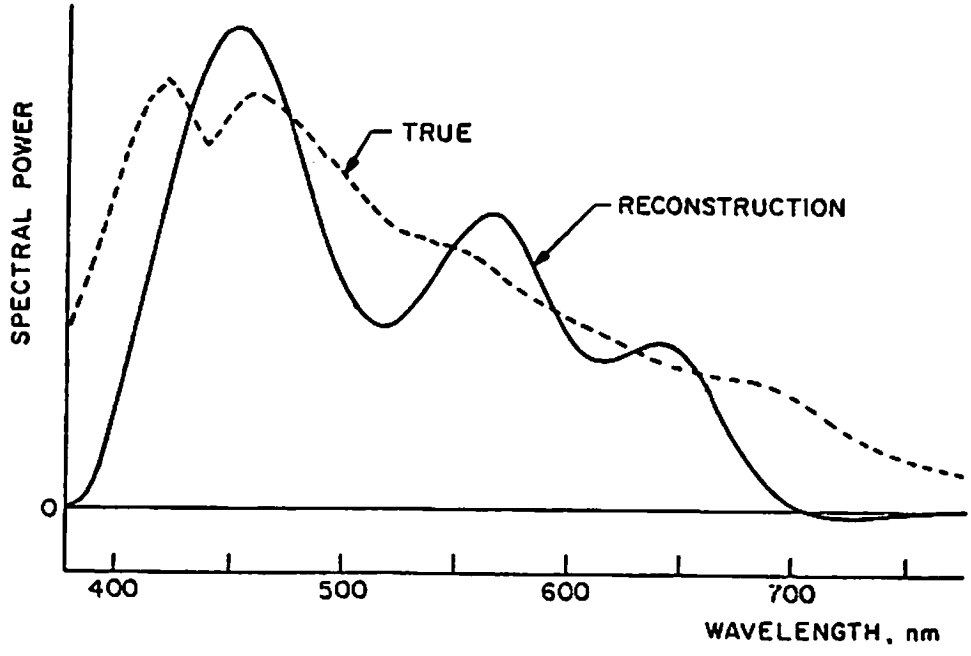

Figure (4-10) Smoothing inverse reconstruction of color 3

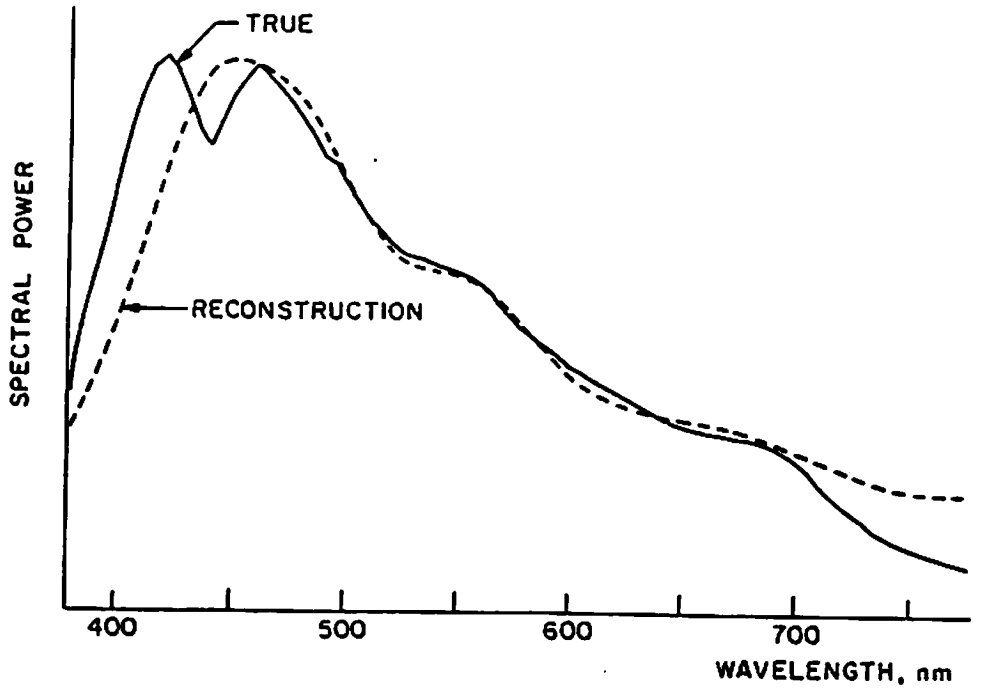

Figure (4-11) Wiener inverse reconstruction of color 3

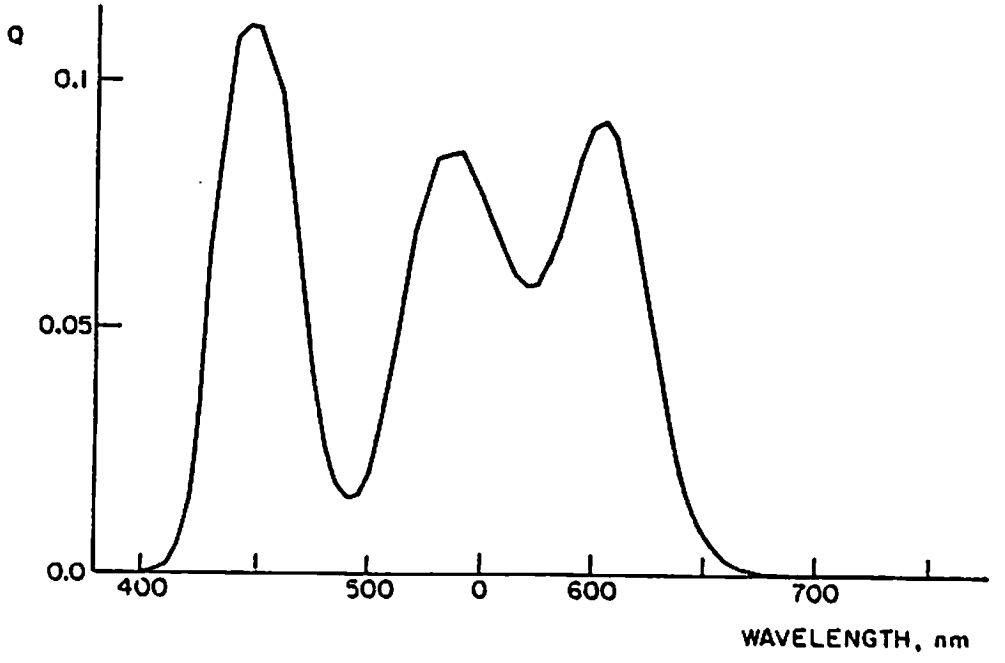

Figure (4-12) Colorimetric quality factor vs wavelength, narrowband sensor

Table (4-1)

Tristimulus Estimator Performance Against Ten Test Colors

Film Sensitivity Characteristics

Color Number	1	2	3	4	5	6	7	8	9	10
True Luminance	.33	.12	.47	.14	.18	.09	.23	.44	.11	.50
Chromaticity u	.24	.19	.18	.28	.25	.15	.14	.21	.38	.20
Chromaticity v	.32	.33	.29	.34	.27	.23	.35	.36	.32	.31
Pseudo-inverse										
Luminance Error	-.05	-.02	-.07	-.02	-.02	-.01	-.04	-.07	-.02	-.07
Chrominance Error	.01	.01	.02	.01	.02	.04	.03	.01	.04	.01
Cube Root Error	4.7	3.3	7.4	3.0	3.7	9.2	5.7	5.0	4.8	5.8
Smoothed Pseudo-inverse										
Luminance Error	-.02	-.01	-.03	-.00	-.00	-.01	-.01	-.02	-.01	-.02
Chrominance Error	.01	.01	.01	.00	.02	.03	.03	.02	.03	.01
Cube Root Error	2.1	1.3	3.3	0.6	2.2	5.4	3.8	2.6	2.7	2.3
Wiener, ρ =0.9,c=0.3I										
Luminance Error	-.01	-.01	-.00	-.00	-.01	-.00	-.00	-.01	-.01	-.00
Chrominance Error	.01	.00	.00	.01	.01	.01	.02	.01	.03	.00
Cube Root Error	1.0	0.3	0.4	0.6	1.7	0.9	2.1	1.8	2.7	0.2

Table (4-2)

Tristimulus Estimator Performance Averaged Over Ten Test Colors, Film Sensitivity Characteristics

Estimator Type	RMS Error Luminance	RMS Error Chrominance	RMS Error Cube Root Space
Pseudo-inverse	0.044	0.022	5.29
Smoothed Pseudo-inverse	0.014	0.019	2.78
Wiener	0.005	0.011	1.35

Table (4-3)

Tristimulus Estimator Performance Averaged Over Ten Test Colors, Narrowband Sensitivity Characteristics

Estimator Type	RMS Error Luminance	RMS Error Chrominance	RMS Error Cube Root Space
Pseudo-inverse	0.272	0.056	39.82
Smoothed Pseudo-inverse	0.211	0.054	28.37
Wiener	0.037	0.040	10.67

cube root uniform perceived error (Euclidean distance in L a b cube root coordinate space).

From Table (4-2), it is apparent that smoothing of $\underline{c}$ reduces the color estimation errors, especially the luminance errors. The minimum norm property of the pseudo-inverse generates a waveform possessing the least energy (sum of the squared waveform samples) of all solutions to $\underline{x}=\underline{S}\underline{c}$. Therefore, positive weighted summations over the estimated waveform tend to be smaller than equivalent summations over the "true" input waveform. For this reason, pseudo-inverse estimates of tristimulus values tend to be on the low side. Note in Table (4-1) that luminance errors using the pseudo-inverse estimator are uniformly negative for all ten test colors. Imposing smoothing on $\hat{\underline{c}}$ by using Wiener estimation generates waveforms whose luminance errors are still more negative than positive (Table 4-1), but whose RMS average luminance error is reduced over the pseudo-inverse RMS luminance error by a factor of nine (Table 4-2) and whose RMS chrominances error is also improved by a factor of two. The net error improvement in the perceptually uniform cube root space is by a factor of about four.

The tristimulus estimators were also tested using the same test color set, but using sets of sensor characteristics which are poorer approximations to color

matching curves than are the film sensitivities just discussed. A set of narrowband sensitivities of unit amplitude peaking at wavelengths of 450, 550 and 650 nanometers were tested. The colorimetric quality factors of these sensors are 0.114, 0.079 and 0.008. These arbitrarily chosen sensors are not the best narrowband sensors colorimetrically. Figure (4-12) shows a graph of the colorimetric quality q for a narrow band filter as a function of its center wavelength. The optimal narrowband wavelengths are approximately 445, 540 and 605 nanometers. The average color errors resulting from application of the tristimulus estimators using the narrowband sensors at 450, 550 and 650 nanometers are summarized in Table (4-3). Again, the Wiener estimator provides the best tristimulus estimation accuracy, although the errors are larger for each estimator type than they were using the film sensitivities. The improvement provided by smoothing when narrowband sensors are used is apparent when the pseudo-inverse and Wiener estimates of color number three are compared. Figure (4-13) shows the pseudo-inverse reconstruction of color three using the narrowband filters. It consists of samples of the input waveform at the narrowband wavelengths. Figure (4-14) shows the corresponding Wiener estimate (ρ=0.9). The waveform values at the filter wavelengths are again correct (as they have to be if $\underline{x}=\underline{\underline{S}}\underline{c}$ and the filters are narrowband) but the

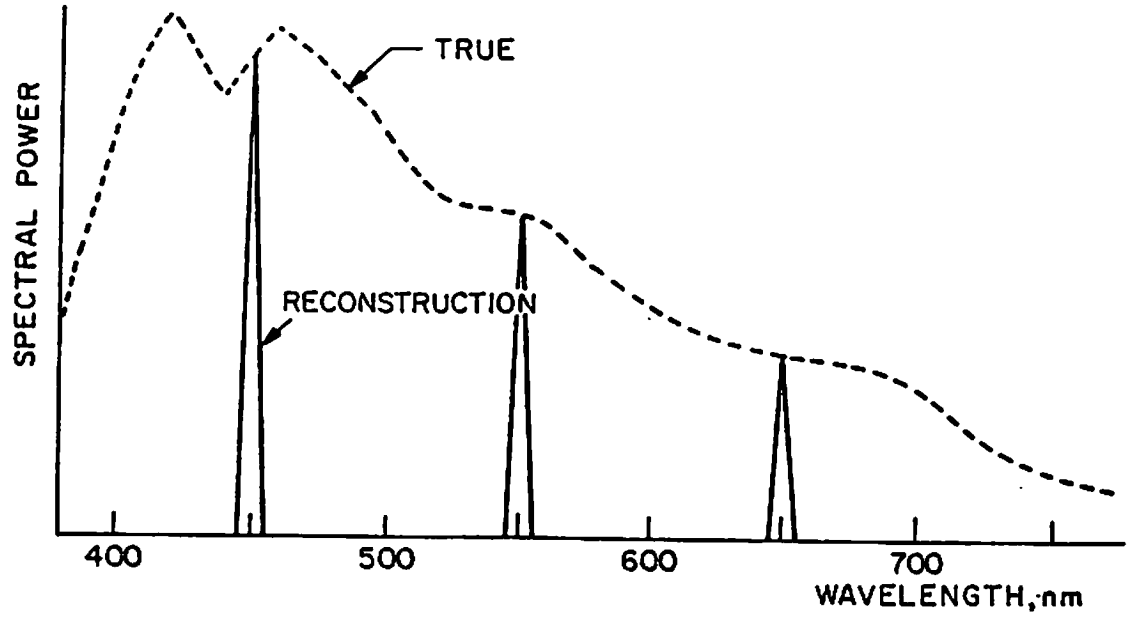

Figure (4-13) Pseudo-inverse reconstruction of color 3, narrowband sensors

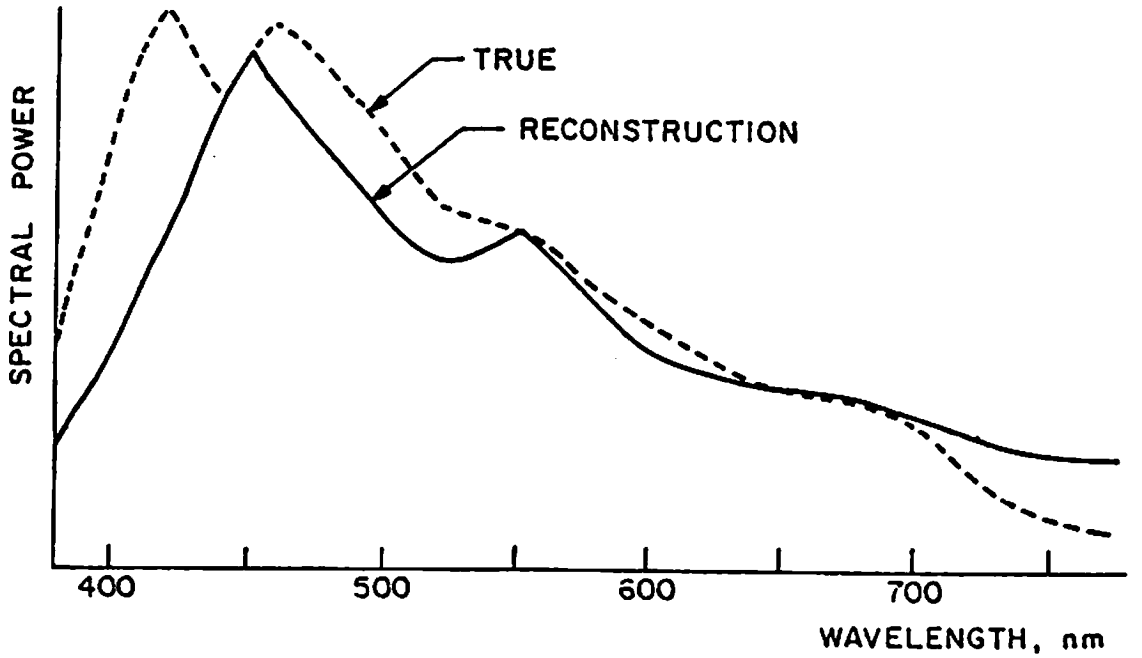

Figure (4-14) Wiener inverse reconstruction of color 3, narrowband sensors

values at other wavelengths are much more accurate because of smoothing. Although tristimulus errors are much improved because of smoothing (see luminance error in Table (4-3)), chrominance errors are improved by a smaller factor. This is because chromaticities are ratios of tristimulus values, and the negative tristimulus errors tend to cancel.

The tristimulus estimators were tested using a real six band multispectral image. The six samples at each image point constituted the elements of $\underline{c}$, the "true" input spectral waveform. The elements of the 3 $\underline{x}$ 6 array $\underline{S}$ could then be selected to simulate any arbitrary set of three taking sensitivities. The $\underline{x}$ vector generated at each image point by $\underline{x}=\underline{S}\underline{c}$ served as an input vector to one of the estimator algorithms, generating an estimated image to be displayed.

The input multispectral image was generated by photographing a table top still life of colored objects through six narrowband interference filters. The filter center wavelengths were 440, 480, 520, 560, 600 and 640 nanometers and their half power bandwidths were about 10 nanometers. Each filter was an element of a sixteen filter set made by Oriel corporation. The spectral passbands of the set are shown in figure (6-2). The exposures were made using Kodak Tri-X film in a 35mm camera with incandescent

illumination. Exposure times were of the order of ten seconds in length, established by trial and error. Care was taken that the field of view of interest was less than twenty degrees in order that the interference filters were not detuned significantly by off-axis rays at the edge of the field. The six negatives were digitized using a flatbed microdensitometer and digitally converted to positive images. Photographs of the six digital images, displayed on a cathode ray tube, are shown in figure (4-15).

After scaling to correspond to the spectral weighting of the illumination, the six images were weighted and summed according to the color matching curves of a set of television display primaries. A photograph of the resulting "true color" image is shown in figure (4-16)(see color plate). The six images were also weighted by factors simulating sets of sensors far removed from ideal color matching curves. One such set consisted of narrowband sensors at 440, 520, and 600 nanometers, weighted by 0.25, 1.0, and 0.5, respectively. The resulting green biased image is shown in figure (4-17). Operating on this image with the pseudo-inverse tristimulus estimator gives the image shown in figure (4-18). The green bias is removed, but the image is dark owing to the tendency of the pseudo-inverse estimator to generate low tristimulus values when the sensors are narrowband. The result of smoothing

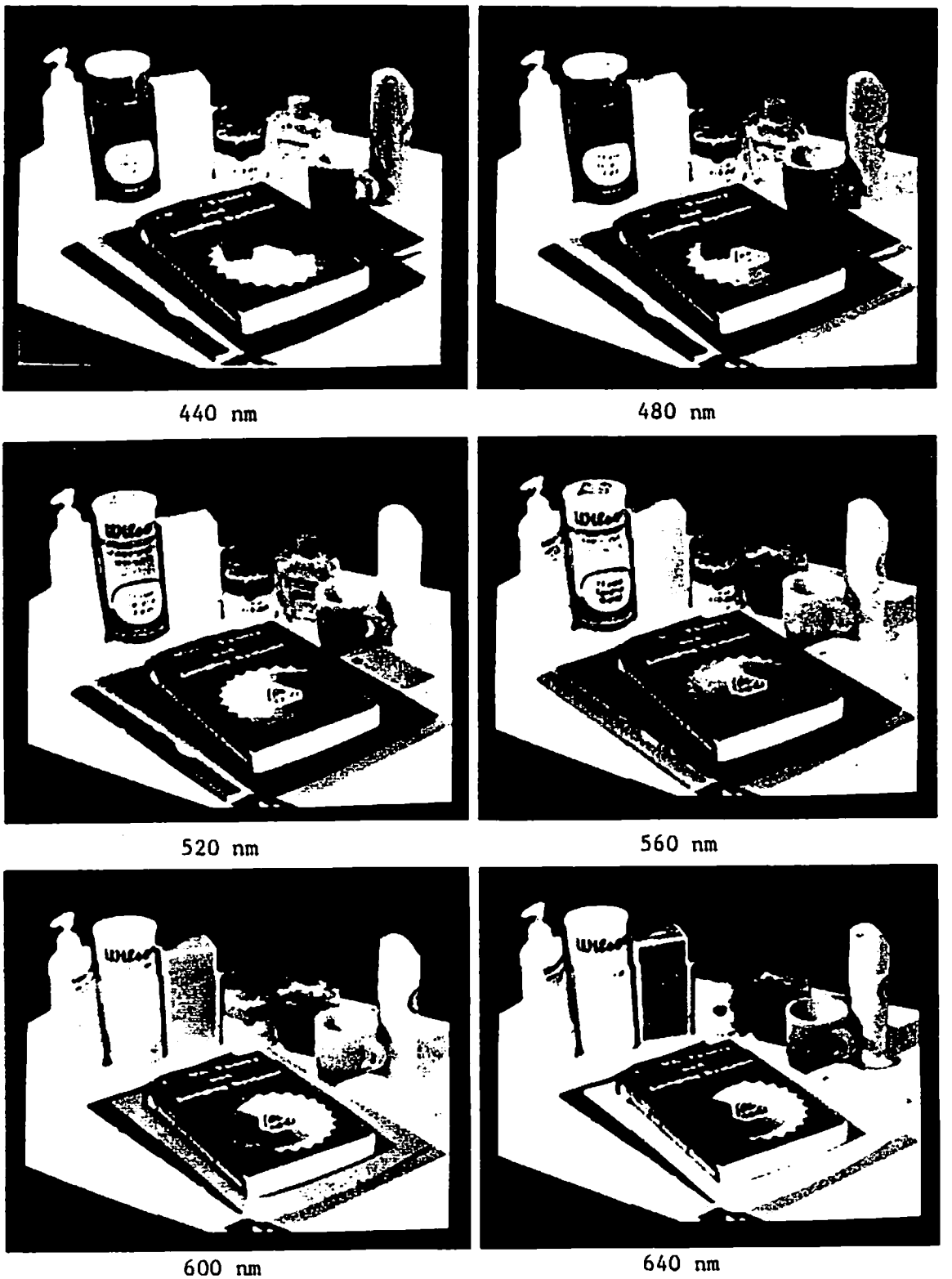

Figure (4-15) Six multispectral images

is shown in the Wiener estimated image of figure (4-19). The image is bright and color balanced. The main color error with respect to the true color image is a desaturation of the bright reds, possiby because of the absence of the deep red 640 nm. component in the input image.

The Wiener estimator performs well with sensors which may not be color balanced and which may be either narrowband or broadband, as long as the three sensors are near the ideal values of 445, 540 and 605 nm. A more severe test takes place when large portions of the visible region are not covered. Figure (4-20) shows the result when the blue, green and red display primaries are driven by equal amplitude narrowband sensors at three long wavelengths, 560, 600 and 640 nm. Since only the green to red components are present at the input, the color distortion is great. Reds map into orange, greens become blue, blues become black, and yellows are white. With this as an input, the Wiener estimated image is as shown in figure (4-21). The primary improvement is in the rendition of the reds. Blues also are now no longer black, because of the smoothing induced blue content in the estimated spectra. On the debit side, oranges and yellows are still rendered as white, and there is a slight overall pink bias to the image. The overall color improvement achieved by using the Wiener estimator can be judged by examining the

color wheel on the book cover of each of figures (4-19), (4-20), and (4-21).

References

1. Papoulis, A., Probability, Random Variables, and Stochastic Processes, McGraw-Hill, New York (1965)

2. Rust, B.W., and W.R. Burrus, Mathematical Programming and the Numerical Solution of Linear Equations, American Elsevier, New York (1972)

3. Lewis, T.O., and P.L. Odell, Estimation in Linear Models, Prentice Hall, Englewood Cliffs, New Jersey (1971)

4. Luenberger, D., Optimization by Vector Space Methods, John Wiley, New York (1969)

5. Rao, C.R., and S.H. Mitra, Generalized Inverse of Matrices and its Applications, John Wiley, New York (1971)

6. Phillips, D.L., "A Technique for the Numerical Solution of Certain Integral Equations of the First Kind," J. Assoc. Comput. Mach., 9, pp. 84-87 (1964)

7. Wyszecki, G., and W.S. Stiles, Color Science: Concepts and Methods, Quantitative Data and Formulas, John Wiley, New York (1967)

8. Glasser, L., A. McKinney, C. Reilley, and P.

Schnelle, "Cube-Root Color Coordinate System," J. Optical Society of America, 48, 10 (1958)

9. Evans, R., W. Hanson, and W. Brewer, Principles of Color Photography, Wiley, New York (1953)

5. Digital Correction of Color Nonlinearities

In Chapter 3 it was stated that an ideal colorimetric reproduction system should have sensor characteristics which are color matching functions, thereby generating signals at each image point which are tristimulus values. It was further stated that the ideal color system should be linear between the sensor outputs and the input to the final display primaries, and should convert the sensor outputs to tristimulus values in the color coordinate system defined by the display primaries. When these conditions fail, as they always do to some extent in real color systems, color errors will be seen in the displayed image. This chapter will examine methods of correcting color errors introduced by the presence of system nonlinearities which cause the second condition stated above to fail.

5.1 Color Imaging System Nonlinearities

Nonlinearities in imaging systems, whether the system is photographic or electronic, can be placed in one of two major categories: invertible or non-invertible.

1) Invertible nonlinearities - In imaging systems, these are usually operations which alter signal values in a smooth, mathematically simple way. An example is the power-law or "gamma" nonlinearity characteristic of some

television camera tubes and cathode ray tubes [1]. If input and output signals are called v_i and v_o, respectively, the functional relationship is given by

$$v_o = v_i^{\gamma}$$

where the constant γ typically has a value between 0.5 and 2.0. When the value of γ is known, and other operations have not also taken place, the gamma nonlinearity can be corrected by raising v_o to the power $1/\gamma$. This may be easily accomplished when signals are digitally stored in a computer. Another important invertible nonlinearity is the density vs. exposure relationship in photographic film. Over some range of exposure (radiant energy per unit area at the film plane, spectrally weighted by the film sensitivity characteristic), the relation between film layer density and exposure is very nearly logarithmic. As will be shown in a later section of this chapter, the relations among exposure x, density d, and transmissivity τ for a layer of reversal color transparency film can be expressed in approximate form as

$$d = b - \gamma \log x \qquad (5\text{-}1)$$

and

$$\tau = 10^{-d} \qquad (5\text{-}2)$$

where b and γ are constants. Substituting (5-2) into (5-1)

gives

$$\tau = 10^{-(b-\gamma \log x)} = 10^{-b}\, x^{\gamma} \qquad (5\text{-}3)$$

From this result, it is clear that when γ differs from unity, there is a power law nonlinearity between the input exposure x and the output transmissivity.

2) Non-invertible nonlinearities - Nonlinearities in imaging systems which cannot be inverted are usually caused by signal limiting. Signals whose values are too large or too small for the dynamic range of the system are mapped into the upper or lower clipping levels of one of the system components. Examples of non-invertible nonlinearities include the clipping action of the density-vs-log exposure curve which takes place in photographic film and the limiting of signals in electronic devices. The film density-vs-log exposure of figure (2-8) is a typical example of the limiting functions present in all image transmission and storage systems.

In Chapter 3, a general digital color analyzing system model was described. The operation of the model on an input color $\underline{c}$ was described by eq. (3-17), repeated below

$$\underline{v} = \underline{HGFc}$$

where the model components are defined and related on the block diagram of figure (3-2). The special case of a film

and scanner color system is also indicated in figure (3-2). The film-scanner color analyzing system will be examined in the remainder of this section, in order to give a concrete and important example of a real system containing nonlinearities. The concepts developed are applicable to a much wider class of color imaging systems. In the section which follows the film-scanner discussion, some methods of correcting invertible nonlinearities will be discussed.

The type of color photographic film which will be examined is reversal color film [2], which produces a three layer positive transparency. In a reversal color film, three light-sensitive layers absorb incident light at a point in the film plane. The spectral irradiance at the object point being imaged is $c(\lambda)$. The spectral sensitivity curves of the layers of a typical reversal color film are shown in figure (5-1). The sensitivities $S_R(\lambda)$, $S_G(\lambda)$, $S_B(\lambda)$ of the three layers are defined by

$$S_i(\lambda) = \frac{1}{E_i(\lambda)} \qquad (5\text{-}4)$$

for i=R,G,B where $E_i(\lambda)$ is the energy per unit area at the film plane at wavelength which is necessary to generate some fixed density value after development. The integrated exposure values of the film layers are given by

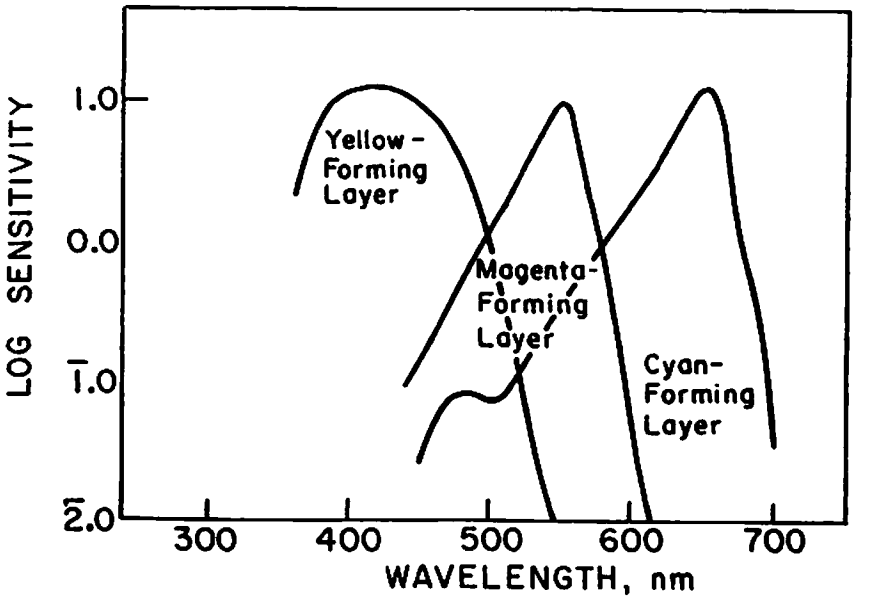

Figure (5-1) Film spectral sensitivities

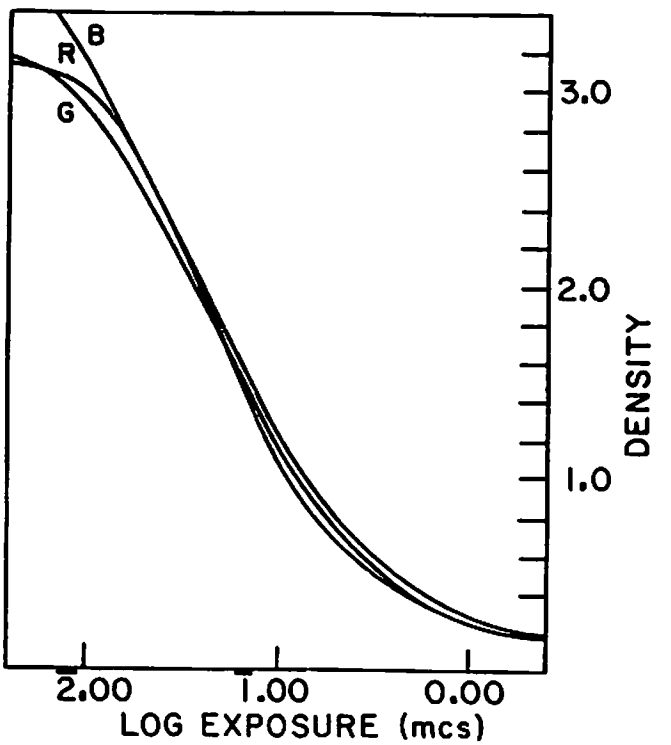

Figure (5-2) Film density vs log exposure curves

$$X_R(C) = d_R \int_{\lambda_L}^{\lambda_U} C(\lambda)\, S_R(\lambda)\, \tau_o(\lambda)\, d\lambda \qquad (5\text{-}5a)$$

$$X_G(C) = d_G \int_{\lambda_L}^{\lambda_U} C(\lambda)\, S_G(\lambda)\, \tau_o(\lambda)\, d\lambda \qquad (5\text{-}5b)$$

$$X_B(C) = d_B \int_{\lambda_L}^{\lambda_U} C(\lambda)\, S_B(\lambda)\, \tau_o(\lambda)\, d\lambda \qquad (5\text{-}5c)$$

where τ_o is the spectral transmissivity of the camera optics and d_R, d_G, d_B are proportionality constants which contain the physical parameters which govern the relationship between the spectral power at a point in the scene being photographed and the spectral energy at the film plane. These parameters include the F number of the camera lens and the duration of the exposure. This allows the exposure values to be defined in terms of the spectral irradiance $c(\lambda)$ at points in the scene rather than in terms of the spectral radiant energy at the film plane. In practice, the values of d_R, d_G, d_B are usually adjusted so that the exposure values X_R, X_G, X_B are equal when the input color is a chosen reference white. Converting eqs. (5-5) to a matrix equation, (see Chapter 2) yields

$$\underline{x} = \underline{S}\underline{c} \qquad (5\text{-}6)$$

where the 3xn matrix $\underline{S}$ contains d_R, d_G, d_B and $\tau_o(\lambda)$ as well

as $S_R(\lambda)$, $S_G(\lambda)$, and $S_B(\lambda)$. The vector $\underline{x}$ is then the exposure vector corresponding to the color vector $\underline{c}$ and the sensitivity matrix $\underline{S}$.

In the development of the film, the layer exposures are converted to dye densities c, m, or y according to relationships such as those shown in figure (5-2). These density vs. log exposure curves are approximate in that the density of a developed layer is dependent not only on its own layer exposure as shown by figure (5-2), but, to a much lesser extent, on the exposures of the other two layers. This phenomenon is called the interimage effect [3]. The densities c, m, y are the dye concentrations of the three dye layers of the developed transparency. The spectral densities $D_c(\lambda)$, $D_m(\lambda)$, $D_y(\lambda)$ (sometimes called spectral analytical densities) of unit concentration of each layer dye of a typical reversal film are shown in figure (2-7). The dye layers are cyan, magenta, and yellow in color and are intended to control the transmission of red, green, and blue light, respectively. The spectral analytical densities of the three superimposed layers is $cD_c(\lambda) + mD_m(\lambda) + yD_y(\lambda)$. The spectral transmittance $\tau(\lambda)$ of the transparency is

$$\tau_T = 10^{-cD_c(\lambda) - mD_m(\lambda) - yD_y(\lambda)} \qquad (5\text{-}7)$$

When dye concentrations of c=m=y=1 are present, the transparency spectral analytical density is the upper curve

of figure (5-3) and the resulting transparency appears to be a neutral gray under illumination by a reference white light.

Equation (5-7) can be converted to vector form using the following definitions:

$$\underline{\tau} = \begin{bmatrix} \tau_T(\lambda_1) \\ \tau_T(\lambda_2) \\ \vdots \\ \tau_T(\lambda_n) \end{bmatrix}$$

$$\underline{w} = \begin{bmatrix} c \\ m \\ y \end{bmatrix}$$

$$\underline{D} = \begin{bmatrix} D_c(\lambda_1) & D_m(\lambda_1) & D_y(\lambda_1) \\ \vdots & \vdots & \vdots \\ D_c(\lambda_n) & D_m(\lambda_n) & D_y(\lambda_n) \end{bmatrix} = \begin{bmatrix} \underline{d}_1^T \\ \vdots \\ \underline{d}_n^T \end{bmatrix} \qquad (5\text{-}8)$$

Equation (5-7) can then be written as

$$\tau_i = 10^{-\underline{d}_i^T \underline{w}} \qquad (5\text{-}9)$$

or, with slightly irregular matrix notation,

$$\underline{\tau} = 10^{-\underline{D}\underline{w}} \qquad (5\text{-}10)$$

In order to digitize the transparency, a scanner samples its transmissivity at each point of some two

dimensional array. Three sensors are used to measure the red, green and blue regions. If the scanner spectral sensitivities are $H_R(\lambda)$, $H_G(\lambda)$, and $H_G(\lambda)$, and V_R, V_G, and V_B are scanner output signals at each image point, then

$$V_R = \int_{\lambda_L}^{\lambda_U} H_R(\lambda)\ \tau_T(\lambda)\ d\lambda \qquad (5\text{-}11a)$$

$$V_G = \int_{\lambda_L}^{\lambda_U} H_G(\lambda)\ \tau_T(\lambda)\ d\lambda \qquad (5\text{-}11b)$$

$$V_B = \int_{\lambda_L}^{\lambda_U} H_B(\lambda)\ \tau_T(\lambda)\ d\lambda \qquad (5\text{-}11c)$$

The H characteristics are obtained by multiplying the spectral characteristics of the scanner light source, the photosensor, the scanner optics and the red, green, or blue filter used for color separation. Substituting from eq. (5-7) gives the scanner signals

$$V_R = \int_{\lambda_L}^{\lambda_U} H_R(\lambda)\ 10^{-[cD_c(\lambda) + mD_m(\lambda) + yD_y(\lambda)]}\ d\lambda \qquad (5\text{-}12a)$$

$$V_G = \int_{\lambda_L}^{\lambda_U} H_B(\lambda)\ 10^{-[cD_c(\lambda) + mD_m(\lambda) + yD_y(\lambda)]}\ d\lambda \qquad (5\text{-}12b)$$

$$V_B = \int_{\lambda_L}^{\lambda_U} H_B(\lambda)\ 10^{-[cD_c(\lambda) + mD_m(\lambda) + yD_y(\lambda)]}\ d\lambda \qquad (5\text{-}12c)$$

as a function of the dye weights c, m, and y.

It is desired, then, to solve eq. (5-12) for c, m, and y after observing V_R, V_G, and V_B, where D_c, D_m, and D_y are known. The solution is difficult because of nonlinearities and undesired absorptions, two of the possible sources of color error which were described in Chapter 2. The nonlinear relationships among c, m, y and V_R, V_G, and V_B are apparent from eq. (5-12). The undesired absorptions occur because the D_c, D_m, and D_y functions are nonzero over the whole spectral region, not just over the appropriate third of the region. If $D_m(\lambda)$ and $D_y(\lambda)$ were zero value over the red spectral region, where $H_R(\lambda)$ is nonzero, then eq. (5-12a) could be solved for c independently of the other two equations. In general, each dye absorbs to some extent over the whole spectral region, and the three equations must be solved simultaneously. Equation (5-12) can be converted to vector form

$$\underline{v} = \underline{\underline{H}}\underline{\tau} \qquad (5\text{-}13)$$

where

$$\underline{v} = \begin{bmatrix} V_R \\ V_G \\ V_B \end{bmatrix}$$

and

$$\underline{H} = \begin{bmatrix} H_R(\lambda_1) & \cdots\cdots & H_R(\lambda_N) \\ H_G(\lambda_1) & \cdots\cdots & H_G(\lambda_N) \\ H_B(\lambda_1) & \cdots\cdots & H_B(\lambda_N) \end{bmatrix}$$

Summarizing, the complete input color-to-scanner output chain in vector notation can be stated as

$$\underline{v} = \underline{H}\tau = \underline{HG}(\underline{w}) = \underline{HGF}(\underline{x}) = \underline{HGFSc} \qquad (5\text{-}14)$$

where $\underline{H}$ and $\underline{S}$ are linear operations which can be described by matrices and $\underline{G}$ and $\underline{F}$ are nonlinear vector operators.

5.2 Exposure Estimation Methods

The equations relating the layer exposures of a color photographic film to the corresponding output signals of a film scanner can be solved exactly, in principle. If the film dye characteristics D_c, D_m, D_y and the scanner spectral responses H_R, H_G, H_B are known, then the three film layer densities c, m, y can be obtained by inverting eq. (5-12). These are three simultaneous nonlinear equations in three unknowns c, m, and y. If the three D log E curves of the film are known, then they, in turn, can be used to obtain the layer exposures X_R, X_G, X_B from c, m, and y.

In practice, there are two reasons why an exact solution cannot be obtained. First, the film and scanner characteristics described above are not known exactly; they are derived from experiments which are subject to some degree of measurement error. Secondly, inversion of a set of nonlinear equations such as eq. (5-12) generally requires iterative solution. Solution algorithms may converge rapidly to the solution of the equations, but there will generally be some residual error remaining after any finite number of iterations. About the first source of error, little can be done except to obtain the best information available on the film and scanner characteristics. The second type of error, computational error in the solution algorithm, can be made almost arbitrarily small at the cost of complexity of the algorithm. However, since the inversion algorithm must be executed at each point of an image array which may contain tens or hundreds of thousands of points, the computer time required for its execution is of great importance. Choosing the optimal inversion algorithm requires a tradeoff between signal error and computation time.

In the following material, a typical set of film dye transmissivity and density vs. log exposure curves and a set of color scanner response curves are substituted into eq. (5-12), and several solution methods of various kinds are employed in order to compare their relative accuracies

and degrees of complexity.

The solution methods which have been investigated can be assigned to one of three general types:

1) An "exact" solution - Equation (5-12) can be solved with arbitrarily small error by employing a Newton-Raphson iteration algorithm which converges to a solution of any desired accuracy in a finite number of steps.

2) Solution by approximation of the original equations - Equation (5-12) can be simplified by making approximations which convert the three nonlinear integral equations to three algebraic equations which may be linear or quadratic, and which may be solved analytically.

3) Solution by table look-up or interpolation - The equations may be solved by substituting values of film density or exposure over some range of possible values into the film-scanner equations, and tabulating the resulting scanner voltages. To keep the number of entries in the three dimensional table within reasonable bounds, coarse quantization of the tabulated values can be combined with linear interpolation between the tabulated values. Alternatively, the whole table can be curve fitted by simple interpolating functions such as polynomials. The exposure values are then obtained, within certain error limits, by inserting the scanner signal values into the

interpolating functions and calculating the result.

The Newton-Raphson algorithm used to give an arbitrarily exact solution of eq. (5-12) is a standard iterative algorithm for solving nonlinear equations [4]. In this algorithm, an approximate solution for c, m, y is substituted into eq. (5-12) to obtain a corresponding set of approximate scanner signals $\tilde{V}_R$, $\tilde{V}_G$, $\tilde{V}_B$. The differences between the observed V_R, V_G, V_B and the approximate signals are then used to generate correction terms Δc, Δm, Δy to the initial approximate values of c, m, y. Thus,

$$\begin{bmatrix} \Delta c \\ \Delta m \\ \Delta y \end{bmatrix} = \begin{bmatrix} \frac{\partial V_R}{\partial c} & \frac{\partial V_R}{\partial m} & \frac{\partial V_R}{\partial y} \\ \frac{\partial V_G}{\partial c} & \frac{\partial V_G}{\partial m} & \frac{\partial V_G}{\partial y} \\ \frac{\partial V_B}{\partial c} & \frac{\partial V_B}{\partial m} & \frac{\partial V_B}{\partial y} \end{bmatrix} \begin{bmatrix} V_R - \tilde{V}_R \\ V_G - \tilde{V}_G \\ V_B - \tilde{V}_B \end{bmatrix} \qquad (5\text{-}15)$$

The process can be iterated until the desired solution accuracy is achieved. The initial approximate solution can be obtained using any of the algorithms to be described in the following material on approximate solutions of eq. (5-12).

Single pass solutions of eq. (5-12) can be obtained in several ways by imposing conditions on the properties of the scanner or photographic film which render eq. (5-12)

directly solvable. One such approximate solution is obtained by assuming that the spectral response curves of the scanner are narrowband and that the density-log exposure curves of the film are linear over all density values of interest. The last condition implies

$$c = \alpha_c + \gamma_c \log X_R \tag{5-16a}$$

$$m = \alpha_m + \gamma_m \log X_G \tag{5-16b}$$

$$y = \alpha_y + \gamma_y \log X_B \tag{5-16c}$$

Substituting these approximations into eqs. (5-12) relates the exposures to the scanner signals V_R, V_G, V_B

$$V_R = k_R \int_{\lambda_L}^{\lambda_U} K(\lambda)\, H_R(\lambda)\, X_R^{\psi_c(\lambda)}\, X_G^{\psi_m(\lambda)}\, X_B^{\psi_y(\lambda)}\, d\lambda \tag{5-17a}$$

$$V_G = k_G \int_{\lambda_L}^{\lambda_U} K(\lambda)\, H_G(\lambda)\, X_R^{\psi_c(\lambda)}\, X_G^{\psi_m(\lambda)}\, X_B^{\psi_y(\lambda)}\, d\lambda \tag{5-17b}$$

$$V_B = k_B \int_{\lambda_L}^{\lambda_U} K(\lambda)\, H_B(\lambda)\, X_R^{\psi_c(\lambda)}\, X_G^{\psi_m(\lambda)}\, X_B^{\psi_y(\lambda)}\, d\lambda \tag{5-17c}$$

where

$$\psi_c(\lambda) = \gamma_c\, D_c(\lambda)$$

$$\psi_m(\lambda) = \gamma_m\, D_m(\lambda)$$

$$\Psi_y(\lambda) = \gamma_y \, D_y(\lambda)$$

$$K(\lambda) = 10^{-[\alpha_c \, D_c(\lambda) + \alpha_m \, D_m(\lambda) + \alpha_y \, D_y(\lambda)]}$$

The narrowband assumption implies that the scanner characteristic H_R, H_G, H_B are nonzero over spectral regions which are so narrow that the other functions of λ are approximately constant. This assumption is very good for laser scanners but less good for broadbanded scanner characteristics. Under the narrowband assumption, eq. (5-17) becomes

$$V_R = A_R \, X_R^{\Psi_c(\lambda_R)} \, X_G^{\Psi_m(\lambda_R)} \, X_B^{\Psi_y(\lambda_R)} \qquad (5\text{-}18a)$$

$$V_G = A_G \, X_R^{\Psi_c(\lambda_G)} \, X_G^{\Psi_m(\lambda_G)} \, X_B^{\Psi_y(\lambda_G)} \qquad (5\text{-}18b)$$

$$V_B = A_B \, X_R^{\Psi_c(\lambda_B)} \, X_G^{\Psi_m(\lambda_B)} \, X_B^{\Psi_y(\lambda_B)} \qquad (5\text{-}18c)$$

where

$$A_R = k_R \, K(\lambda_R) \int_{\lambda_L}^{\lambda_U} H_R(\lambda) \, d\lambda$$

$$A_G = k_G \, K(\lambda_G) \int_{\lambda_L}^{\lambda_U} H_G(\lambda) \, d\lambda$$

$$A_B = k_B K(\lambda_B) \int_{\lambda_L}^{\lambda_U} H_B(\lambda)\, d\lambda$$

and $\lambda_R, \lambda_G, \lambda_B$ are the centroid wavelengths of the scanner functions H_R, H_G, H_B, respectively. Taking the logarithm of each side of eq. (5-18) gives the matrix equation

$$\begin{bmatrix} \ln V_R \\ \ln V_G \\ \ln V_B \end{bmatrix} = \begin{bmatrix} \Psi_c(\lambda_R) & \Psi_m(\lambda_R) & \Psi_y(\lambda_R) \\ \Psi_c(\lambda_G) & \Psi_m(\lambda_G) & \Psi_y(\lambda_G) \\ \Psi_c(\lambda_B) & \Psi_m(\lambda_B) & \Psi_y(\lambda_B) \end{bmatrix} \begin{bmatrix} \ln \hat{X}_R \\ \ln \hat{X}_G \\ \ln \hat{X}_B \end{bmatrix} + \begin{bmatrix} \ln A_R \\ \ln A_G \\ \ln A_B \end{bmatrix} \qquad (5\text{-}19)$$

Inverting this equation and exponentiating gives the estimated exposures $\hat{X}_R$, $\hat{X}_G$, $\hat{X}_B$.

Another approximation can be made in eqs. (5-12) which renders the equations solvable in closed form. The necessary approximation is that the film dyes are ideal block dyes; that is, the three layer absorption curves are spectrally nonoverlapping and are constant with wavelength over their absorption regions as shown in figure (2-8). Under this assumption, eq. (5-12) reduce to the following equations

$$V_R = b_{11}\, 10^{-cD_c} + b_{12}\, 10^{-mD_m} + b_{13}\, 10^{-yD_y} \qquad (5\text{-}20a)$$

$$V_G = b_{21}\, 10^{-cD_c} + b_{22}\, 10^{-mD_m} + b_{23}\, 10^{-yD_y} \qquad (5\text{-}20b)$$

$$V_B = b_{31}\, 10^{-cD_c} + b_{32}\, 10^{-mD_m} + b_{33}\, 10^{-yD_y} \qquad (5\text{-}20c)$$

where D_c, D_m, D_y are the constant ideal dye absorptions over their absorption regions and where

$$b_{ij} = \int_{\lambda_{Lj}}^{\lambda_{Uj}} H_i(\lambda)\, d\lambda$$

for i=R,G,B;j=c,m,y and where λ_{lc} and λ_{uc} define the lower and upper spectral limits of the cyan dye absorption region, with similar definition for the magenta and yellow absorption region. In matrix form, eq. (5-20) becomes

$$\begin{bmatrix} V_R \\ V_G \\ V_B \end{bmatrix} = \begin{bmatrix} & B & \end{bmatrix} \begin{bmatrix} 10^{-cD_c} \\ 10^{-mD_m} \\ 10^{-yD_y} \end{bmatrix} \qquad (5\text{-}21)$$

Inverting this matrix equation, taking the base 10 logarithm of the components of the resulting vector, and dividing by the appropriate constants $-D_c$, $-D_m$, or $-D_y$ gives the approximate values of c, m, and y under the ideal dye approximation. The accuracy of the answer is determined by the closeness of the actual dye absorption

curves to the nearest set of ideal dye curves. As was stated in Chapter 2, real dyes have some degree of absorption in undesired spectral regions, and do not have constant absorption over the desired absorption region.

Inversion of the system of equations defined by the density-log exposure curves and eq. (5-12) can be accomplished in other approximate ways by first substituting a range of exposure values $\underline{x}$ into the equations and tabulating the resulting scanner signals $\underline{v}$. Determination of $\underline{x}$ from $\underline{v}$ can then be accomplished by any of the following:

1) choosing the tabulated $\underline{v}$ nearest to the observed $\underline{v}$ and looking up the corresponding $\underline{x}$ in the table.

2) curve fitting the $\underline{x}$ values to the $\underline{v}$ values using a set of algebraic interpolating functions, thus obtaining estimated values of $\underline{x}$ from observed values of $\underline{v}$ by inserting the observed $\underline{v}$ into the interpolating function and calculating the corresponding value of $\underline{x}$.

3) using a combination of the above.

For example, a coarsely quantized table of $\underline{x}$ vs. $\underline{v}$ might be used along with a simple, perhaps linear, interpolation algorithm for obtaining values when $\underline{v}$ is not equal to one of the relatively small number of $\underline{v}$'s in the coarse lookup table.

The curve fitting and interpolation algorithms can be simplified by using the logarithms of the variables rather than the variables themselves, since the logarithms of the components of $\underline{x}$ and $\underline{v}$ are very nearly linearly related. This may be inferred by observing that under the narrowband scanner assumption, eqs. (5-12) simplify to eqs. (5-19) which are exactly linear in the logarithms of $\underline{x}$ and $\underline{v}$.

5.3 Exposure Estimation Results

In this section, the exposure estimation algorithms which have been described are compared by testing them with exposure and scanner signal values obtained using a computer simulation of a typical film-scanner color analyzing system. The film properties are those of a typical reversal color film (Kodak Ektachrome-X). The density vs. log exposure and layer dye spectral densities of the film are shown in figures (5-2) and (2-7). The scanner simulation represented a flying spot scanning system consisting of a cathode ray tube light source, a photomultiplier tube sensor with an S20 sensitivity characteristic, and color filters which are Kodak Wratten filters number 25 (red), 58 (green) and 47B (blue). In addition, the spectral absorption of a typical set of lenses was incorporated. The overall spectral responses of the simulated scanner in its red, green, and blue channels are shown in figure (5-3).

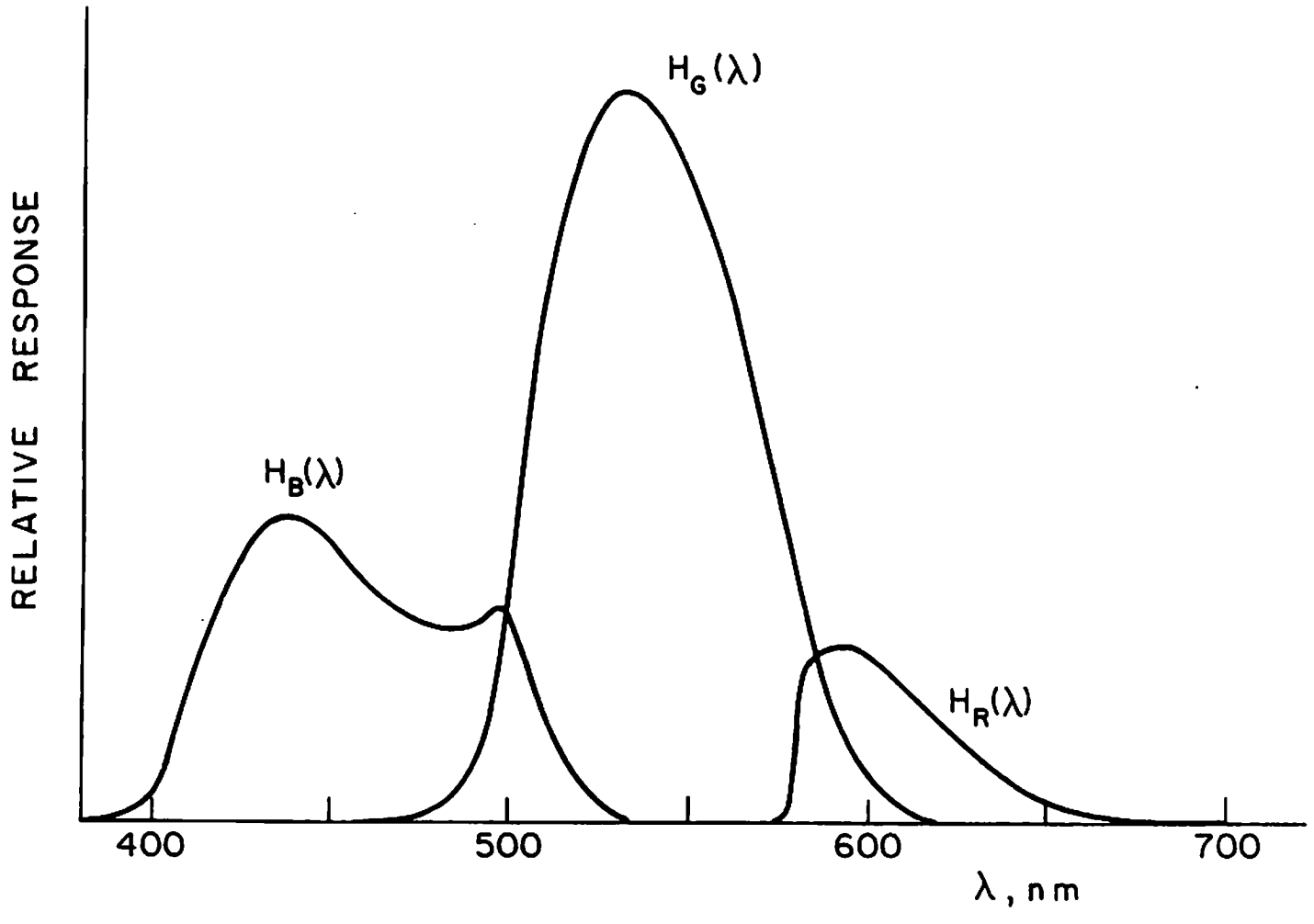

Figure (5-3) Scanner spectral response

The algorithms which were tested as exposure estimators were the following:

1) Newton-Raphson

2) Narrowband

3) Ideal Dye

4) Quadratic Curve Fit

5) Table Look-up with Iterative Correction

The parameters of the algorithms were adjusted to the particular film-scanner system being considered in the following ways:

1) Newton-Raphson - The Newton-Raphson solution method was carried out for each input color until the change in estimated exposure values for iteration was sufficiently small. The iterations were stopped when the RMS fractional change in the estimated exposures averaged over the three exposure values, was less than 0.01. This was achieved, on the average, after about six iterations.

2) Narrowband - The narrowband spectral sensitivities were placed at the centroids of the three scanner response curves, which are at wavelengths of 610, 535, and 440 nanometers for the red, green and blue scanner channels, respectively.

3) Ideal Dye - The dye spectral density functions which were assumed under the ideal dye model were of the

ideal rectangular shape as shown in figure (2-8) where the wavelengths separating the three dye absorption curves were chosen to be the intersection wavelengths of the actual dyes, and the constant densities of the ideal dyes were selected so that their densities integrated over all wavelengths equalled the integrated densities of the actual dyes.

4) Quadratic Curve Fit - A quadratic polynomial exposure estimator was derived by obtaining a least squares curve fit between a set of exposure vectors $\underline{x}$ and the corresponding scanner signal vectors $\underline{v}$, obtained by substituting the $\underline{x}$ vectors into the equations which model the film and scanner properties

$$\underline{v} = \underline{HGF}(\underline{x})$$

The polynomial expression which approximates the components of $\underline{x}$ from the components of $\underline{v}$ was selected to be a quadratic expression in the logarithms of the components

$$(\log \hat{X}_i) = \sum_j a_{ij} \log V_j + \sum_{jk} b_{ijk} \log V_i \log V_k + c_i$$

where i,j,k = R,G or B. This was done since it was known that the relationship between the log V and log X quantities is exactly linear in the narrowband scanner case (equation 5-19), and it was hoped that many of the quadratic coefficients could be neglected in the general scanner approximation. This indeed turned out to be the

case, and it was found that the quadratic coefficients which were the largest were those corresponding to the channel being approximated. That is, in approximating log X_R, the coefficient of the $(\log V_R)^2$ term was much larger than that of the $(\log V_R \log V_G)$ term or the $(\log V_G)^2$ term. This allows the approximation to take the simple form

$$(\log \hat{X}_i) = \sum_j a_{ij} \log V_j + b_i (\log V_i)^2 + c_i$$

Expressed in matrix form, this becomes

$$\begin{bmatrix} \log X_R \\ \log X_G \\ \log X_B \end{bmatrix} = \begin{bmatrix} a_{11} & a_{12} & a_{13} & b_1 & 0 & 0 \\ a_{21} & a_{22} & a_{23} & 0 & b_2 & 0 \\ a_{31} & a_{32} & a_{33} & 0 & 0 & b_3 \end{bmatrix} \begin{bmatrix} \log V_R \\ \log V_G \\ \log V_B \\ (\log V_R)^2 \\ (\log V_G)^2 \\ (\log V_B)^2 \end{bmatrix} \begin{bmatrix} C_1 \\ C_2 \\ C_3 \end{bmatrix} \quad (5\text{-}22)$$

The a, b, and c coefficients were determined by least squares curve fitting over 125 points, 5 in each dimension of x. The five values each of log X_R, log X_G and log X_B were chosen to cover in equal increments most of the linear region of the density-log exposure curves of the film.

5) Linear Correction Scheme using Table Look-up for Initialization - An efficient iterative method for solving

for the layer dye weights c, m, y was derived from a method of Eugene Allen [5] for solving a related problem, that of determining the dye weights which give a colorimetric match to a given sample. Details of the method can be found in reference [5]. The only change required for the film-scanner problem is the substitution of the scanner characteristics for the color matching curves used by Allen. The method essentially linearizes the relations between c,m,y and the scanner signals about the initial values of c,m,y and generates a linear corrective term which is added to the initial values.

The method was tested using as initial estimates values obtained from a coarse three-dimensional (5x5x5) look-up table,followed by one step of linear correction using the Allen method. The table was obtained by inputting a range of 125 density vectors $\underline{w}$, spaced uniformly, into the film-scanner simulation and forming a three-dimensional table of the output vectors $\underline{v}$ and the input $\underline{w}$'s. Given an observed $\underline{v}$, the nearest smaller $\underline{v}$ components in the table were selected, and the corresponding $\underline{w}$ was used as an initial point.

The results of a computer simulation testing of the various exposure estimation algorithm are summarized in Table (5-1), along with the results of using no correction for film and scanner nonlinearities. The simulation

Table (5-1)

Exposure Estimator Error Performance

Exposure Estimation Algorithm	Normalized Exposure Error
Narrowband Approximation	0.0392
Ideal Dye Approximation	0.0662
Quadratic Curve Fit	0.0110
Table Lookup With Linear Correction	0.0213
Newton-Raphson Iterative Method	0.0061
No Correction (Scanner Signals Treated as Exposures)	0.1045

modelled the whole photographic film and color scanner system whose characteristics are given by the curves of figures (2-7),(5-1), (5-2) and (5-3). The input colors were the ten reflectivities of figure (4-1) illuminated by CIE Illuminant C.

The results indicate, as expected, that the more complex methods were more accurate. Of the two simplest methods, the narrowband approximation was more accurate than the ideal dye approximation, although both were much better than no correction at all. The slightly more complex quadratic curve fit was better than either of the simpler methods, by a factor of four or more, and was also more accurate than the more complex table lookup with linear correction. The table lookup with one step of correction was far surpassed by the Newton-Raphson method, which executed six iterative steps per solution.

References

1. L. DeMarsh, "Color Reproduction in Color Television," in Color: Theory and Imaging Systems, Soc.Photog.Scientists and Engineers publication, 1973.

2. R. Evans, W. Hanson, and W. Brewer, Principles of Color Photography, John Wiley and Sons, New York, (1953).

3. F. Clapper, R. Gendron, and S. Brownstein, "Color Gamuts of Additive and Subtractive Color-Reproduction Systems," J. Optical Society of America, 63, 5, p. 625 (1973).

4. K.S. Kunz, Numerical Analysis, McGraw-Hill, New York, 1957.

5. E. Allen, "Basic Equations Used in Computer Color Matching," J. Optical Society of America, 56, 9, p. 1256, (1966).

6. Related Applications of Digital Color Methods

The vector space description of color analysis which was described in Chapter 3 and the generalized inverse methods which were used for tristimulus estimation in Chapter 4 can be applied to a wide variety of color problems. In this chapter, two problems will be discussed. The first, spectral calibration of an optical sensor using readings from test samples, is a practical problem which arises when direct spectrophotometric measurement of the sensor spectral characteristic is impossible. The second problem, that of computer generation of spectral waveforms with desired properties, arises in the simulation of color or multi-spectral sensing and recording systems.

6.1 Estimation of Color Scanner Spectral Characteristics

The spectral response of an optical sensing system, such as a color image scanner or a densitometer, is often difficult to measure directly. The spectral response is typically the product of a series of spectral characteristics of the system's component parts, such as the emission characteristic of the light source, the transmissivity of the system optics and the response characteristic of the sensor. The spectral response of the system as a whole can be measured directly only by placing a wavelength variable narrowband device, such as a calibrated monochromator, in the system light path. This

may be impossible because of physical size limitations, accuracy requirements, or other reasons. An alternative approach is to take readings with the scanner using a series of test color samples whose spectral characteristics are known, and to reconstruct the scanner spectral response from these readings. The vector equation relating the scanner characteristic $\underline{h}$, the i th color sample transmissivity $\underline{c}_i$ and the corresponding scanner output x_i is given by

$$x_i = \underline{c}_i^T \underline{h} + n_i \qquad (6\text{-}1)$$

where $\underline{c}_i$ and $\underline{h}$ are Qx1 vectors of quadrature samples of the test color sample transmissivity curve and the scanner response curve, respectively. The observation noise error on the i th observation is given by n_i. By combining the P observations x_i (i=1,...,P) into a Px1 vector $\underline{x}$, eq. (6-1) becomes the matrix equation

$$\underline{x} = \underline{C}\,\underline{h} + \underline{n} \qquad (6\text{-}2)$$

where $\underline{c}_i^T$ is the i th row of the PxQ matrix $\underline{C}$. Since the number of quadrature mesh points Q is usually much larger than the number of test samples P, eq. (6-2) is underdetermined, and the tools which were used to solve the same equation (eq.4-1) in Chapter 4 can be again applied. The mathematical solution for $\underline{h}$ in eq. (6-2) is equivalent to solving for $\underline{c}$ in eq. (4-1) because of the symmetry

between $\underline{c}$ and $\underline{h}$ in eq. (6-1). In the tristimulus problem the sensor response was known and the input color was being estimated. Now, the input color is known and the sensor characteristic is being estimated.

The three types of solutions developed in Chapter 4 are the pseudo-inverse solution, the generalized inverse with a smoothness constraint, and the Wiener solution. All three are applicable to the scanner spectral characteristic problem. The smoothness constraints imposed on the estimated characteristic by the constrained generalized inverse solution and the Wiener solution are desirable since the spectral response of a broad banded color sensor can be assumed a priori to be a smooth function. The three solutions to eq. (6-2) are

(1) pseudo-inverse solution

$$\underline{\hat{h}} = \underline{C}^T (\underline{C}\,\underline{C}^T)^{-1}\,\underline{x} \qquad (6\text{-}3)$$

(2) generalized inverse solution with smoothness constraint

$$\underline{\hat{h}}_S = \underline{N}^{-1}\,\underline{C}^T (\underline{C}\,\underline{N}^{-1}\,\underline{C}^T)^{-1}\,\underline{x} \qquad (6\text{-}4)$$

where $\underline{N}$ is a suitably chosen smoothing matrix such as that of equation (4-29), which minimizes the average squared difference over all solutions to $\underline{x}=\underline{C}\underline{h}$.

(3) Wiener solution

$$\hat{\underline{h}}_w = \underline{m}_h + \underline{M}\,\underline{C}^T\,(\underline{C}\,\underline{M}\,\underline{C}^T + \underline{K})^{-1}\,(\underline{x} - \underline{C}\,\underline{m}_h) \qquad (6\text{-}5)$$

where $\underline{m}_h$ is the mean vector and $\underline{M}$ is the covariance matrix of the vector random process from which $\underline{h}$ is assumed to be a sample, and $\underline{K}$ is the covariance of the observation noise.

The three solutions were used in the spectral calibration of an Optronics Model S2000 flat bed scanning microdensitometer. The test samples were two sets of spectrally selective filters, each set covering the spectral region of interest, roughly 400 to 700 nanometers in wavelength. The first set consisted of nine absorption filters, four gelatin (Kodak Wratten) filters and five glass absorption filters. Their transmissivities are shown in figure (6-1). These were obtained by sampling the continuous transmissivities at 80 points at 5 nm. intervals. The resulting $\underline{C}$ matrix was therefore 9x80. The second set of filters consisted of 16 Oriel narrowband interference filters, shown in figure (6-2). These are spectrally spaced from 400 to 700 nanometers in increments of 20 nanometers and have half power bandwidths of 10 nanometers. The transmissivities were sampled at 160 points in steps of 2.5 nm. (380 to 777.5 nm.), giving a 16x160 $\underline{C}$ matrix.

The $\underline{N}$ matrix used in the constrained generalized

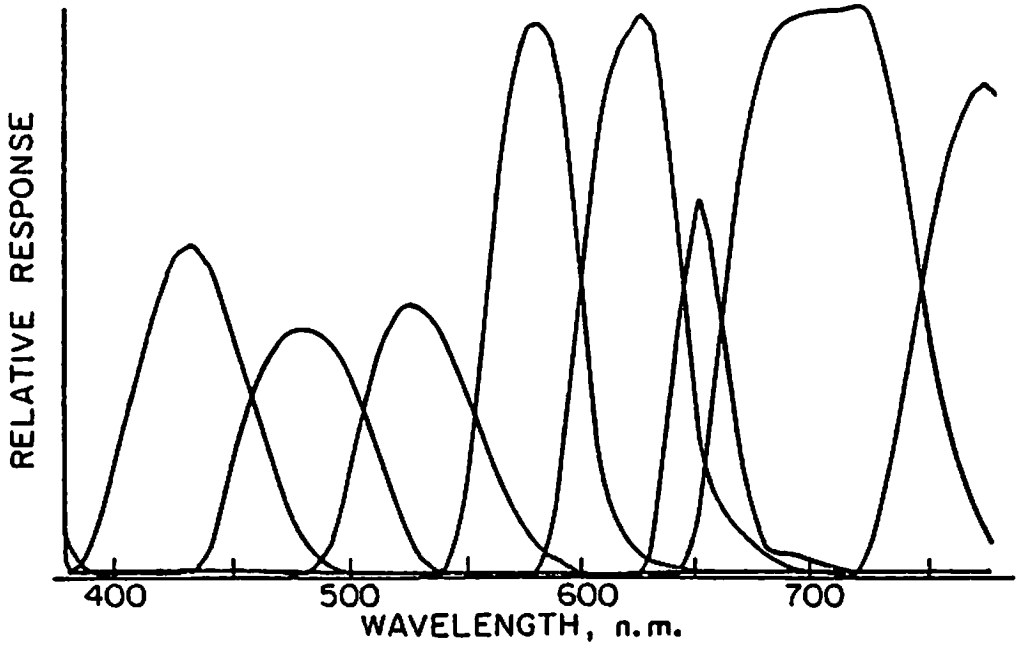

Figure (6-1) Absorption filter characteristics

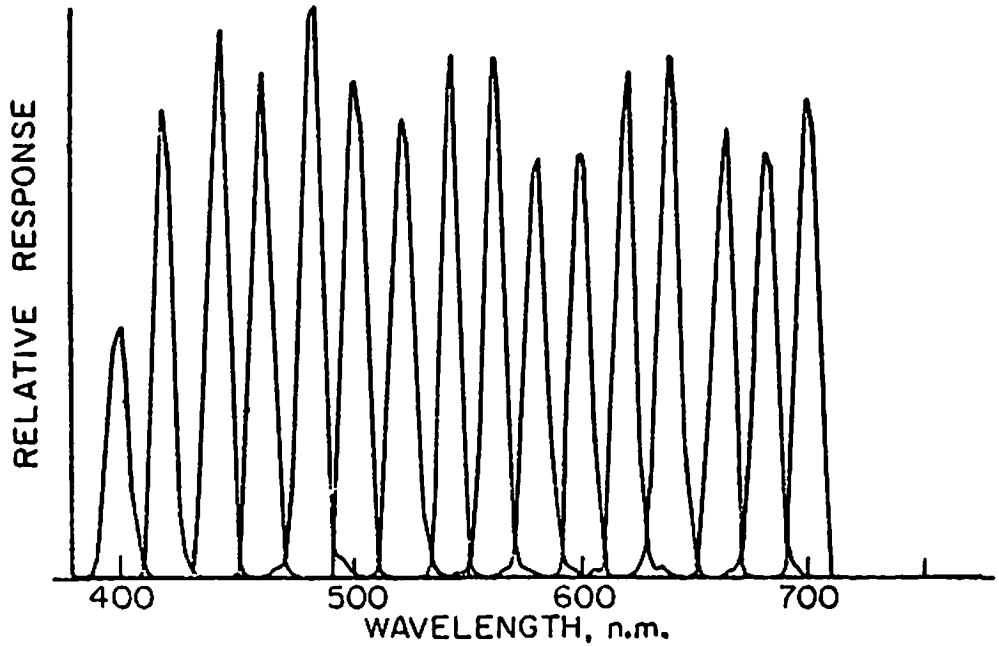

Figure (6-2) Interference filter characteristics

inverse solution was the smoothing matrix of equation (4-29) and the Wiener solution assumed a zero mean vector, a first order Markov covariance matrix, and negligible observation noise.

Figure (6-3) shows the estimated response for the three types of estimator using the measurements taken with the absorption filters. Figure (6-3a) shows the pseudo-inverse estimate, figure (6-3b) shows the constrained generalized inverse estimate and figure (6-3c) shows the Wiener solution with three different values of assumed interelement correlation. Figure (6-4) gives the estimates obtained using the same types of estimators but with data obtained using the narrowband interference filters. The Wiener estimates with the highest correlation values (Ø.9 or Ø.95) give the smoothest curves obtained with both the absorption and interference filter data, and may be presumed to be the best estimates of the true response. The interference filter estimate might be expected to be more accurate than the absorption filter estimates, since there were more of the interference filters and since their passbands do not overlap significantly, making eq. (6-2) extremely well conditioned. The "true" spectral response curve is not available, however, but since the Wiener estimates with the two filter sets are in fairly good agreement, it may be concluded that both estimated responses are a good

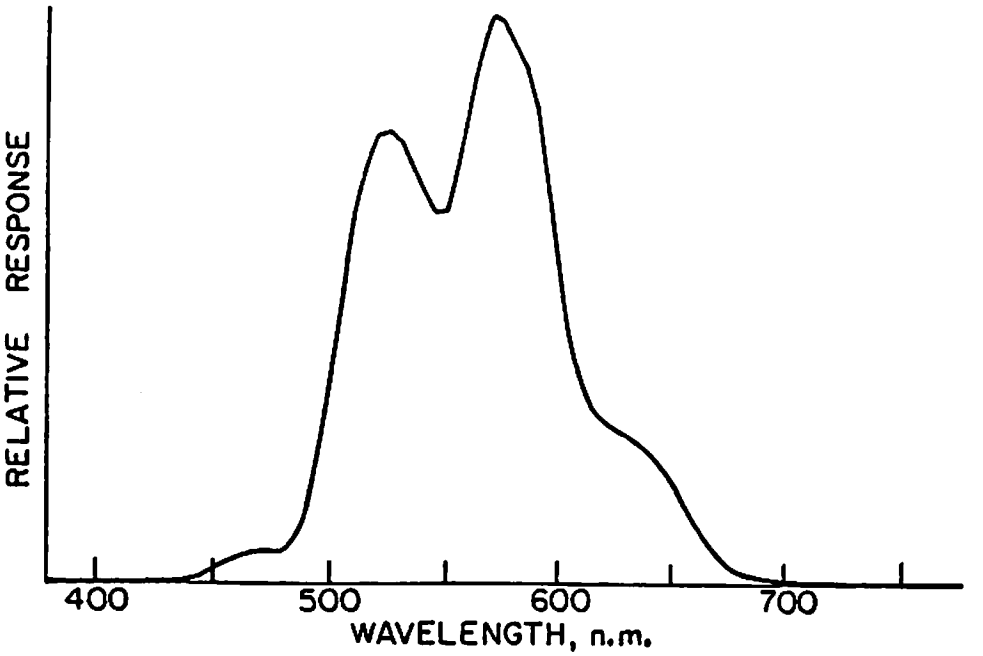

Figure (6-3a) Estimated scanner response, pseudo-inverse, absorption filters

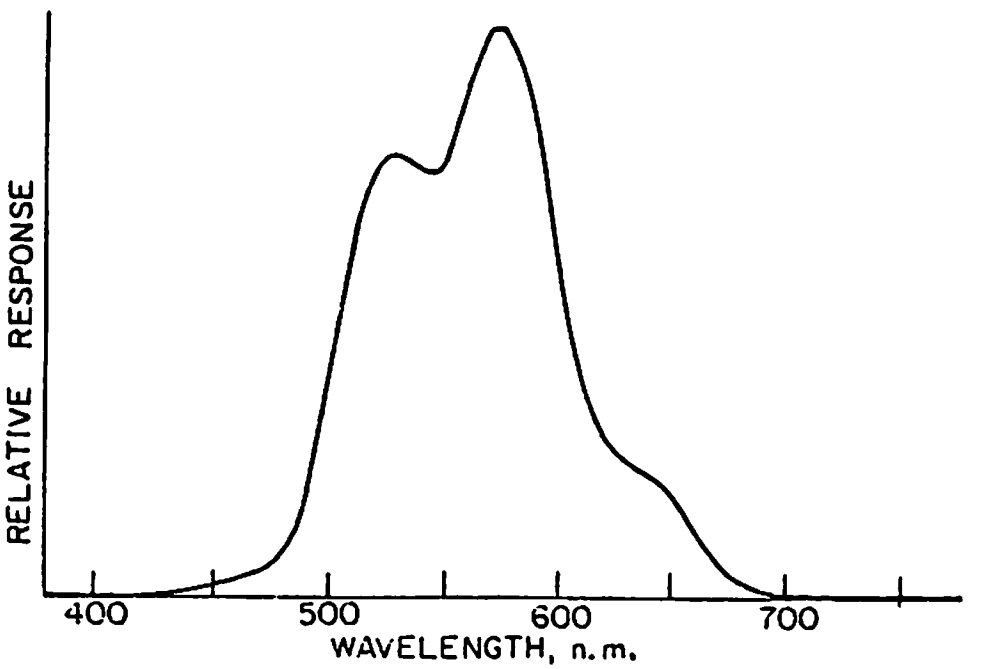

Figure (6-3b) Estimated scanner response, smoothing inverse, absorption filters

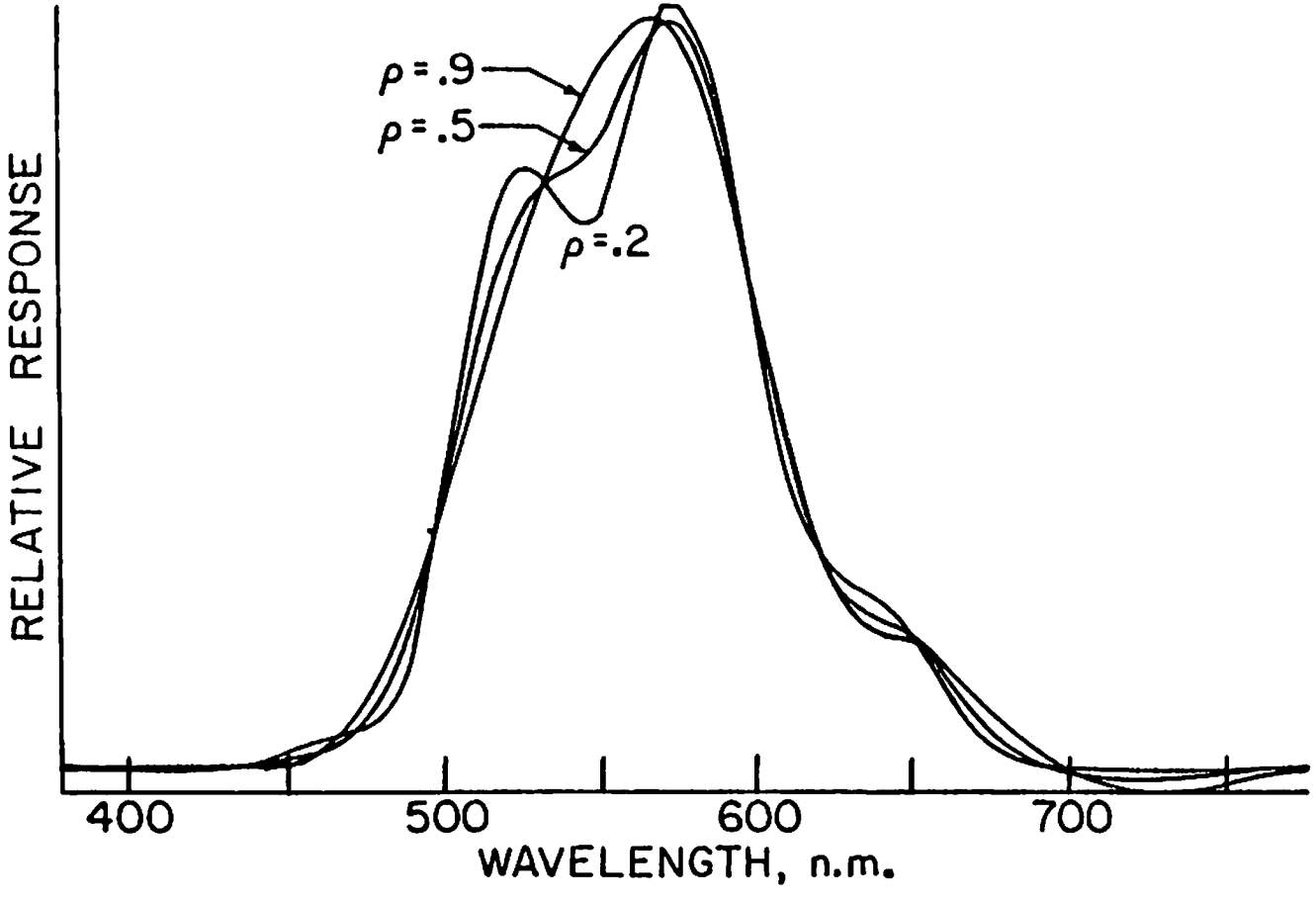

Figure (6-3c) Estimated scanner response, Wiener inverse, absorption filters

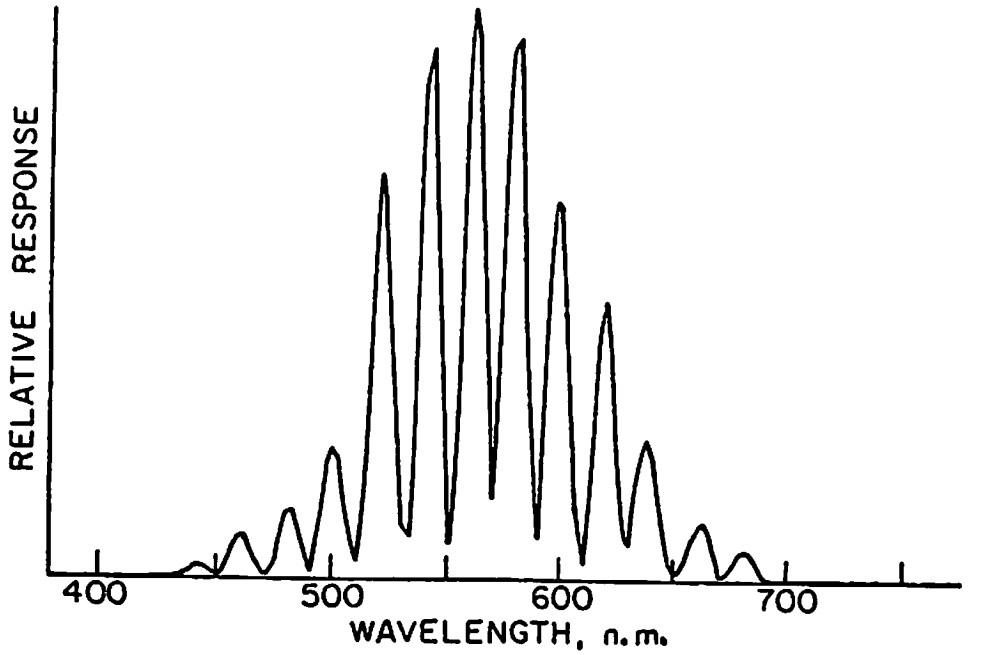

Figure (6-4a) Estimated scanner response, pseudo-inverse interference filters

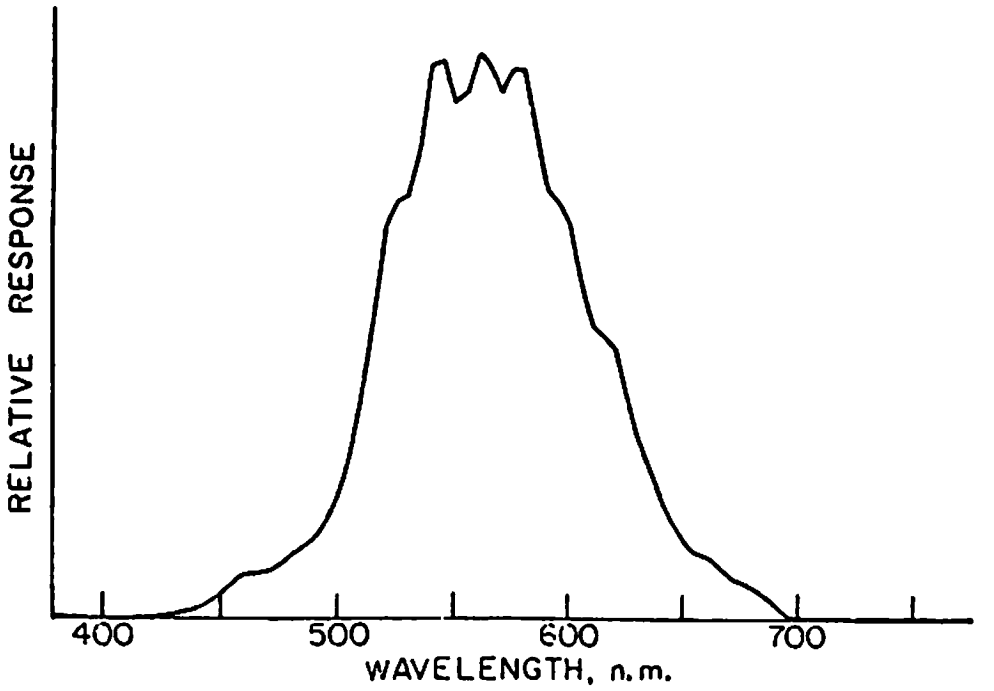

Figure (6-4b) Estimated scanner response, smoothing inverse, interference filters

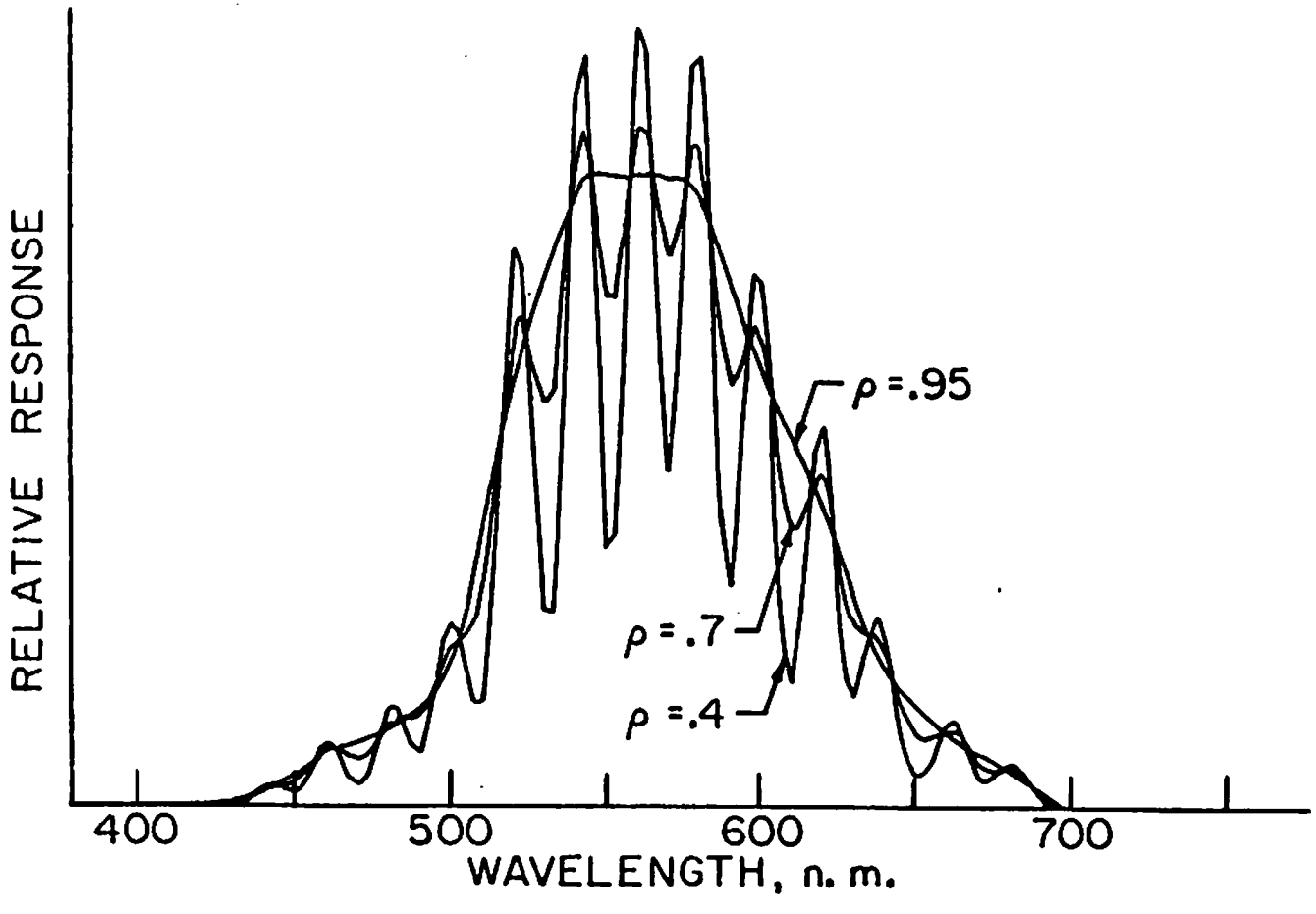

Figure (6-4c) Estimated scanner response, Wiener inverse, interference filters

approximation to the actual spectral response.

6.2 Computer Generation of Spectral Waveforms

The computer simulation of color and multispectral sensing and recording systems often requires the generation of spectral waveforms which simulate the spectral power distributions existing at points in the sensor field of view. It may be desired that the n-vector which represents the sampled spectral waveform possess certain properties expressible as linear equality constraints. For example, it might be desired to generate a spectral waveform, or color, whose tristimulus values are specified. In addition, the generated waveform should exhibit properties which are characteristic of spectral waveforms existing in nature, such as smoothness and non-negativity. These requirements are nearly identical to those of the waveforms generated in the tristimulus estimation methods of Chapter 4. The difference is that the matrix $\underline{S}$ in the constraining equation $\underline{x}=\underline{S}\underline{c}$ need not represent a set of real sensor characteristics, but instead may represent any linear operation on the waveform $\underline{c}$, such as a tristimulus constraint of the form $\underline{t}=\underline{T}\underline{c}$.

The generation of spectral waveforms metameric to a given color is a special case of waveform generation which has been the subject of some study. This is equivalent to generating waveforms with desired tristimulus values. The

methods which have been derived usually construct the waveform as weighted sums of three or four simple functions such as narrowband functions (see reference [1], p. 344-357) for a summary of methods to 1967). A recent method developed by Takahama and Nayatani [2] is derived using calculus of variations, and constructs the function $\underline{c}$ as a weighted sum of color matching curves. The Takahama algorithm expressed in sampled data form is equivalent to the pseudo-inverse solution of the constraining equation, $\underline{c}=\underline{T}^{+}\underline{t}$. To generate many metameric waveforms satisfying the constraint, $\underline{c}_o$ is varied and the solution $\underline{c}=\underline{c}_o+\underline{T}^{+}(\underline{t}-\underline{T}\underline{c}_o)$ is the solution of $\underline{t}=\underline{T}\underline{c}$ which is nearest in the least squares sense to $\underline{c}_o$.

The Wiener and smoothing inverses described in Chapter 4 can be applied to the generation of metameric waveforms with some advantages. The imposition of smoothing can, for example, generate waveforms which are very broad and smooth while still, satisfying $\underline{t}=\underline{T}\underline{c}$. The general waveform expression is given by

$$\underline{c} = \underline{c}_o + \underline{M}\underline{T}^{T}(\underline{T}\underline{M}\underline{T}^{T})^{-1}(\underline{t} - \underline{T}\,\underline{c}_o) \qquad (6\text{-}6)$$

where $\underline{t}$ is the desired tristimulus vector, $\underline{T}$ is the matrix whose rows are color matching curves, $\underline{c}_o$ is an arbitrary waveform, and $\underline{M}$ is a smoothing matrix. Waveforms generated by this algorithm are shown in Figure (6-5). A test color is shown as a dotted line, with waveforms metameric to the

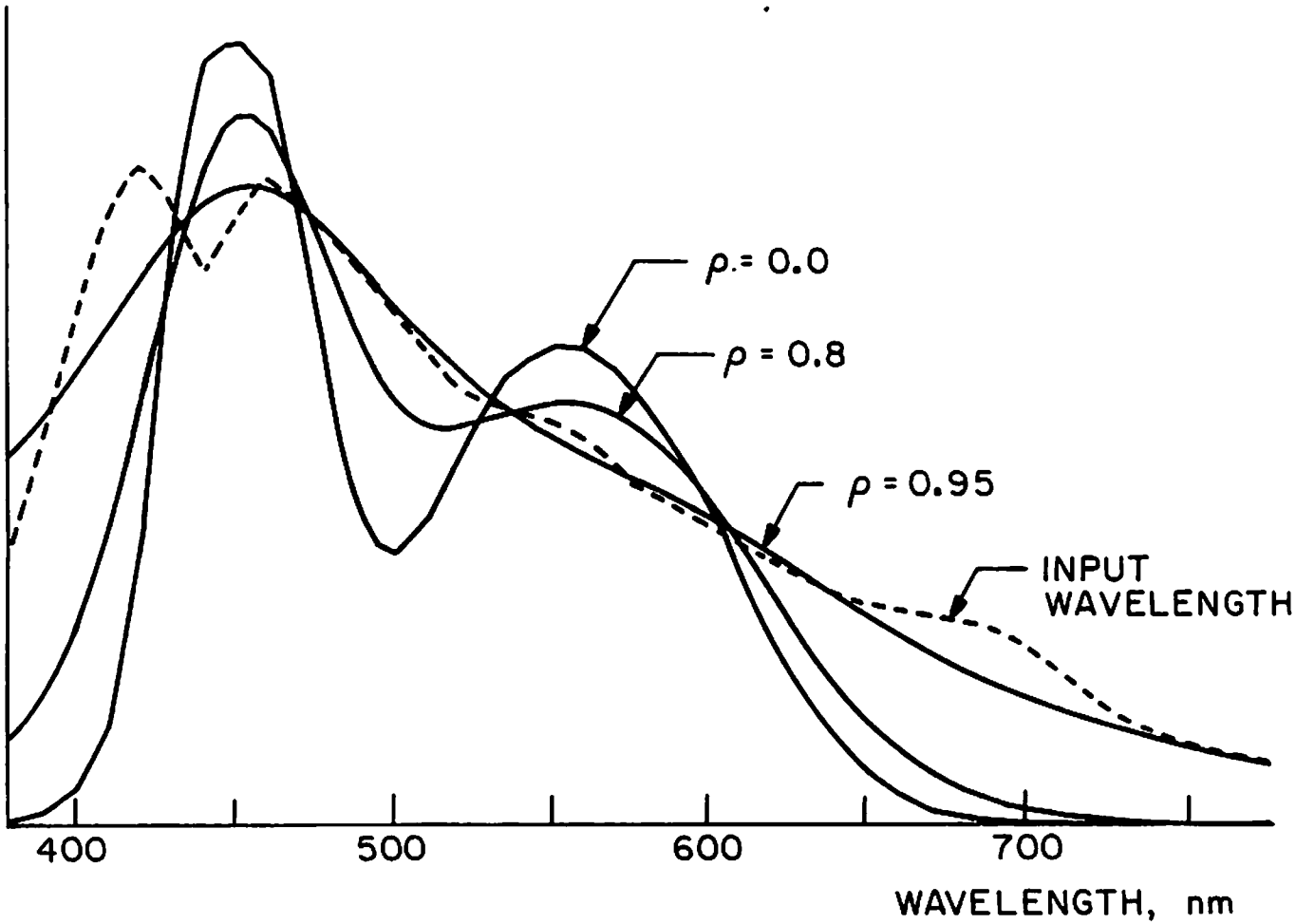

Figure (6-5) Computer generated metameric spectral waveforms

test color (with respect to illuminant C) shown as solid lines. The metameric waveforms were generated using eq.(6-6) with $\underline{c}_o=0$ and the Markov matrix of eq.(4-64) replacing $\underline{M}$. The values of ρ were 0.0, 0.8, and 0.95.

References

1. Wyszecki, G., Color Science , John Wiley,New York (1967).

2. Takahama, K., and Y.Nayatani, "New Method for Generating Metameric Stimuli of Object Colors," J.Opt.Soc.Am., 62, p.1516 (1972)

7. Conclusions and Topics for Further Study

This dissertation has presented a variety of techniques for digitally restoring digital color images. The methods which were treated included ways of correcting for colorimetrically imperfect sensors and correcting errors introduced by color system nonlinearities and undesired film absorption. In addition, methods for estimating the spectral response of a broadband sensor from sample readings and for computer generation of waveforms with desired colormetric properties were treated.

The correction for sensor spectral imperfections, or tristimulus estimation, was best accomplished using a wiener estimation algorithm which imposed a large smoothing effect on the spectral waveforms generated as intermediate steps in the estimation of tristimulus values. The RMS error in UCS chromaticity space was 0.011 averaged over ten test colors using color film taking sensitivities. The method has the advantages of simplicity, linearity, optimality (under a mean squared tristimulus error criterion) and generality. The property of generality assures that the estimator can easily be re-optimized when the taking sensitivities or the assumed statistical properties of the input colors are changed. Although the method was restricted in this report to the estimation of three tristimulus values from three outputs of imperfect

spectral sensors, it is easily generalized to other dimensionalities. The outputs of m sensors of arbitrary spectral response could be used to estimate the outputs of n other arbitrary sensors, where m is greater than, equal to, or less than n. Applications of the method might include the filling of spectral gaps in multi-spectral sensor data, or the generation of "true color" imagery from multi-spectral data. All that is required is that the spectral correlation properties of the incoming radiation are known with some degree of accuracy, and that there is significant correlation between the observed spectral regions and those being estimated.

The material dealing with correction of color system nonlinearities and undesired absorption showed that the resulting color errors can be greatly reduced, for a typical film-scanner system, by using relatively simple computer algorithms. Simple linear and quadratic approximations to an exact solution proved capable of reducing errors in estimated film exposures by a factor of about ten, for the system which was simulated.

The chapter on applications related to digital color restoration used as its primary mathematical tool the generalized matrix inverse, used previously in the chapter on tristimulus estimation. In fact, the most important single result of this report may be the demonstration of

the great utility of the generalized inverse as applied to color systems. The applications treated in this dissertation included tristimulus estmation, estimation of sensor spectral responses, and computer generation of spectral waveforms. The generalized matrix inverse is applicable to a great many other problems connected with color and multi-spectral analyzing and imaging systems. Any problem requiring the solution or inversion of a set of linear vector equations, subject to the minimization of a vector quadratic form, is a candidate for generalized inverse methods. This is true whether the equations are deterministic or stochastic, overdetermined, underdetermined or exactly determined. Typical problems might include the estimation of the spectral properties of sample reflectivities, sensors, illuminants, atmospheric transmissivity, lens or filter absorption characteristics, etc.

A fruitful area for further study is in determining the best quadratic forms for use as error criteria with linear estimation techniques. A quadratic form which best measures the departure of a spectral waveform from the smoothness or correlation properties of natural object colors would be useful. The optimal quadratic forms for converting the vector of tristimulus errors or the vector of spectral distribution errors to a number measuring the total perceived color error would also be of some benefit

in color estimation problems.

In conclusion, it is hoped that the contents of this dissertation are of some value in advancing the science and art of digital color image processing. The field of digital color image processing is in its infancy, and will doubtless evolve far beyond its current state. The uneasy marriage of colorimetry and linear system theory, characteristic of the methods described here, will someday be supplanted as newer, more complex and more accurate mathematical models of the human visual systems are created. Still, in spite of the obvious limitations of linear estimation, quadratic error criteria, and present day colorimetry, methods such as those described here are effective. With the increasing power of digital computation the digital processing of color imagery will become even more effective and more widespread.